

MCGILL UNIVERSITY

**Using external fields to control
topological insulators and topological
superconductors**

Aaron Farrell

Department of Physics

April 2016

McGill University, Montreal, Quebec

A thesis submitted to McGill University in partial fulfillment of the requirements of the
degree of Doctor of Philosophy

©Aaron Farrell, 2016

Abstract

The work in this thesis is dedicated to creating and manipulating topological states of matter in condensed matter systems through the use of external fields. In particular, the research in this dissertation is focused on topological superconductors and topological insulators. These states of matter are of interest because of their unique edge-states. In a topological superconductor the edge-states are Majorana modes and have potential applications in quantum computation. Meanwhile, in a topological insulator the edge-states amount to counter propagating, helical channels with interesting transport and photo-voltaic properties. Topological states of matter are also of interest for more fundamental reasons. This is because they represent a strong departure from our standard understanding of states of matter.

The ability to tune a topological state of matter is of vital importance to both isolating these states in the laboratory, and to utilizing the properties of these states in physical applications. The work in this document begins by focusing on creating a topological superconductor by using an externally applied (and therefore tunable) magnetic field. The remainder of the thesis will be dedicated to using externally applied electromagnetic radiation to create and manipulate the properties of a topological insulating state.

Résumé

Les travaux de cette thèse sont consacrés à la création et la manipulation des états topologiques de la matière dans les systèmes de matière condensée par l'utilisation de champs extérieurs. En particulier, la recherche dans cette thèse se concentre sur les supraconducteurs topologiques et les isolants topologiques. Ces états de la matière sont d'intérêt en raison de leurs états de bord uniques qui peuvent être utiles pour des applications technologiques. Dans un supraconducteur topologique, les états de bord sont des modes de Majorana et ont des applications potentielles dans le calcul quantique. Par ailleurs, dans un isolant topologique, les états de bord sont des canaux hélicoïdaux qui propagent dans le sens inverse avec des propriétés photovoltaïques et de transports intéressants. Les états topologiques de la matière sont également intéressants pour des raisons plus fondamentales. En effet, ils dévient énormément de notre compréhension standard des états de la matière.

La capacité de manipuler un état topologique de la matière est importante pour isoler ces états dans un laboratoire et pour utiliser les propriétés de ces états dans des applications physiques. Ce document commence en décrivant la création d'un supraconducteur topologique en utilisant un champ magnétique appliqué. Le reste de la thèse sera consacré à l'utilisation du rayonnement électromagnétique pour créer et manipuler les propriétés d'un état isolant topologique.

Acknowledgments

I would like to begin by thanking my friends and family for their continued support throughout my studies. This work would not have been possible without their ongoing encouragement. Second, I would like to express my gratitude to my supervisor, Dr. Tami Pereg-Barnea, for her advice, encouragement, and support over the last five years. The work in this thesis was funded by the Walter C. Sumner Memorial Fellowship and the Canada Vanier Graduate Scholarships program.

Contributions of authors

This dissertation is formatted as a manuscript based thesis with all the papers (Chapters 2, 3, 4, and 5) having been published, accepted for publication or submitted for publication during my candidature. I am the principal author of each chapter and considered as the sole author of the thesis and fully responsible for everything contained in it. The contributions of the other authors to each of the three manuscripts are listed below.

Zeeman field induced non-trivial topology in a spin-orbit coupled superconductor

Aaron Farrell:

Co-proposed the idea for the work and performed the analytical and numerical analyses of the problem. Compiled and interpreted the results of these calculations and shared editing responsibilities during the preparation of the manuscript.

T. Pereg-Barnea:

Co-proposed the idea for the work and supervised its development. Provided critical evaluation, advice, and interpretation of results as the work progressed and shared the responsibilities of editing the manuscript.

Photon Inhibited Topological Transport in Quantum Well Heterostructures

Aaron Farrell:

performed the analytical and numerical analyses of the problem. Compiled and interpreted the results of these calculations, and shared in the editing responsibilities during the preparation of the manuscript.

T. Pereg-Barnea:

Originally proposed the idea for the work and supervised its development. Provided critical evaluation, advice, and interpretation of results as the work progressed and shared in the the responsibilities of editing the manuscript.

Edge State Transport in Floquet Topological Insulators**Aaron Farrell:**

performed the analytical and numerical analyses of the problem. Compiled and interpreted the results of these calculations and shared editing responsibilities during the preparation of the manuscript.

T. Pereg-Barnea:

Originally proposed the idea for the work and supervised its development. Provided critical evaluation, advice, and interpretation of results as the work progressed and shared in the the responsibilities of editing the manuscript.

Time-dependent population of sidebands in a Dirac system**Aaron Farrell:**

Co-proposed the idea for the work and performed the analytical and numerical analyses of the problem. Compiled and interpreted the results of these calculations and shared in the editing responsibilities during the preparation of the manuscript.

T. Pereg-Barnea:

Co-proposed the idea for the work and supervised its development. Provided critical evaluation, advice, and interpretation of results as the work progressed and shared the responsibilities of editing the manuscript.

Contents

1	Introduction	1
1.1	Topological States of Matter	1
1.2	Externally Induced Topological Superconductivity	4
1.3	Non-equilibrium Topological Insulators	8
1.4	Outline of this Thesis	11
	Preface to Chapter 2	15
2	Zeeman field induced non-trivial topology in a spin-orbit coupled superconductor	17
2.1	Introduction	19
2.2	Preliminary Discussion	21
2.3	Model and Method	25
2.4	Summary of RG Analysis	32
2.5	Mean Field Topological Classification	38
2.6	Conclusion	42
2.7	Acknowledgements	43
2.A	Interaction Vertex in the Band Basis	43
2.B	Three-Loop Expansion for S'_{int} on the Lattice	45
2.C	Continuum Limit	50
	Preface to Chapter 3	63
3	Photon Inhibited Topological Transport in Quantum Well Heterostructures	65
3.1	Introduction	67
3.2	Methods	68
3.3	Transport Results	70
3.4	Connection to Floquet Sum Rule	75
3.5	Conclusions	77
3.6	Acknowledgements	77

3.A Floquet-Landauer Formula for Transport	78
3.B Effective Hamiltonian	83
Preface to Chapter 4	95
4 Edge State Transport in Floquet Topological Insulators	97
4.1 Introduction.	99
4.2 Model.	101
4.3 Two Terminal Conductivity.	104
4.4 Photon Inhibited Transport and Floquet Sum Rule.	106
4.5 Hall Bar Geometry and Edge States	109
4.6 Conclusions.	112
4.7 Acknowledgments	113
4.A Floquet-Landauer Formulism for Transport	113
4.B Approximate Result for the Conductivity	116
Preface to Chapter 5	131
5 Time-dependent population of sidebands in a Dirac system	133
5.1 Introduction	135
5.2 Preliminaries	137
5.3 Results and Discussion	146
5.4 Conclusions	155
5.5 Acknowledgements	156
5.A Integrals Involving the Pump Envelope	157
5.B Green's Function	158
5.C Gauge Choice	160
5.D Linearly Polarized Light	162
5.E Circularly Polarized Light	163
6 Conclusions	169
6.1 Summary of this Thesis	169
6.2 Future Directions	171

List of Figures

1.1	Edge channels in a two-terminal conduction set-up in a 2D topological insulator. . .	10
2.1	Schematic picture of our linearized bands. The different horizontal lines correspond to values of the chemical potential creating a single Fermi surface (μ_A) and to two Fermi surfaces (μ_B and μ_C).	35
2.2	Plot of the integral $v(m_z) = v_{-1,-1}(m_z)$ as a function of A . Above we have set $B = 0$, $M = -0.3t$ and $\mu = 0$. We note that for the range of parameters chosen the $m_z = -2$ channel is by far the most negative channel.	37
2.3	Diagrams contributing to the renormalization of the BCS coupling function up to one-loop.	45
3.1	The two device geometries considered in this work. Left is a two-terminal device labeled with leads left ('L'), and right ('R'). On the right is a six terminal device labeled with leads 1 through 6 . The sites coupled to leads have a solid rectangle around them.	69
3.2	Plots of the differential two-terminal conductivity as a function of V_{ext} . Left: results for various disorder strengths, right: various values of the system size (L) and the lead coupling parameter (Γ).	71
3.3	Disorder averaged summed conductivity, Eq. (3.4.1). The inset shows a zoomed in picture of the first area of conductivity quantization. Note some error bars in the insets are too small to see.	75
4.1	Two geometries considered in this work. On the left we have the two-terminal set-up with a bias voltage V/e offsetting the two Fermi energies ϵ_L and ϵ_R . On the right we have the six terminal set-up with a current I being driven between leads 1 and 4	104

- 4.2 Two terminal conductivity in units of e^2/h . The left shows the conductivity at $E = \Omega/2$ in a two terminal set up as a function of external potential strength for various disorder strengths W and system size $L = 20$. The right is the conductivity for various values of the system size, L , and the lead coupling parameter Γ over a region where edge states are present. 105
- 4.3 Quasi-energy spectrum of a topologically trivial sample at different driving amplitudes in a semi-infinite cylindrical geometry. The left plot is for $V_{ext} = 0.1|M|$, the middle $V_{ext} = 0.3|M|$, and the right $V_{ext} = 0.9|M|$ 106
- 4.4 Results for disorder averaged summed conductivity, *i.e.* Eq. (4.4.4) in the text, with $M = -1$ and $E = \Omega/2$ and in units of e^2/h for various disorder strengths W . The inset shows a zoomed in picture of the first area of conductivity quantization. The disorder plots are constructed by averaging over 40 randomly drawn collection of disorder potentials while the error bars represent one standard deviation of this data. Note some error bars in the insets are too small to see. This data has been obtained from a calculation on a 20×20 lattice. 110
- 5.1 Schematic picture of the main results of this paper. The original Dirac cone is split into sidebands, with sidebands further away from the original cone receiving less "weight". In the figure this is signified using lighter colours for less probable sidebands. Now, if the operator describing the time periodic field, $V(t)$, commutes with the original Hamiltonian, $H_{\mathbf{k}}(t)$, then this splitting is all that happens. If these two operators do not commute sidebands hybridize and the band structure becomes modified by, e.g., having gaps opened. 140
- 5.2 Comparison of numerical results found by integrating the time dependent Dirac equation and the analytic approximation in Eq. (5.3.6) for $I(k_x, 0, \omega, t_{\mathcal{O}})$. The left plots $I(0, 0, \omega, t_{\mathcal{O}})$ for different delay times $t_{\mathcal{O}}$ while the right plots $I(0.05\text{\AA}^{-1}, 0, \omega, t_{\mathcal{O}})$ also for different delay times. In these plots the bottom plot is for $t_{\mathcal{O}} = -500\text{fs}$, the middle for $t_{\mathcal{O}} = -100\text{fs}$ and the top is for $t_{\mathcal{O}} = 0\text{fs}$. In all plots the solid line is the approximation in Eq. (5.3.6) while the circles are numerical results. There is excellent agreement between the numerics and our approximation for all three delay times. 142
- 5.3 Plot of the photocurrent $I(k_x, 0, \omega, t_{\mathcal{O}})$ at various values of the delay time $t_{\mathcal{O}}$ for linearly polarized light. In the distant past we see only the Dirac cone, as the pump field starts to turn on we see copies of this cone (sidebands) begin to develop. As the field envelope becomes larger weight of the original Dirac cone is shifted into other sidebands. 147
- 5.4 Plot of the photocurrent $I(0, k_y, \omega, t_{\mathcal{O}})$ at various values of the delay time $t_{\mathcal{O}}$ for linearly polarized light. In the distant past we again only see the Dirac cone, as the pump field starts to turn on we see copies of this cone (sidebands) begin to develop and these copies develop avoided crossings. As the field becomes fully turned on the weight of the original Dirac cone is shifted into other sidebands and these gaps become more evident. 147

-
- 5.5 Comparison of numerical results found by integrating the time dependent Dirac equation and the analytic approximation in Eq. (5.3.15) for $I(0, 0, \omega, t_{\mathcal{O}})$. The left shows $I(0, 0, \omega, t_{\mathcal{O}})$ for different delay times $t_{\mathcal{O}}$ while the right shows $I(0, 0, \omega, t_{\mathcal{O}})$ also for different delay times but this time with a pulse FWHM of 500fs instead of 250fs. In these plots the bottom plot is for $t_{\mathcal{O}} = -500$ fs, the middle for $t_{\mathcal{O}} = -100$ fs and the top is for $t_{\mathcal{O}} = 0$ fs. In all plots the solid line is the approximation in Eq. (5.3.15) while the circles are numerical results. On the top row we see reasonable agreement between numerics and our approximation for all three delay times. When we turn up the pulse width, which effectively makes the "turn-on" time slower, we see that the agreement becomes excellent. 151
- 5.6 Plot of the photocurrent $I(k_x, 0, \omega, t_{\mathcal{O}})$ at various values of the delay time $t_{\mathcal{O}}$ for circularly polarized light. In the distant past we see only the Dirac cone, as the pump field starts to turn on we see copies of this cone (sidebands) begin to develop and the Dirac cone becomes gapped out. At $t_{\mathcal{O}} = 0$ we can plainly see only two sidebands through the cut $k_x = 0$ 151

Introduction

1.1 Topological States of Matter

The last several years of research in the field of condensed matter physics have seen rapid expansion in, and unrelenting excitement about, topological states of matter. This enthusiasm is rooted not only in the important potential applications of these states, but also in the deep shift in our fundamental understanding of matter that they represent. This thesis contains a collection of manuscripts that all share the common goal of creating and manipulating topological states of matter through the use of applied fields.

As stated above, topological phases of matter represent a paradigm shift in our understanding of states of matter. This is rooted in the fact that until recently it was believed that all quantum states of matter could be classified using the principle of spontaneous symmetry breaking[1]. As an example of this classification scheme, consider a crystalline solid. The solid is made up of atomic centers whose interactions are translational invariant. Nonetheless, the solid breaks this translational symmetry; its atomic centers occupy fixed points in space.

The paradigm of classifying a quantum state of matter only in terms of its spontaneously

broken symmetries has recently been disrupted. Physicists have begun to appreciate that two states with the same broken symmetry properties can have significantly different physical properties. These differences can be understood by allowing for another distinguishing characteristic between the states, their topology.

The notion of topological classification is borrowed from mathematics. Mathematicians originally introduced the concept of topological invariance to classify different geometrical objects into broad categories. The simplest example of this scheme is 2D surfaces. These surfaces are classified by the number of holes in them, a measure called the genus of the surface. Surfaces that can be transformed into one another without creating new holes are said to be topologically equivalent. This leads to the famous example that a coffee cup is topologically equivalent to a doughnut; these two surfaces can be smoothly deformed into one another without creating any new holes.

In order to understand the topological classification of quantum states of matter one must generalize the concepts of a smooth deformation and therefore what it means to create holes. Systems that can be connected to one another without creating holes can then be said to belong to the same topological class.

In a quantum system these concepts are defined in relation to the Hamiltonian. In a many-particle system we consider a Hamiltonian with an energy gap separating the ground state and the excited states. The available deformations are then all of the ways in which we can change this Hamiltonian. The analogue of creating a hole is closing the energy gap in this Hamiltonian. Smooth deformations are then all of the changes that we can make to the Hamiltonian that do not close the energy gap. In this way two quantum mechanical states that are connected through changes to the Hamiltonian that leave the gap intact are said to be topologically equivalent [2, 3]. The above understanding leads to the conclusion that two states of matter that both spontaneously break the same symmetries can still be topologically distinct and therefore have different properties. This is possible if the two

states have Hamiltonians that are not connected through smooth deformations.

The implication of a state's topology are most profound when studying its boundary. When two states in a different topological class are put in contact with one another nature must find a way to accommodate for the change in topology in moving from one state to another. This is done by closing the quantum mechanical gap only on the boundary between the systems, giving rise to edge or surface states whose energies lie within the (bulk) gap of the system. Depending on the system of interest, these edge-states can have very rich physical properties. One ubiquitous property is their robustness. These states exist because of a difference in topology between two systems. As long as this difference in topology exists the states will persist. The difference in topology will of course be maintained so long as only smooth deformations are made to the Hamiltonians of the respective systems. Therefore making changes to the system of interest (e.g. adding disorder or applying a field) will not destroy the edge states unless these changes are drastic enough to close the gap in the system.

It has become common to call certain states topological states of matter. In keeping with the discussion above, this designation can be thought of as being short-hand for states that belong to a different topological class than the vacuum. Thus the natural boundary of the materials in these states play host to interesting edge physics.

Topological states of matter come in several flavours depending on how they are related to their trivial counterparts[4]. Topological states that are only different from their trivial counterpart because a symmetry that forbids deformations that would change the topological system into the trivial system are called symmetry-protected topological states. Such states will be the focus of this work. Specifically, this thesis will be concerned with two such topological materials: topological superconductors, protected by particle-hole symmetry, and topological insulators, protected by time-reversal symmetry. The following two sections will introduce the key features of these states, outline present challenges and

discuss the problems addressed in this thesis.

1.2 Externally Induced Topological Superconductivity

The first topological state this thesis will focus on will be a topological superconductor. As discussed in the previous section, this topological state will play host to edge-states. In the case of a topological superconductor these edge-states are very special, as they are predicted to be Majorana modes.

To understand why Majorana modes are special we must first make a brief digression into the field of particle physics, and in particular the Dirac equation. Complex valued solutions to Dirac's equation provide a description of relativistic, spin- $\frac{1}{2}$ particles, such as electrons and protons. These complex valued solutions provide a description of particles that have unique anti-particles.

Shortly after Dirac proposed his now famous relativistic wave-equation an Italian physicist known as Ettore Majorana proposed a modification to the Dirac equation which would lead to purely real solutions [5]. These real valued solutions, since termed Majorana fermions, have the novel property that they describe spin-1/2 particles (i.e. fermions) that are their own anti-particles. After Majorana published his findings in 1937, experimentalists became interested in the possible existence of a Majorana fermion and began searching for a fundamental particle having these unique properties. Despite these effort, all fundamental fermions discovered to date (perhaps excepting the neutrino) have had unique anti-particles.

In addition to being elusive and fundamentally interesting, Majorana fermions are of interest for more practical reasons. In a condensed matter context the analogue of these particles may be created as quasiparticle excitations, these quasiparticles can then bind to a defect at zero energy to create an object known as a Majorana mode. These Majorana

rana modes are expected to belong to a group of particles known as non-abelian anyons[6, 7]. Non-abelian anyons have non-trivial exchange statistics; the exchange of two of these particles changes the ground state of the system by more than just a phase. Moreover, the exchange of non-abelian anyons is non-commutative. Owing to these properties, non-abelian anyons (e.g. Majorana modes) are largely believed to be important components in the design of quantum computers; as the exchange of these particles can be used to store information in a many-body system [7].

Moving back towards topological superconductors, these materials are believed to be a promising route for realizing Majorana modes. This is because in superconductors Gauge symmetry is spontaneously broken and as a result particle number is not conserved. In such a system the fundamental excitations of interest are a superposition of particles and holes. In condensed matter systems, holes can be thought of as antiparticles and therefore the excitations in a superconductor are a superposition of particles and anti-particles. One can imagine that an equal superposition of particle and hole would then result in a particle that is its own antiparticle, and therefore potentially a Majorana fermion and eventually a Majorana mode.

Unfortunately typical superconductors, i.e. spin-singlet superconductors, are described by a superposition of electrons and holes with *opposite* spin and therefore do not provide the proper superposition to constitute a Majorana fermion. The proper conditions for this superposition are met in a topological, spin-triplet $p_x + ip_y$ superconductor. Alas, with a few unverified exceptions[8], there are currently no naturally occurring materials with topological p -wave pairing. Nonetheless, many proposals have focused on indirect routes to creating this important type of pairing [9–18]. Understanding these proposals will be the prerequisite to the first manuscript in this thesis.

The pioneering proposal for how one can create an effective $p+ip$ -wave superconductor was made by Fu and Kane[9]. Their proposal showed that a three dimensional topologi-

cal insulator placed near a conventional s -wave superconductor will develop topological superconductivity. One can understand this phenomenon at a high level by realizing that the topological insulator already has non-trivial topology, and the pairing necessary for superconductivity is induced by its proximity to the superconductor.

The proposal of Fu and Kane has been continually refined by several groups [12–18]. The most relevant for understanding the work in this thesis are the proposals of Sau, Lutchyn, Tewari [10] and Das Sarma, and also the work of Alicea [11]. Sau and coworkers envisioned a two-dimensional electron gas (2DEG) with Rashba spin-orbit coupling. They then imagined connecting one side of this system to a ferromagnetic insulator and the other to a conventional s -wave superconductor. The combination of these three puzzle pieces creates a topological p -wave superconductor without the need for the potentially difficult to work with topological insulator involved in the original proposal of Fu and Kane.

Shortly after the work of Sau *et al*, Alicea set out to further simplify this set-up[11]. The main success of Alicea’s work was the elimination of the ferromagnetic insulating layer in favour of an external, and therefore tunable, magnetic field. This was accomplished by considering a 2DEG with a mix of Dresselhaus and Rashba spin-orbit coupling.

The ability to add tunability to a potentially topological system is one of the two main themes of this thesis. In the case of topological superconductors our main inspiration comes from Alicea’s work. The principle goal of the first manuscript in this thesis will be to further simplify the process of inducing a p -wave superconductor.

The key features of creating an effective topological state in the proposals discussed in the last several paragraphs is the proper combination of spin-orbit coupling and Zeeman field. We are interested in determining if the need for the superconducting layer can be alleviated by allowing for the spin-orbit coupled, two-dimensional electrons to interact with each other. The motivation for this work is to find a material that is either a trivial superconductor or in some other phase to start with. The hope is then that by properly

applying a Zeeman field (either via a magnetic field or some other effective means) we can induce a topological superconducting phase.

The groundwork for this problem has been laid in a collection of preliminary papers written during the author's Master of Science study[19–21]. These preliminary studies take a relatively simple approach to the problem in order to establish proof-of-principle. The manuscript presented in Chapter 2 of this thesis should be considered a rigorous and culminating work on this problem. It reviews these earlier studies as well as providing a detailed description of the proposals for topological superconductivity surveyed at a high level in this introduction. It then dives deep into the problem of interest by analyzing the system from a Renormalization Group point of view. This analysis concludes that topological superconductivity induced by an applied field is possible in a system with interaction driven superconductivity. Such a set-up represents the opportunity to drive and manipulate a topological state with an externally applied mechanism without the need for the additional superconducting layer.

The study of topological superconductivity outlined above constitutes the first part of this thesis. The second part will focus on the driving and manipulation of a topological insulator (TI). Here our drive of interest will be a time-periodic perturbation, typically assumed to be electromagnetic radiation. The two main experimental tools that have historically been used to probe topological insulators are transport measurements and angle-resolved photoemission spectroscopy (ARPES). We study how the expected results of both of these methods change in the presence of time-periodic modulations. A more detailed introduction to this system will be the central point of the next section.

1.3 Non-equilibrium Topological Insulators

1.3.1 Introduction

The beginning of the story of topological insulators can probably be placed at the discovery of the quantum Hall effect (QHE) in 1980[22]. A quantum Hall state is realized in a 2DEG with an applied magnetic field. In the quantum Hall state the bulk of the two-dimensional system is insulating, but nonetheless the edge plays host to a unidirectional current. This unidirectional current is topologically protected (see the first section of this introduction) and gives rise to a precise quantization of the Hall conductance in the sample[23, 24].

In the two decades following the discovery of the QHE a great deal of effort was put into finding a new state of matter with similar conduction properties to the QHE, but without the presence of the applied magnetic field, i.e. a system with time-reversal (TR) invariance [25–28]. This search ultimately led to the discovery of topological insulators.

In a topological insulator time-reversal invariance is maintained and so there is no applied magnetic field. An essential component in topological insulators (at least up until the time of writing) has been the role of spin-orbit coupling (SOC). Spin-orbit coupling can be thought of as playing the same role as the applied field in the QHE. The crucial difference in a TI is that the effective magnetic field felt by electrons in the presence of SOC has a different direction depending on the spin of the electrons. That is to say, if a spin-up electron sees an effective field in the z -direction, then a spin-down electron will see an effective field in the negative z -direction. This feature not only maintains TR-invariance, but also permits the transport properties of a TI to be thought about as two copies of a QH state. In these copies, spin-up electrons have a unidirectional flow in one direction while spin-down electrons flow in the opposite direction. This state is commonly called the spin-QHE.

The discussion so far has been focused on 2D systems, however three dimensional generalizations of topological insulators also exist[29, 30]. Both 2D and 3D TIs demonstrate

Dirac-like, in-gap, spectra along their edges. Depending on the dimensionality of the TI, there are different experimental signatures of the topological state that are easiest to observe experimentally. In a 2D system the topologically robust transport properties of the system are easiest to observe[31], meanwhile in a 3D dimensionality the spectral properties of the edge-states are the signature that is looked for. These experiments will be the central focus of the second part of this thesis and we will briefly outline them here before introducing the notion of driven topological insulators.

We will first focus on the transport properties of topological insulators. Here we will give a general overview of these properties, a detailed description can be found in the excellent review article [2]. First, we will discuss two-terminal transport in these systems. This involves biasing the left and right edges of a sample relative to each other and measuring the resulting conductance. In a TI the bulk is insulating and provided the bias lies in the bulk gap charge can only be carried by the edge modes. As discussed above, these edge modes amount to spin-up electrons circulating in one direction, while spin-down electrons circulate in the opposite direction, see Fig. 1.1. In the absence of magnetic impurities these edge states do not interact with each other and therefore amount to two copies of 1D channels that carry charge from a source to a drain. Each 1D edge channel comes with a conductance of e^2/h and so TIs are expected to have a two-terminal conductance of $2e^2/h$ [2, 26]. This robust conductance signature has been measured for a 2D TI[31].

To close this subsection we will quickly discuss a second experimental confirmation of the properties found in topological insulators. This signature comes from ARPES experiments conducted on 3D TIs. ARPES experiments have been able to confirm the 3D in-gap, Dirac cone structure of the surface states in these materials [30].

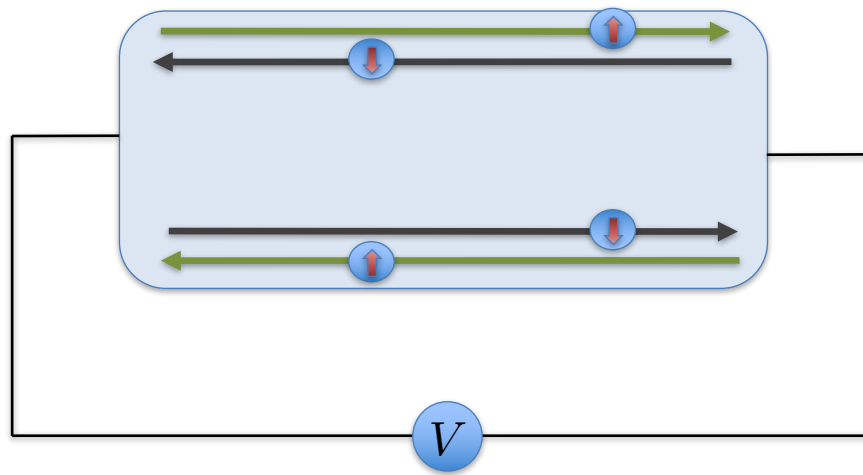


Figure 1.1: Edge channels in a two-terminal conduction set-up in a 2D topological insulator.

1.3.2 Floquet Topological Insulators

Despite the numerous experimental successes surrounding the discovery of TIs, there are still numerous challenges surrounding these materials. One of the central challenges involves isolating a TI. Finding a material with the correct properties to support a topological band-structure relies to a great degree on good fortune. The tunability of these devices, both in the sense of creating the topological state and manipulating it, remains an experimental hurdle.

In addition, the topological states of matter discussed so far have been limited to time-independent, or equilibrium, systems. An interesting question is how the topological properties of the system will behave in a time-dependent scenario. One can imagine both trying to understand how these topological properties can be manipulated using a time-dependent perturbation, and also if the time-dependent perturbation can be used to create new topological properties of the system.

In an effort to begin to explore both of the avenues outlined above, the group of Refael *et al* [32] proposed a way to start with a trivial (in the topological sense) material and drive this material into a topological state using a time-periodic external field. Topological

insulators created in this way have been named Floquet Topological Insulators (FTI).

This proposal to create a topological state using a time-periodic perturbation has great experimental potential. That fact notwithstanding, the manner in which the experimental signatures of a topological insulator generalize to a FTI must be established. This task is the focus of the second, third, and fourth manuscripts of this thesis.

In the second and third manuscripts we address the problem of transport in FTIs. We begin with an understanding of the transport behaviour of an equilibrium TI under a periodic perturbation. This involves generalizing a sum rule established previously in the context of a topological superconductor[33]. We then use this intuition, and sum rule, to build an understanding of transport in a FTI. In the end, we find that the time-periodic perturbation can be used to manipulate the signature two-terminal conductance of $2e^2/h$ to take on significantly smaller values. In spite of this reduction in the signature conductivity, we establish that by using a sum rule, which sums the conductance over several bias voltages, we can recover the signature conductivity value of $2e^2/h$.

The fourth manuscript of this work builds on the physical understanding established in manuscripts 2 and 3 in order to build a theory of ARPES in TIs in the presence of a time-periodic perturbation. With this work in place we are able to make connection to recent experimental time-resolve ARPES work[34].

1.4 Outline of this Thesis

The remainder of this manuscript based thesis is organized as follows. Chapter 2 contains a Renormalization Group Flow calculation in a spin-orbit coupled 2D system of interaction electrons. The focus of this study is to establish whether an applied Zeeman field can be used to drive and manipulate a topological superconducting state. Chapter 3 begins the second focus of this thesis, which is the use of electromagnetic radiation to drive and/or

manipulate a topological insulating state. Chapter 3 itself begins the first step of this study by delving into how a time-periodic perturbation may be used to manipulate the now famous transport properties of a 2D topological insulator. Chapter 4 continues this work, but shifts gears to a system where the topological state itself only exists because of the applied, time-periodic field. Chapter 5 remains focused on the manipulation of a topological insulator with applied electromagnetic radiation. Unlike the previous two chapters, this chapter focuses on 3D topological insulators. Chapter 5 explores how a time-periodic perturbation changes the edge-states of a 3D TI and makes connection with recent time-resolved ARPES experiments. Finally, Chapter 6 closes this thesis with a summary and concluding remarks.

Before moving on to the first manuscript of this thesis, some remarks on organization are in order. Each of the four manuscripts is written to be both self-contained but also to provide a natural progression in the theme of this work. In an effort to make the manuscripts self-contained, each work has its own bibliography and appendices. To aid in the flow of the thesis, each chapter contains a preface which sets the stage for the manuscript by providing context to the work, and by connecting it to preceding and proceeding chapters.

References

- ¹P. Anderson, Basic Notions of Condensed Matter Physics (Boulder, CO), 1997.
- ²X.-L. Qi and S.-C. Zhang, Rev. Mod. Phys. **83**, 1057–1110 (2011).
- ³S.-c. Zhang, Physics **1**, 6 (2008).
- ⁴A. M. Turner, A. Vishwanath, and C. O. Head, Topological Insulators **6**, 293 (2013).
- ⁵E. Majorana, Nuovo Cimento **5**, 171 (1937).
- ⁶M. Franz, Physics **3**, 24 (2010).
- ⁷C. Nayak, S. H. Simon, A. Stern, M. Freedman, and S. D. Sarma, Reviews of Modern Physics **80**, 1083 (2008).
- ⁸C. Kallin and A. Berlinsky, Journal of Physics: Condensed Matter **21**, 164210 (2009).
- ⁹L. Fu and C. L. Kane, Physical review letters **100**, 096407 (2008).
- ¹⁰J. D. Sau, R. M. Lutchyn, S. Tewari, and S. D. Sarma, Physical review letters **104**, 040502 (2010).
- ¹¹J. Alicea, Physical Review B **81**, 125318 (2010).
- ¹²A. Cook and M. Franz, Physical Review B **84**, 201105 (2011).
- ¹³Y. Tanaka, T. Yokoyama, and N. Nagaosa, Physical review letters **103**, 107002 (2009).
- ¹⁴R. M. Lutchyn, J. D. Sau, and S. D. Sarma, Physical review letters **105**, 077001 (2010).
- ¹⁵Y. Oreg, G. Refael, and F. von Oppen, Physical review letters **105**, 177002 (2010).
- ¹⁶J. Klinovaja, S. Gangadharaiyah, and D. Loss, Physical review letters **108**, 196804 (2012).
- ¹⁷L. Fu and E. Berg, Physical review letters **105**, 097001 (2010).
- ¹⁸S. Tewari, T. D. Stanescu, J. D. Sau, and S. D. Sarma, New Journal of Physics **13**, 065004 (2011).

-
- ¹⁹A. Farrell and T. Pereg-Barnea, *Physical Review B* **87**, 214517 (2013).
- ²⁰A. Farrell and T. Pereg-Barnea, *Phys. Rev. B* **89**, 035112 (2014).
- ²¹A. Farrell, arXiv preprint arXiv:1308.3724 (2013).
- ²²K. v. Klitzing, G. Dorda, and M. Pepper, *Physical Review Letters* **45**, 494 (1980).
- ²³R. B. Laughlin, *Physical Review B* **23**, 5632 (1981).
- ²⁴D. Thouless, M. Kohmoto, M. Nightingale, and M. Den Nijs, *Physical Review Letters* **49**, 405 (1982).
- ²⁵F. D. M. Haldane, *Physical Review Letters* **61**, 2015 (1988).
- ²⁶B. A. Bernevig, T. L. Hughes, and S.-C. Zhang, *Science* **314**, 1757–1761 (2006).
- ²⁷C. L. Kane and E. J. Mele, *Physical review letters* **95**, 226801 (2005).
- ²⁸C. L. Kane and E. J. Mele, *Physical review letters* **95**, 146802 (2005).
- ²⁹J. E. Moore and L. Balents, *Physical Review B* **75**, 121306 (2007).
- ³⁰D. Hsieh, D. Qian, L. Wray, Y. Xia, Y. S. Hor, R. Cava, and M. Z. Hasan, *Nature* **452**, 970–974 (2008).
- ³¹M. König, H. Buhmann, L. W. Molenkamp, T. Hughes, C.-X. Liu, X.-L. Qi, and S.-C. Zhang, *Journal of the Physical Society of Japan* **77**, 031007 (2008).
- ³²N. H. Lindner, G. Refael, and V. Galitski, *Nature Physics* **7**, 490–495 (2011).
- ³³A. Kundu and B. Seradjeh, *Physical review letters* **111**, 136402 (2013).
- ³⁴Y. Wang, H. Steinberg, P. Jarillo-Herrero, and N. Gedik, *Science* **342**, 453–457 (2013).

Preface to Chapter 2

The first manuscript of this thesis is concerned with driving a topological superconducting state in a system of interacting, spin-orbit coupled electrons. This work builds on the previous work in [1] which was done in the mean field context. This opening manuscript employs renormalization group (RG) methods to provide a more rigorous treatment of the problem. This RG approach establishes that an externally applied Zeeman field may be used to drive, and manipulate, a topological superconducting state.

**Zeeman field induced non-trivial
topology in a spin-orbit coupled
superconductor**

Aaron Farrell¹ and T. Pereg-Barnea¹

¹Department of Physics and the Centre for Physics of Materials, McGill University, Montreal, Quebec, Canada H3A 2T8

This chapter has been published in Physical Review B. Journal Reference: Physical Review B 90, 144518 (2014)

Abstract

The hope to realize Majorana fermions at the vortex core of a two dimensional topological superconductor has led to a variety of proposals for devices which exhibit topological superconductivity. Many of these include superconductivity through the proximity effect and therefore require a layer of a conventional superconductor deposited on top of another system, which lends its topological properties. The necessity of the superconducting layer poses some technical complications and, in particular, makes it harder to probe the Majorana state. In this work we propose to replace the proximity effect pairing by an innate tendency for pairing, mediated by interactions. We use a model system with spin orbit coupling and on-site repulsion and apply renormalization group to the interaction vertex. Without a Zeeman field this model exhibits pairing instabilities in different channels depending on the tuning of parameters. Once a Zeeman field is introduced the model favors topological superconductivity where the order parameter winds an odd number of times around the Fermi surface. This suggests that certain superconductors, with strong spin-orbit coupling, may go through a topological phase transition as a function of applied magnetic field.

2.1 Introduction

Majorana fermions, interesting in their own right, are desirable components of topological, fault tolerant, quantum computations. In order to perform such computations it is necessary to move Majorana fermions and in particular exchange their position in a braiding fashion. While it is probably easiest to achieve Majorana fermions in one dimensional systems[2–4], controlling their motion seems more natural in two dimensions. This reason and others inspire the search for two dimensional topological superconductors which are known to support Majorana fermions at their vortex cores[5, 6].

Some of the prominent ideas for two dimensional topological superconductivity include a multi-layer heterostructure[7–14]. In the proposed structures one or more layers provide the topological properties, i.e, a winding of the electron spin around the Brillouin zone while another layer provides the tendency for pairing through the proximity effect. For example, in a heterostructure of spin-orbit coupled semiconductors in proximity to a simple s -wave superconductor topological superconductivity arises as the pairing gap inherits the winding of the spins and forms a $p_x + ip_y$ state. Besides SOC and pairing, a key ingredient in the above proposal is a Zeeman field. The importance of the Zeeman field is in ensuring that only one Fermi surface with spin-momentum locking participates in the pairing. Without the Zeeman field there are two spin-orbit coupled bands with opposite spin chirality in each energy. This leads to an overall cancelation of the topology which is manifested in a trivial Z_2 invariant.

Inspired by the above proposals we set out to answer the following question. Can the combined effect of spin-orbit coupling and electron-electron interaction lead to topological superconductivity? Our study suggests that the answer is affirmative with the help of a Zeeman field. Similarly to the semiconductor proposals, in our system the Zeeman field ensures that only one spin orbit coupled band is paired, producing a topological superconductor. We therefore speculate that there may exist a spin-orbit coupled superconductor

whose topology is trivial due to the multiplicity of Fermi surfaces[15, 16]. This superconductor can be rendered topological by the application of a magnetic field. Of course one may worry that the magnetic field has an orbital effect which ultimately leads to the suppression of superconductivity. We therefore look at interaction driven superconductors which has the potential for a high critical field such that a topological superconductor phase may appear *before* superconductivity is completely turned off.

The model we use is an extension of the Hubbard model on the square lattice with Rashba spin orbit coupling (SOC). Without SOC this model leads to a d -wave superconductor when treated in the strong coupling limit away from half filling[17–19]. In the presence of SOC coupling there are various phases depending on parameters. While we have recently analyzed a similar model in weak[1] and strong coupling[20], in this paper we focus on its continuum analogue and find the possible pairing channels in an RG analysis. We find that when the Fermi level cuts only one of the spin-orbit coupled bands the interaction induces topological superconductivity. This superconductor is of either f -wave or p -wave symmetry, depending on the direction of the Zeeman field relative to the spin winding. This type of pairing comes about as a combination of two effects. Without SOC the preferred channel of pairing is a spin-singlet d -wave. The SOC couples the two spin directions and produces two bands in which the spin winds by 2π as one encircles the Brillouin zone mid point. This winding is superimposed on the $\pm 4\pi$ phase winding of the d -wave order parameter and leads to either a 2π (p -wave) or a 6π (f -wave) winding of the order parameter as seen by the band electrons. Our renormalization group analysis shows that the above topological channels are dominant when there is a single Fermi surface.

This paper is laid out as follows. In Section 2.2 we discuss and review past heterostructure devices. In particular, we highlight the necessity for a description of the problem in a band basis. In this case the wave function of Cooper pairs is a mixture of singlet and triplet pairing[21]. This section aims to frame the results we present in relation to the current

literature on this problem. It also gives an overview of our main results. Section 2.3 defines the model we study and reviews the basics of the RG method we will employ. We then begin discussing our results in Section 2.4 by first looking at the general problem and then specializing to systems with a single Fermi surface. After finding the potential for topological superconductivity in Section 2.4 we follow up in Section 2.5 by developing a simple mean-field model from our RG results and showing that for the correct combinations of parameters we get a topological superconductor. We close the main text in Section 2.6 with some concluding remarks. A detailed appendix gives an overview of more technical details of our RG analysis.

2.2 Preliminary Discussion

2.2.1 Superconductivity with lifted spin degeneracy

As discussed in the introduction the goal of this paper is to address interaction driven superconductivity in a system of spin-orbit coupled electrons. We would first like to acquaint the reader with superconductivity in systems with a “lifted spin degeneracy”. Without spin-orbit coupling (and Zeeman field) the model we will use in this work simplifies to a tight binding model with spin-degenerate bands. Such a dispersion is typical in the studies of superconductivity with which most readers are familiar. In this case it is natural to discuss the formulation of Cooper pairs in singlet or triplet spin configurations.

Once spin-orbit coupling is introduced the two-fold spin-degeneracy of the bands is lifted and singlet and triplet pairings become mixed in the wave function of the Cooper pairs[21]. Put another way, once spin-orbit coupling is considered the z projection of the electron spins is no longer a good quantum number. Instead we are left with what will be referred to as a band index. We can then see Cooper pairs form between two electrons in the same band (intra-band pairing) or between electrons in different bands (inter-band

pairing). These two types of pairs can, of course, be thought of as superpositions of the more traditional singlet and triplet pairs.

A clear illustration of this was given by Alicea in Ref. [8]. If one considers a system of spin-orbit coupled electrons, in this case a quantum well system, placed in proximity to an s -wave (singlet) superconductor an interpretation of such a system in terms of interband and intraband pairs is as follows. Proximity effect *forces* the electrons to pair in a spin-singlet state, symbolically we can think of this as adding a term $\Delta_0 \int d\mathbf{k} \left(\psi_{\uparrow}^{\dagger}(\mathbf{k})\psi_{\downarrow}^{\dagger}(-\mathbf{k}) + \text{h.c.} \right)$ to the Hamiltonian. However, in the quantum well the states (\mathbf{k}, σ) (where $\sigma = \uparrow$ or \downarrow) are no longer good states and one must instead describe the system in a “band” basis. Quantitatively this amounts to transforming the operators $\psi_{\sigma}^{\dagger}(\mathbf{k})$ into operators creating/destroying electrons in each band which we denote as $\psi_{\pm}(\mathbf{k})$. Carrying out this transformation the superconducting contribution to the Hamiltonian becomes (schematically)

$$H_{SC} = \int d\mathbf{k} (\Delta_{++}(\mathbf{k})\psi_{+}^{\dagger}(\mathbf{k})\psi_{+}^{\dagger}(-\mathbf{k}) + \Delta_{--}(\mathbf{k})\psi_{-}^{\dagger}(\mathbf{k})\psi_{-}^{\dagger}(-\mathbf{k}) + \Delta_{+-}(\mathbf{k})\psi_{+}^{\dagger}(\mathbf{k})\psi_{-}^{\dagger}(-\mathbf{k}) + \text{h.c.}) \quad (2.2.1)$$

The functions $\Delta_{++}(\mathbf{k})$, $\Delta_{--}(\mathbf{k})$, and $\Delta_{+-}(\mathbf{k})$ play the role of the superconducting order parameter for, respectively, intraband pairing between two electrons in the upper band, two electrons in the lower band, and inter band pairing between one electron in the upper band and one in the lower band.

One additional, important observation when dealing with superconductivity with lifted spin degeneracy is that the symmetry of the pairing in the spin basis is not generally the same as the symmetry in the band basis. For the example above, Alicea begins with a system that has simple s -wave pairing in the spin basis; however, this pairing drives band Cooper pairs to form with the order parameters $\Delta_{++}(\mathbf{k})$, $\Delta_{--}(\mathbf{k})$, and $\Delta_{+-}(\mathbf{k})$ which are non-trivial functions of \mathbf{k} . In particular, $\Delta_{++}(\mathbf{k})$ and $\Delta_{--}(\mathbf{k})$ are odd under $\mathbf{k} \rightarrow -\mathbf{k}$ while

$\Delta_{+-}(\mathbf{k})$ is even.

2.2.2 Spinless p -wave Pairing in the band basis

Superconductivity with $p \pm ip$ pairing is highly desirable as it is the canonical example of a topological superconductor[5]. The example above can be argued to be a spinless $p - ip$ superconductor. In order to review this argument let us first quickly review the band structure of these systems. One begins with two, spin degenerate, quadratic bands. When spin-orbit coupling is added these bands are split and the degeneracy is lifted. If the bands are parabolic they cross at $\mathbf{k} = 0$. When a Zeeman field is applied the crossing is avoided and a gap is opened around $\mathbf{k} = 0$. Therefore, for any energy within this $\mathbf{k} = 0$ gap there is a single circular contour of constant energy on which the spin is locked to the momentum direction. Please note that when we discuss a Zeeman field opening a gap in the rest of this paper we are referring to this scenario. An example of this type of band structure can be seen in Fig. 2.1. If the chemical potential of the system is tuned so that the Fermi surface lies in this gap, and superconductivity is not strong enough to induce transitions between bands (through $\Delta_{+-}(\mathbf{k})$) then the upper band of the problem plays no role and can be projected out. This leaves only a Hamiltonian

$$H_{eff} = \int d\mathbf{k} (\epsilon_{-}(\mathbf{k}) \psi_{-}^{\dagger}(\mathbf{k}) \psi_{-}(\mathbf{k}) + \Delta_{--}(\mathbf{k}) \psi_{-}^{\dagger}(\mathbf{k}) \psi_{-}^{\dagger}(-\mathbf{k}) + \Delta_{--}^{*}(\mathbf{k}) \psi_{-}(-\mathbf{k}) \psi_{-}(\mathbf{k})) \quad (2.2.2)$$

where $\epsilon_{-}(\mathbf{k})$ is some dispersion. This is exactly a spinless $p - ip$ superconductor.

While the above idea was proposed for a system with s -wave pairing the same principle can be applied for other singlet superconductors. Of interest for the current work is that $d \pm id$ -wave singlet pairing leads to $f + if$ and $p - ip$ intraband pairing which are both topologically non-trivial[1, 22]. That is, as in the example of Alicea[8] above, one begins

with a $d \pm id$ -wave superconductor in the traditional sense. We can think of this schematically as a term in the Hamiltonian of the form $H_{SC}^{d-wave} = \left(\Delta_d(\mathbf{k}) \psi_{\uparrow}^{\dagger}(\mathbf{k}) \psi_{\downarrow}^{\dagger}(-\mathbf{k}) + \text{h.c.} \right)$ where $\Delta_d(\mathbf{k})$ has either $d + id$ or $d - id$ -wave symmetry. Once spin-orbit coupling is added the hamiltonian is no longer diagonal in the usual Nambu space and we should transform the states to describe them in the band basis discussed above. Projecting onto a band basis yields a superconducting contribution of the form of Eq. (2.2.1). During this projection the phase $e^{\pm i\theta_{\mathbf{k}}}$ coming from the spin-orbit coupling is attached to the original $\Delta_d(\mathbf{k})$ to give $\Delta_{--}(\mathbf{k}) \sim e^{i\theta_{\mathbf{k}}} \Delta_d(\mathbf{k})$ and $\Delta_{++}(\mathbf{k}) \sim e^{-i\theta_{\mathbf{k}}} \Delta_d(\mathbf{k})$, meanwhile $\Delta_{+-}(\mathbf{k})$ is just proportional to $\Delta_d(\mathbf{k})$. Similar to the s -wave case, when the chemical potential lies in the gap one can focus on the lower energy band and the problem is mapped to a spinless superconductor with the sole order parameter $\Delta_{--}(\mathbf{k})$. If we begin with $d - id$ symmetry then $\Delta_{--}(\mathbf{k})$ will have $p - ip$ symmetry while beginning with $\Delta_d(\mathbf{k})$ being a $d + id$ -wave order parameter leads to a $\Delta_{--}(\mathbf{k})$ with symmetry $f + if$.

The approach taken in this paper, although highly motivated by the above discussion, works in the opposite direction. Instead of inducing pairing *via* proximity effect we look at driving pairing by interactions. Rather than forcing pairs to develop in, say, the s -wave singlet channel as the heterostructure devices above do, we utilize renormalization group methods to look at instability for pairing between band electrons. We focus on the topologically relevant band structure discussed above, that is not just a spin-orbit split band structure but one with a gap opened *via* a some sort of mass (Zeeman) term.

It has been shown in Refs. [15, 16] that spin-orbit coupling in an otherwise quadratic band structure leads to enhancement of superconductivity. These works find an instability towards pairing with the symmetry of the order parameter (or at least the dominant term) dependent on how the relative strength of the spin-orbit coupling and fermi energy are tuned. Here we follow a similar program but with the introduction of a mass term into the model. This term opens a gap between the spin-orbit split bands in the *non-interacting*

band structure and we focus on what happens when the chemical potential is tuned to lie in the gap. For this choice of parameters there is only a single Fermi surface and we find that the pairing that develops has either $p - ip$ or $f + if$ symmetry depending on the sign of the Zeeman mass term. In either case we expect the superconductivity that develops to be topological in nature, i.e., to support Majorana fermions in its vortex cores.

2.3 Model and Method

2.3.1 Model

Definition

Here we would like to introduce our model and the language of a band basis that the rest of this work will be framed in. Our initial focus is on the Hamiltonian studied in [1] and [20]:

$$H = H_1 + H_{int} \quad (2.3.1)$$

where $H_1 = H_{KE} + H_{SO}$ is a quadratic Hamiltonian and H_{int} contains interactions effects.

For H_1 we take the following model

$$H_1 = \sum_{\mathbf{k}, \alpha, \beta} c_{\mathbf{k}, \alpha}^\dagger (\xi_{\mathbf{k}} \delta_{\alpha, \beta} + \mathbf{d}_{\mathbf{k}} \cdot \vec{\sigma}_{\alpha, \beta}) c_{\mathbf{k}, \beta} \quad (2.3.2)$$

where $\xi_{\mathbf{k}} = \epsilon_{\mathbf{k}} - \tilde{\mu}$ with $\epsilon_{\mathbf{k}} = -2t(\cos(k_x) + \cos(k_y))$ and $\mathbf{d}_{\mathbf{k}} = (d_1(\mathbf{k}), d_2(\mathbf{k}), d_3(\mathbf{k})) = (A \sin k_x, A \sin k_y, 2B(\cos k_x + \cos k_y - 2) + M)$ where $t, A, B, M, \tilde{\mu}$ are material parameters giving the strength of the hopping amplitude, in plane spin-orbit coupling, out-of-plane spin-orbit coupling, Zeeman field and chemical potential respectively. Above $\vec{\sigma}$ is a vector of Pauli matrices and α and β are spin labels.

The model above has been chosen for the sake of versatility. We have discussed numer-

ous possible applications in past work[23], they include cold atomic systems with synthetic gauge fields, transition-metal oxides (*e.g.* pyrochlore iridates), quantum wells, and insulating oxide interfaces (*e.g.* the interface of LaAlO₃ and SrTiO₃). From this point of view the parameters A and B could come from traditional spin-orbit coupling such as Rashba or Dresselhaus, they could find their origins in systems like quantum wells[24], or they could be created in a cold atomic system. Further, the parameter M could also have numerous origins, here we outline only a few possible sources. An applied magnetic field is perhaps the most obvious choice. In this case one must be dealing with a system where orbital effects are small so as to minimize the suppression of superconductivity. Additionally, this Zeeman field may come from a band gap, which would be the case if we are dealing with quantum well like structures[24]. In the case of a band gap the orbital effects are avoided altogether. Finally, this term may come from proximity to a FM insulator, similar to heterostructure proposals in the past[9].

To account for interactions we take a simple on-site coulomb repulsion given by

$$\begin{aligned}
 H_{int} &= \sum_{\mathbf{k}_1, \mathbf{k}_2, \mathbf{k}_3, \mathbf{k}_4} \sum_{\alpha_1, \alpha_2, \alpha_3, \alpha_4} \delta_{\mathbf{k}_1 + \mathbf{k}_2, \mathbf{k}_3 + \mathbf{k}_4} \\
 &\times U_{\alpha_1, \alpha_2, \alpha_3, \alpha_4}(\mathbf{k}_1, \mathbf{k}_2, \mathbf{k}_3, \mathbf{k}_4) c_{\mathbf{k}_1, \alpha_1}^\dagger c_{\mathbf{k}_2, \alpha_2}^\dagger c_{\mathbf{k}_3, \alpha_3} c_{\mathbf{k}_4, \alpha_4}
 \end{aligned} \tag{2.3.3}$$

where

$$\begin{aligned}
 U_{\alpha_1, \alpha_2, \alpha_3, \alpha_4}(\mathbf{k}_1, \mathbf{k}_2, \mathbf{k}_3, \mathbf{k}_4) &= \\
 \frac{U}{4N} (\sigma_{\alpha_1, \alpha_2}^x \delta_{\alpha_1, \alpha_4} \delta_{\alpha_2, \alpha_3} - \sigma_{\alpha_2, \alpha_1}^x \delta_{\alpha_2, \alpha_4} \delta_{\alpha_1, \alpha_3}) &.
 \end{aligned} \tag{2.3.4}$$

Note that it is enough to take a *repulsive* interaction since it leads to pairing in a strong coupling treatment (in contrast to Ref. [1] where near-neighbor attraction was introduced to mimic this effect in the weak coupling treatment).

Transformation to the Band Basis

We now diagonalize H_1 in order to recast our problem in terms of band electrons. This is done by making the unitary transformation

$$\begin{pmatrix} c_{\mathbf{k},\uparrow} \\ c_{\mathbf{k},\downarrow} \end{pmatrix} = \begin{pmatrix} f_{+1}(\mathbf{k}) & f_{-1}(\mathbf{k}) \\ e^{i\theta_{\mathbf{k}}} f_{-1}(\mathbf{k}) & -e^{i\theta_{\mathbf{k}}} f_{+1}(\mathbf{k}) \end{pmatrix} \begin{pmatrix} b_{\mathbf{k},+} \\ b_{\mathbf{k},-} \end{pmatrix} \quad (2.3.5)$$

where the $+1, -1$ label a band and we have defined the following

$$\begin{aligned} e^{i\theta_{\mathbf{k}}} &= \frac{d_1(\mathbf{k}) + id_2(\mathbf{k})}{\sqrt{d_1(\mathbf{k})^2 + d_2(\mathbf{k})^2}} \\ f_{\lambda}(\mathbf{k}) &= \sqrt{\frac{d + \lambda d_3}{2d}} \end{aligned} \quad (2.3.6)$$

where $\lambda = \pm 1$ and $d = |\mathbf{d}_{\mathbf{k}}|$. Written in the new basis,

$$H_1 = \sum_{\mathbf{k},\lambda} E_{\mathbf{k},\lambda} b_{\mathbf{k},\lambda}^{\dagger} b_{\mathbf{k},\lambda} \quad (2.3.7)$$

where $b_{\mathbf{k},\lambda}$ are annihilation operators in the band λ and $E_{\mathbf{k},\lambda} = \xi_{\mathbf{k}} + \lambda d$ labels the energy of the bands relative to the Fermi energy μ .

Before we move on to the RG calculations we express H_{int} in terms of band electrons. This requires some tedious manipulation which we defer to the Appendix. After some work we obtain:

$$\begin{aligned} H_{int} &= \sum_{\mathbf{k}_1, \mathbf{k}_2, \mathbf{k}_3, \mathbf{k}_4} \sum_{\lambda_1, \lambda_2, \lambda_3, \lambda_4} \delta_{\mathbf{k}_1 + \mathbf{k}_2, \mathbf{k}_3 + \mathbf{k}_4} \\ &\times W_{\lambda_4, \lambda_3, \lambda_2, \lambda_1}(\mathbf{k}_4, \mathbf{k}_3, \mathbf{k}_2, \mathbf{k}_1) b_{\mathbf{k}_4, \lambda_4}^{\dagger} b_{\mathbf{k}_3, \lambda_3}^{\dagger} b_{\mathbf{k}_2, \lambda_2} b_{\mathbf{k}_1, \lambda_1} \end{aligned} \quad (2.3.8)$$

where

$$\begin{aligned}
W_{\lambda_4, \lambda_3, \lambda_2, \lambda_1}(\mathbf{k}_4, \mathbf{k}_3, \mathbf{k}_2, \mathbf{k}_1) &= -\frac{U}{4N} w_{\lambda_4, \lambda_3}(\mathbf{k}_4, \mathbf{k}_3) \\
&\times w_{\lambda_2, \lambda_1}^*(\mathbf{k}_2, \mathbf{k}_1)
\end{aligned} \tag{2.3.9}$$

where $w_{\lambda_i, \lambda_j}(\mathbf{k}_i, \mathbf{k}_j) = \lambda_i e^{-i\theta_{\mathbf{k}_i}} F_{j,i} - \lambda_j e^{-i\theta_{\mathbf{k}_j}} F_{i,j}$ with $F_{i,j} = f_{\lambda_i}(\mathbf{k}_i) f_{-\lambda_j}(\mathbf{k}_j)$. We see that in the band basis electrons in bands λ_2 and λ_1 can scatter to bands λ_3 and λ_4 , that is to say there is no ‘‘band conserving condition’’. The δ -function ensures that the momentum is conserved.

Partition Function

We can now recast our model in the language of coherent state path integral. First we define the quadratic part of the action as

$$S_0 = \int_0^\beta d\tau \sum_{\mathbf{k}, \lambda} b_{\mathbf{k}, \lambda}^*(\tau) \left(\frac{\partial}{\partial \tau} + E_{\mathbf{k}, \lambda} \right) b_{\mathbf{k}, \lambda}(\tau) \tag{2.3.10}$$

with Grassman variables $b_{\mathbf{k}, \lambda}^*(\tau)$ and $b_{\mathbf{k}, \lambda}(\tau)$ and inverse temperature β . The interaction part is:

$$S_{int} = \sum_{1,2,3,4} V(4, 3, 2, 1) b^*(4) b^*(3) b(2) b(1) \tag{2.3.11}$$

where we simplified the notation by defining $i = (\lambda_i, \mathbf{k}_i, \tau_i)$ and

$$\begin{aligned}
V(4, 3, 2, 1) &= -\frac{U}{4N} \int_0^\beta d\tau \left(\prod_{j=1}^4 \delta(\tau - \tau_j) \right) \delta_{\mathbf{k}_1 + \mathbf{k}_2, \mathbf{k}_3 + \mathbf{k}_4} \\
&\times w_{\lambda_4, \lambda_3}(\mathbf{k}_4, \mathbf{k}_3) w_{\lambda_2, \lambda_1}^*(\mathbf{k}_2, \mathbf{k}_1).
\end{aligned} \tag{2.3.12}$$

The partition function is given by:

$$Z = \int \mathcal{D}(b_\lambda^*(\tau), b_\lambda(\tau)) e^{-S_0 - S_{int}} \quad (2.3.13)$$

2.3.2 Renormalization Group Approach

We now take the standard steps in finding the renormalization group flow of our model[25].

We begin by separating the Grassman variables into fast and slow modes:

$$\begin{aligned} b_{\mathbf{k},\lambda}(\tau) &= \theta(\Lambda/s - |E_{\mathbf{k},\lambda}|) b_{\mathbf{k},\lambda}^<(\tau) \\ &+ \theta(\Lambda - |E_{\mathbf{k},\lambda}|) \theta(|E_{\mathbf{k},\lambda}| - \Lambda/s) b_{\mathbf{k},\lambda}^>(\tau) \end{aligned} \quad (2.3.14)$$

where Λ is our energy cut-off and s is a flow-parameter. While fast and slow modes are decoupled in S_0 , they are coupled in S_{int}

$$S = S_0 + S_{int} = S_0(<) + S_0(>) + S_{int}(<, >) \quad (2.3.15)$$

Integrating over all of the fast modes gives

$$Z = \int \mathcal{D}(b_{<}, b_{<}^*) e^{-S_0(<) - S'_{int}(<)} \quad (2.3.16)$$

where $-S'_{int}(<) = \ln [\langle e^{-S_{int}(<, >)} \rangle_{0, >}]$ where the average is over fast modes with respect to $e^{-S_0(>)}$. We can obtain an approximation of S'_{int} by performing a cumulant expansion:

$$\begin{aligned} -S'_{int}(>) &= -\langle S_{int}(<, >) \rangle_{0, >} \\ &+ \frac{1}{2} (\langle S_{int}^2(<, >) \rangle_{0, >} - \langle S_{int}(<, >) \rangle_{0, >}^2) \\ &- \frac{1}{3!} \langle \langle S_{int}^3(<, >) \rangle \rangle_{0, >} + \frac{1}{4!} \langle \langle S_{int}^4(<, >) \rangle \rangle_{0, >} \end{aligned} \quad (2.3.17)$$

where the double angled brackets denote, respectively, the third and fourth order cumulants of S_{int} (with respect to $e^{-S_0(>)}$). Using the above perturbative expression we calculate a new effective interaction for the slow modes of the theory. We would like to point out that all of the results we derive are perturbative *only* in the interaction strength U , while t , A , B , M and $\tilde{\mu}$ are not assumed small in any way.

We use Feynman diagrams in order to evaluate the above expression[25]. The relevant Feynman rules are as follows:

- Each vertex diagram contains 4 external lines, two incoming and two outgoing. All other lines will be referred to as internal.
- Label every line with a momentum \mathbf{k} , a band index λ and a Matsubara frequency $i\omega_m$.
- For every internal line write a bare propagator $G_{\mathbf{k},\lambda}(i\omega_m) = \frac{1}{i\omega_m - E_{\mathbf{k},\lambda}}$.

- Every vertex in the diagram has a factor of
$$V_{\lambda_4,\lambda_3,\lambda_2,\lambda_1}(\mathbf{k}_4, \mathbf{k}_3, \mathbf{k}_2, \mathbf{k}_1) = -\frac{U(\lambda_4 e^{-i\theta\mathbf{k}_4} F_{3,4} - \lambda_3 e^{-i\theta\mathbf{k}_3} F_{4,3})(\lambda_2 e^{i\theta\mathbf{k}_2} F_{1,2} - \lambda_1 e^{i\theta\mathbf{k}_1} F_{2,1})}{4N}$$

where the numbers 1 through 4 *must* be assigned in the following way: For propagators coming into the vertex, the one from the left is 1 and the one from the right is 2, for propagators leaving the vertex the one to the left is 3 and to the right is 4.

- Conserve total momenta and frequency at each vertex.
- Sum over all internal frequencies $\frac{1}{\beta} \sum_{i\omega_m}$.
- Sum over all internal momenta, with the restriction that these are fast modes $\sum_{\mathbf{k},>}$.
- Sum over all internal band indices.
- Determine the overall multiplicative factor by multiplying by how many independent ways there are of drawing a specific diagram and for n^{th} order diagrams divide by $n!$.

- Multiply by the appropriate sign in the cumulant expansion and determine the sign coming from the contractions required to draw a given diagram

Once the above steps have been completed we have a *general* expansion. We focus on the “BCS” (pairing) channel by setting the incoming external momenta to $\pm\mathbf{k}'$ and band indices to λ' and the outgoing external momenta to $\pm\mathbf{k}$ and band indices to λ . We focus solely on the BCS pairing channel for several reasons. First, as mentioned before, we have studied the same model outlined above in a mean field context[1] and have found that there is an instability to superconductivity over much of parameter space. There is one exception to this where an antiferromagnet is found but only for larger B and large interaction strength. Second, in models similar to ours *without* spin-orbit coupling it is known[26] that for weak, repulsive interactions the Cooper instability is the only generic instability unless model parameters are fine-tuned. Finally, from a practical point of view our goal is to establish that topological superconductivity could possibly be driven by repulsive electron-electron interactions. Thus we focus only on this problem.

Further, here we are interested in only intraband pairing and so we set both incoming external band indices to λ' and the outgoing ones to λ . In mean-field this describes pairing between electrons in the same band index (intraband pairing) whereas setting band indices to $\pm\lambda$ on the incoming (or outgoing) electrons would represent interband pairing. We focus only on intraband pairing both because it is the interesting pairing from a topological standpoint and because we expect interband pairing to be suppressed relative to its interband counterpart. For example, for the BCS diagram (see the appendix of this paper) we find a relative suppression of $\left(\frac{M}{Ak_f}\right)^2$ when comparing interband pairing to intraband pairing. The calculation is also further simplified by only considering diagrams that contain logarithmic divergences as $s \rightarrow \infty$ [15, 16], as these dominate the vertex function.

2.4 Summary of RG Analysis

2.4.1 General Results

Here we discuss the results of our analysis. We will only include details where it is absolutely essential; a full treatment and discussion of our analysis is included in the appendix. We have calculated diagrams up to fourth order in the interaction parameter U and with logarithmic divergences for our lattice model. The need to go to 3-loops in our calculation is rooted in the flow the interaction channels. Our goal is to find a pairing instability in this system, we therefore look for couplings which flow to large negative values. At one-loop and at two-loop we find couplings that are only marginal, or marginally irrelevant[25]. It is not until 3-loop that we find marginally relevant flow, and therefore instability.

Although we have successfully obtained an expression of the renormalized interaction up to this order it is rather intractable to work with this form. In order to make analytic progress we take the continuum limit by replacing $\sin k_i \rightarrow k_i$, $\cos k_i \rightarrow 1 - k_i^2/2$. Taking the continuum limit not only makes our mathematical expressions analytically tractable but also makes the dispersion a function of $k = |\mathbf{k}|$ only, such that the contours of constant $E_{\mathbf{k},\lambda}$ are circular in \mathbf{k} -space. This enables two simplifications[16, 25]: (1) We can set all external momenta to lie on the Fermi surface (or Fermi surfaces) as any other external momenta correspond to processes that are irrelevant under RG flow and (2) due to the circular symmetry the coupling function in the BCS channel can be a function of $\phi = \theta_{\mathbf{k}} - \theta_{\mathbf{k}'}$ only.

When considering the BCS channel we can think of the RG procedure as renormalizing the interaction as $H_{int}^{eff} = \sum_{\mathbf{k}, \mathbf{k}', \lambda, \lambda'} V'_{\lambda, \lambda'}(\mathbf{k}, \mathbf{k}', s) c_{\mathbf{k}, \lambda}^\dagger c_{-\mathbf{k}, \lambda}^\dagger c_{-\mathbf{k}', \lambda'} c_{\mathbf{k}', \lambda'}$. In the continuum limit the interaction takes the form

$$V'_{\lambda, \lambda'}(\mathbf{k}, \mathbf{k}', s) \equiv V'_{\lambda, \lambda'}(\phi, s) = \frac{e^{i\phi}}{N} v'_{\lambda, \lambda'}(\phi, s) \quad (2.4.1)$$

Where we have used primed variables to distinguish renormalized parameters from the non-primed bare variables. The indices λ and λ' label the Fermi surface of the outgoing and incoming band electrons.

Using this symmetry of the coupling allows us to decouple the interaction into angular momentum channels:

$$\begin{aligned} v'_{\lambda,\lambda'}(\phi, s) &= \sum_{m_z} e^{im_z\phi} v'_{\lambda,\lambda'}(m_z, s) \\ v'_{\lambda,\lambda'}(m_z, s) &= \frac{1}{2\pi} \int_0^{2\pi} e^{-im_z\phi} v'_{\lambda,\lambda'}(\phi, s) \end{aligned} \quad (2.4.2)$$

We now address the question of how does the function $v'_{\lambda,\lambda'}(m_z, s)$ flow as the RG parameter s is tuned and calculate its beta-function. In our full expression for $v'_{\lambda,\lambda'}(m_z, s)$ (see the appendix of this paper) the matrix entries for different λ 's are coupled. Fortunately we can obtain a simple beta function by following a method proposed by Raghu *et al*[26] and further employed by Vafeek and Wang[15, 16]. To this end we define the g' matrix

$$g'_{\nu,\mu}(s, m_z) = \sqrt{N_\nu N_\mu} v'_{\nu,\mu}(s, m_z) \quad (2.4.3)$$

In this definition N_μ is the density of states at the Fermi energy for the band μ . We then obtain the following beta function for the eigenvalues of each g' -matrix

$$\frac{d\lambda_i^{m_z}(s)}{d \ln(s)} = -2(\lambda_i^{m_z}(s))^2 \quad (2.4.4)$$

where $\lambda_i^{m_z}(s)$ is the i^{th} eigenvalue of $g'_{\nu,\mu}(s, m_z)$. With the above beta-function,

$$\lambda_i^{m_z}(s) = \frac{\lambda_i^{m_z}(1)}{1 + 2\lambda_i^{m_z}(1) \ln(s)}. \quad (2.4.5)$$

From this solution we see that if $\lambda_i^{m_z}(1) < 0$ the renormalized coupling diverges at $s =$

$e^{-\frac{1}{2\lambda_i^{m_z}(1)}}$. Thus for any i or m_z , if $\lambda_i^{m_z}(1) < 0$ superconductivity will develop in this channel[16] with a superposition of intraband pairing given by the eigenvector corresponding to $\lambda_i^{m_z}(1)$. The temperature scale at which it will develop is given by the value of the lower cut-off Λ/s at which the above solution diverges, namely [15, 16, 26] $T_c \sim \Lambda e^{\frac{1}{2\lambda_i^{m_z}(1)}}$. Although this argument does not allow us to quantitatively determine T_c due to the lack of a proportionality constant, it does allow us to compare the transition temperatures of different channels (i and m_z) for a given set of parameters. The more negative the eigenvalue $\lambda_i^{m_z}(1)$ the higher T_c will be. Therefore we can think of $\lambda_i^{m_z}(1)$ as a measure of the instability of a particular channel. For a given set of parameters, the value of m_z and i with the most negative $\lambda_i^{m_z}(1)$ is the dominant superconductivity channel.

In addition to the above it is worth noting that our results, like those of Refs. [15, 16], show a BCS instability that is *enhanced* by the presence of spin-orbit coupling. Namely, in a purely parabolic system repulsive interactions cannot create an instability at second order in U , but such an instability occurs in the presence of spin-orbit coupling. Therefore this system falls in the line of reasoning of Ref. [27] where it has been shown that perturbations can significantly enhance superconductivity. Owing to this we note that, as proposed in Ref. [15], the spin-orbit coupling results in stronger superconductivity than would otherwise be present.

The above discussion is general for intraband pairing for any choice of parameters in the model. Let us now specialize to the case of interest, a single Fermi surface.

2.4.2 Pairing on a Single Fermi Surface

First let us describe the two band dispersion $\epsilon_{k,\pm 1}$. The upper band $\lambda = +1$ is a monotonically increasing function of k and parabolic like. For $\lambda = -1$ there are two possible functional forms depending on parameters. The first is a parabolic-like, monotonically increasing function of k . The second has a Mexican hat shape with a value of $-|M|$ at $k = 0$

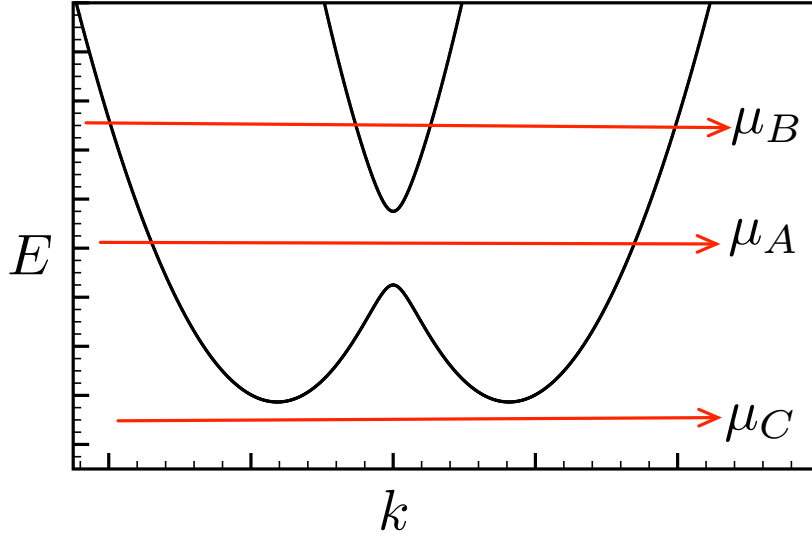


Figure 2.1: Schematic picture of our linearized bands. The different horizontal lines correspond to values of the chemical potential creating a single Fermi surface (μ_A) and to two Fermi surfaces (μ_B and μ_C).

and a minimum at some finite momentum $k = k_{min}$. Above this value of k the band energy is monotonically increasing. A schematic plot of $\epsilon_{\mathbf{k},\pm 1}$ is shown in Fig. 2.1.

Regardless of the functional form of $\epsilon_{\mathbf{k},-1}$ the two bands are separated at $k = 0$ by an energy $2|M|$. The interesting regime is when $|\mu| < |M|$. In this regime there is a single fermi surface, marked by the line μ_A in Fig. 2.1. For $|\mu| > |M|$ we have either two or zero Fermi surfaces; these regimes are marked by the lines μ_B and μ_C in Fig. 2.1.

Here we focus on the region $|\mu| < |M|$ where there is a single, circular Fermi surface with radius $k = k_F$. For this band structure slow modes must belong to the $\lambda = -1$ band. We thus focus on intra-band pairing of electrons in the $\lambda = -1$ band. This is the interacting analogue of the intraband pairing discussed in Refs. [8, 9]. Note that our RG description naturally dispenses with interband pairing for this choice of parameters, *i.e* the Fermi surface contains only $\lambda = -1$ electrons and so we do not expect any interesting flow between electrons in opposite bands. In the language developed in Section 2.2 this would

seem to suggest we would not expect to see $\Delta_{+-}(\mathbf{k})$ type pairings. Additionally, for similar reasons we do not expect to see $\Delta_{++}(\mathbf{k})$ type pairings either.

For this particular choice of parameters $N_{+1} = 0$ as there are no states in the band +1 inside the Fermi surface. The matrix g reduces to a scalar which is obtained by setting $\lambda = \lambda' = -1$ and

$$\lambda^{m_z}(1) = \frac{U^2}{2^6} N_{-1} v_{-1,-1}(m_z). \quad (2.4.6)$$

Where $v_{-1,-1}(m_z)$ is a numerical constant for a given set of material parameters and is defined in the appendix. From the above we see that the channel m_z with the most negative value of $v_{-1,-1}(m_z)$ will be the dominant channel for pairing, as $\frac{U^2}{2^6} N_{-1}$ is a positive constant. The corresponding critical temperature can be roughly estimated as $T_c \sim e^{\frac{2^5}{U^2 N_{-1} v_{-1,-1}(m_z)}}$.

As shown in the appendix $v_{-1,-1}(m_z)$ is a complicated integral. Setting $B = 0.0$ for both simplicity and to make a closer analogy with the work in [9], we have evaluated $v_{-1,-1}(m_z)$ numerically over the range of values, $A \leq t$, $|M| \leq .3t$ and $|\mu| < |M|$. For the parameters we have looked at, we find quite generally that for $M > 0$ the dominant angular momentum channel is $m_z = 2$ while for $M < 0$ it is $m_z = -2$. As an example of the data we have plotted $v_{-1,-1}(m_z)$ as a function of A in Fig. 2.2. We note that in the absence of the mass term M there is a degeneracy between $v_{-1,-1}(m_z)$ and $v_{-1,-1}(-m_z)$, quite simply $v_{-1,-1}(m_z) = v_{-1,-1}(-m_z)$ for all parameter values[16]. This means that for $M = 0$ the m_z channel and the $-m_z$ channel are equally favorable. When we allow for a finite M this degeneracy lifts. For the choice of parameters in Fig. 2.2 there is a large difference between the m_z and $-m_z$ couplings and there is only a single dominant channel.

Looking back at the original pairing function $V'_{\lambda,\lambda'}(\phi, s) = \frac{e^{i\phi}}{N} v'_{\lambda,\lambda'}(\phi, s)$ and replacing $v'_{\lambda,\lambda'}(\phi, s)$ with its most dominant $m_z = \pm 2$ component we see that for $|M| > 0$ our

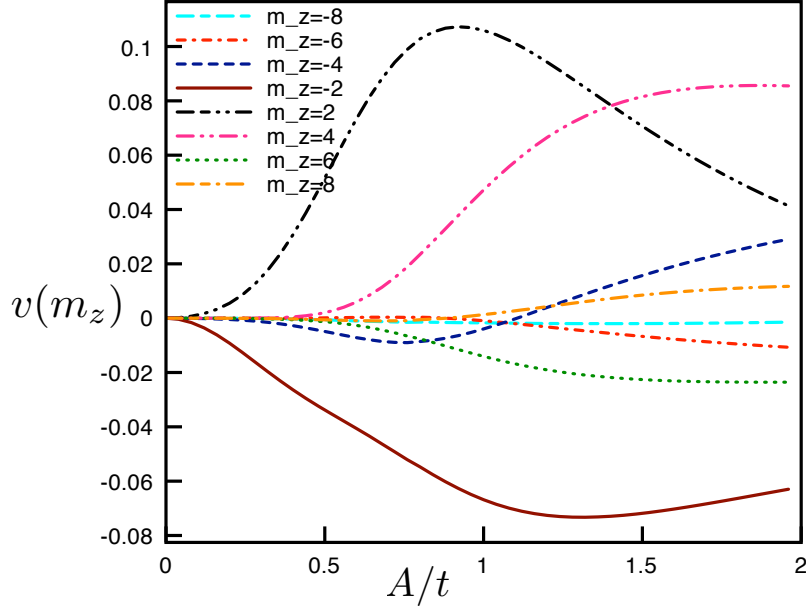


Figure 2.2: Plot of the integral $v(m_z) = v_{-1,-1}(m_z)$ as a function of A . Above we have set $B = 0$, $M = -0.3t$ and $\mu = 0$. We note that for the range of parameters chosen the $m_z = -2$ channel is by far the most negative channel.

RG analysis gives an attractive interaction with f -wave (p -wave) symmetry. Owing to the extra phase factor in this basis, this leads, in a mean field description (discussed in the next section) to an order parameter $\Delta_{--}(\mathbf{k})$ with f -wave or p -wave symmetry. In Section 2.2 we argued that a p -wave (and later an f -wave) $\Delta_{--}(\mathbf{k})$ intraband order parameter with the chemical potential tuned in the gap should constitute a spinless topological superconductor. Here the same argument holds and we have found, within our analysis, that neither $\Delta_{++}(\mathbf{k})$ nor $\Delta_{+-}(\mathbf{k})$ type pairing develops.

Another encouraging comparison comes from connecting our RG calculation with the earlier mean-field work on the same model in [1]. The dominant $m_z = \pm 2$, representing f -wave or p -wave band pairing leads to $d \mp id$ -wave spin-singlet pairing and $p + ip$ and $f + if$ -wave spin-triplet pairing when transformed back to the usual spin basis. Therefore, as we've seen in Section 2.2, once spin degeneracy is broken superconductivity may be

a superpositions of spin-singlet and spin-triplet. The connection to Ref. [1] comes from noting that in this study $d + id$ singlet pairing was found using a variational mean field theory technique. That study did not include p - or f - triplet pairing in the variational wave function and therefore those were not obtained.

2.5 Mean Field Topological Classification

In order to gain more intuition and allow a simple evaluation of the topological invariant we resort to an effective mean field theory. The RG analysis above points to the important component of the interaction and we therefore include only this component in the effective model. To this end, we dispense with any interactions between $\lambda = +1$ band electrons and furthermore only consider the dominant $m_z = m_z^{opt}$ interaction channel between our $\lambda = -1$ band electrons. We therefore write the following dominant channel Hamiltonian,

$$\begin{aligned}
 H_{eff} &= \sum_{\mathbf{k}, \lambda} (\epsilon_{\mathbf{k}} + \lambda d_{\mathbf{k}} - \mu) b_{\mathbf{k}, \lambda}^\dagger b_{\mathbf{k}, \lambda} \\
 &+ \sum_{\mathbf{k}, \mathbf{k}'} V_{eff}(\phi) b_{\mathbf{k}, -1}^\dagger b_{-\mathbf{k}, -1}^\dagger b_{-\mathbf{k}', -1} b_{\mathbf{k}', -1}
 \end{aligned} \tag{2.5.1}$$

where $V_{eff}(\phi)$ represents the part of the interaction which favors superconductivity in the dominant channel, denoted by $m_z \equiv m_z^{opt} = \pm 2$ and therefore $V_{eff}(\phi) \simeq \frac{e^{i(m_z^{opt}+1)\phi}}{N} v_{eff}(m_z^{opt})$.

We perform a mean-field decoupling of the interaction term:

$$\begin{aligned}
 H_{eff, MF} &= \sum_{\mathbf{k}, \lambda} \xi_{\mathbf{k}, \lambda} b_{\mathbf{k}, \lambda}^\dagger b_{\mathbf{k}, \lambda} \\
 &+ \frac{1}{2} \sum_{\mathbf{k}} \left(\Delta_0 e^{-i(m_z+1)\theta_{\mathbf{k}}} b_{\mathbf{k}, -1}^\dagger b_{-\mathbf{k}, -1}^\dagger \right. \\
 &\left. + \Delta_0 e^{i(m_z+1)\theta_{\mathbf{k}}} b_{-\mathbf{k}, -1} b_{\mathbf{k}, -1} \right)
 \end{aligned} \tag{2.5.2}$$

where we have dropped the ‘opt’ superscript on m_z , defined $\xi_{\mathbf{k},\lambda} \equiv \epsilon_{\mathbf{k}} + \lambda d_{\mathbf{k}} - \mu$, and the parameter Δ_0 must be determined self-consistently through the equation

$$1 = -\frac{v_{eff}(m_z^{opt})}{N} \sum_{\mathbf{k}} \frac{\tanh\left(\frac{E_{\mathbf{k}}}{2k_B T}\right)}{E_{\mathbf{k}}} \quad (2.5.3)$$

where $E_{\mathbf{k}} = \sqrt{\xi_{\mathbf{k},-1}^2 + \Delta_0^2}$. The wave function of the above is also of interest. For μ set in the gap in the spin-orbit split bands we have a vacuum of $b_{\mathbf{k},+}$ particles, as all possible ‘+’ states lie above μ , meanwhile we have a superconducting condensate of $b_{\mathbf{k},-}$ particles. These two observations give rise to the ground state

$$|\psi\rangle = \prod_{\mathbf{k}} \left(u_{\mathbf{k},-} + \exp(-i(m_z + 1)\theta_{\mathbf{k}}) v_{\mathbf{k},-} b_{\mathbf{k},-1}^\dagger b_{-\mathbf{k},-1}^\dagger \right) |0\rangle \text{ where } |0\rangle \text{ is the vacuum of band electrons, } u_{\mathbf{k},-} = \sqrt{\frac{E_{\mathbf{k}} + \xi_{\mathbf{k},-1}}{2E_{\mathbf{k}}}} \text{ and } v_{\mathbf{k},-} = \sqrt{\frac{E_{\mathbf{k}} - \xi_{\mathbf{k},-1}}{2E_{\mathbf{k}}}}$$

To obtain a description in terms of traditional spin states we transform $H_{eff,MF}$ back to a spin basis by inverting the transformation in Eq. (2.3.5) and arrive at

$$H_{eff,MF} = \frac{1}{2} \sum_{\mathbf{k}} \psi_{\mathbf{k}}^\dagger \mathcal{H}_{\mathbf{k}} \psi_{\mathbf{k}} \quad (2.5.4)$$

where $\psi_{\mathbf{k}} = (c_{\mathbf{k},\uparrow}, c_{\mathbf{k},\downarrow}, c_{-\mathbf{k},\downarrow}^\dagger, -c_{-\mathbf{k},\uparrow}^\dagger)^T$ and

$$\mathcal{H}_{\mathbf{k}} = \begin{pmatrix} h_{\mathbf{k}} & \hat{\Delta}_{\mathbf{k}} \\ \hat{\Delta}_{\mathbf{k}}^\dagger & -\sigma_y h_{-\mathbf{k}} \sigma_y \end{pmatrix} \quad (2.5.5)$$

with $h_{\alpha,\beta} = (\epsilon_{\mathbf{k}} - \mu)\delta_{\alpha,\beta} + \mathbf{d}(\mathbf{k}) \cdot \vec{\sigma}_{\alpha,\beta}$ and

$$\hat{\Delta}_{\mathbf{k}} = \begin{pmatrix} \Delta_s & -\Delta_t^\uparrow \\ \Delta_t^\downarrow & \Delta_s \end{pmatrix} \quad (2.5.6)$$

where

$$\Delta_s = \frac{\Delta_0}{2} \left(\frac{Ak}{d} \right) e^{-im_z \theta_{\mathbf{k}}} \quad (2.5.7)$$

$$\Delta_t^\uparrow = \frac{\Delta_0}{2} \left(\frac{d-d_3}{d} \right) e^{-i(m_z+1)\theta_{\mathbf{k}}} \quad (2.5.8)$$

$$\Delta_t^\downarrow = -\frac{\Delta_0}{2} \left(\frac{d+d_3}{d} \right) e^{-i(m_z-1)\theta_{\mathbf{k}}} \quad (2.5.9)$$

where d and d_3 are functions of $k = |\mathbf{k}|$. From this we can see that for $m_z = \pm 2$ we get $d \mp id$ -wave singlet pairing and $f \mp if$ and $p \pm ip$ -wave triplet pairing.

We now calculate the Chern number of this effective mean field Hamiltonian. The BdG Hamiltonian $\mathcal{H}_{\mathbf{k}}$ has particle-hole symmetry which greatly simplifies the evaluation as noted by Ghosh *et al*[28]. We define

$$Q(\mathbf{k}) = -\text{sgn}(\text{Pf}(\mathcal{H}_{\mathbf{k}}\Gamma)) \quad (2.5.10)$$

where $\Gamma = \sigma_y \otimes \tau_y$ and ‘Pf’ stands for the Pfaffian of the matrix argument. The Chern number is a function of $Q(\mathbf{k})$ evaluated at the time reversal invariant momenta (TRIM) and in the square lattice this amounts to

$$C_1 = \frac{1}{i\pi} \ln \left[\frac{Q(0,0)Q(\pi,\pi)}{Q(\pi,0)Q(0,\pi)} \right] \quad (2.5.11)$$

where in the logarithm we have taken a branch such that $\ln(-1) = i\pi$. We can easily calculate Q and find

$$Q(\mathbf{k}) = \text{sgn}(|\Delta_s(\mathbf{k})|^2 + (\epsilon_{\mathbf{k}} - \mu)^2 - d_{\mathbf{k}}^2) \quad (2.5.12)$$

Evaluating this at the TRIM points we note the following interesting observations. The first is that $Q(0,\pi) = Q(\pi,0)$ and so the denominator in Eq. (2.5.11) does not contribute to C_1 .

Second, at the point (π, π) we can make a similar argument to that made in Ref. [28]. In units of the lattice constant, if $\pi^2 \gg M, B, \Delta_0, \mu$ then we can focus only on the k^4 term in $Q(\pi, \pi)$. This term is simply $t^2 - B^2$. Finally we have $Q(0, 0) = \mu^2 - M^2$ leading to our result for C_1

$$C_1 = \frac{1}{i\pi} \ln \text{sgn} [(t^2 - B^2)(\mu^2 - M^2)] \quad (2.5.13)$$

If $|B| < t$ then the topology of the system is entirely determined by whether or not μ falls in the gap in the spin-orbit split bands opened by M . If $|\mu| < |M|$ (Fermi surface in the gap) then $C_1 = 1$ and the system has non-trivial topology. Note that Δ_s is not technically defined at $(0, 0)$, this is likely an artifact of our continuum theory and we have replaced it with its limiting value here. We have checked our observations here using the numerical formula for the calculation of C_1 given in Eq. (11) of Ref. [1].

The parameter range $|M| > |\mu|$ is of course the type of system we have considered in our renormalization group approach in the previous section. Thus any superconductivity that develops in the system for this range of parameters will have non-trivial topology.

Although we have performed our calculation on a clean system, we expect our results to be robust against disorder. Our confidence in this comes from our finding that C_1 is non-zero for the relevant parameter regime. A topological system is, by its nature, resilient to disorder[29, 30]. In addition to this, the state we find is a fully gapped superconductor and should therefore be robust to defects for this reason as well.

The effect of temperature has also not been studied here and is left for subsequent studies. We expect that the above topological superconductor be stable at temperatures lower than the mean field gap scale.

2.6 Conclusion

We have studied a model of interacting, spin-orbit coupled electrons using renormalization group methods. After simplifying the model of Ref. [1] by taking the continuum limit, we have applied the methods developed in Refs. [15],[16],[26],[27] to our model and focused on a system with a single Fermi surface. Our analysis shows that for this range of parameters the most dominant angular momentum pairing channel under RG has p -wave or f -wave symmetry depending on the sign of the Zeeman parameter M . Such an interaction should lead to a superconductor with intraband Cooper pairs and a p -wave or f -wave order parameter.

To verify the topology of the state we simplified our model to include only the dominant interaction channel and performed a mean field analysis of the resultant effective Hamiltonian. This analysis shows that the system develops topological superconductivity. The condition for non-trivial topology in the physical case, $|B| < t$, is that $|\mu| < |M|$, that is that the Fermi surface must lie in the gap in the spin-orbit split bands opened by M . This is similar to the condition discussed by Sau[9] and Alicea[8] in the context of spin-orbit coupled bands in proximity to a superconductor. Thus the results here provide added justification to the case that interactions, rather than proximity effect, may be used to obtain topological superconductivity[1, 20, 31]. Moreover, we see the potential for the following physical scenario. In a topologically trivial superconductor with spin-orbit coupling the topology may change to a non-trivial one upon applying a Zeeman field. This occurs since the Zeeman field provides the necessary gapping of one of the bands, leaving one band whose electron spins are locked to the momentum direction.

2.7 Acknowledgements

The authors are thankful for useful discussions with J. Alicea, B. A. Bernevig and Y. Bresler. Financial support for this work was provided by the NSERC and FQRNT (TPB) the Vanier Canada Graduate Scholarship (AF) and the Walter C. Sumner Memorial Fellowship (AF). Numerical calculations for this work were performed using CLUMEQ/McGill HPC super-computing resources.

2.A Interaction Vertex in the Band Basis

We now write the interaction Hamiltonian in terms of the new band operators. We note that our unitary transformation can be written as

$$c_{\mathbf{k},\alpha} = \sum_{\lambda} W_{\alpha,\lambda}(\mathbf{k}) b_{\mathbf{k},\lambda} \quad (2.A.1)$$

where $W_{\alpha,\lambda}(\mathbf{k}) = \exp\left(\left(\frac{1-\sigma_{\alpha,z}}{2}\right)\theta_{\mathbf{k}}\right) f_{\sigma_{\alpha,z}\lambda}(\mathbf{k})\eta_{\sigma,\lambda}$ with $\eta_{\downarrow,-} = -1$ and $\eta_{\alpha,\lambda}$ for all other combinations of α and λ . Meanwhile we have

$$c_{\mathbf{k},\alpha}^{\dagger} = \sum_{\lambda} W_{\alpha,\lambda}^*(\mathbf{k}) b_{\mathbf{k},\lambda}^{\dagger} \quad (2.A.2)$$

Making use of the above we then have the interaction contribution

$$\begin{aligned} H_{int} &= \sum_{\mathbf{k}_1, \mathbf{k}_2, \mathbf{k}_3, \mathbf{k}_4} \sum_{\lambda_1, \lambda_2, \lambda_3, \lambda_4} \delta_{\mathbf{k}_1 + \mathbf{k}_2, \mathbf{k}_3 + \mathbf{k}_4} \\ &\times V_{\lambda_1, \lambda_2, \lambda_3, \lambda_4}(\mathbf{k}_1, \mathbf{k}_2, \mathbf{k}_3, \mathbf{k}_4) b_{\mathbf{k}_1, \lambda_1}^{\dagger} b_{\mathbf{k}_2, \lambda_2}^{\dagger} b_{\mathbf{k}_3, \lambda_3} b_{\mathbf{k}_4, \lambda_4} \end{aligned} \quad (2.A.3)$$

where

$$V_{\lambda_1, \lambda_2, \lambda_3, \lambda_4}(\mathbf{k}_1, \mathbf{k}_2, \mathbf{k}_3, \mathbf{k}_4) = \sum_{\alpha_1, \alpha_2, \alpha_3, \alpha_4} U_{\alpha_1, \alpha_2, \alpha_3, \alpha_4}(\mathbf{k}_1, \mathbf{k}_2, \mathbf{k}_3, \mathbf{k}_4) \quad (2.A.4)$$

$$W_{\alpha_1, \lambda_1}^*(\mathbf{k}_1) W_{\alpha_2, \lambda_2}^*(\mathbf{k}_2) W_{\alpha_3, \lambda_3}(\mathbf{k}_3) W_{\alpha_4, \lambda_4}(\mathbf{k}_4).$$

The above describes scattering events between electrons in the two bands; electrons in eigenstates $(\mathbf{k}_4, \lambda_4)$ and $(\mathbf{k}_3, \lambda_3)$ scatter to states $(\mathbf{k}_2, \lambda_2)$ and $(\mathbf{k}_1, \lambda_1)$ with some associated interaction strength $V_{\lambda_1, \lambda_2, \lambda_3, \lambda_4}(\mathbf{k}_1, \mathbf{k}_2, \mathbf{k}_3, \mathbf{k}_4)$ which depends on momenta and band index. Finally the delta function conserves momentum in this scattering process. A more convenient form for the interaction strength V is given by

$$\tilde{V}_{\lambda_1, \lambda_2, \lambda_3, \lambda_4}(\mathbf{k}_1, \mathbf{k}_2, \mathbf{k}_3, \mathbf{k}_4) = \frac{U}{2N} \sum_{\alpha_1} W_{\alpha_1, \lambda_1}^*(\mathbf{k}_1) W_{\bar{\alpha}_1, \lambda_2}^*(\mathbf{k}_2)$$

$$\times W_{\bar{\alpha}_1, \lambda_3}(\mathbf{k}_3) W_{\alpha_1, \lambda_4}(\mathbf{k}_4) \quad (2.A.5)$$

where we have used a bar symbol, $\bar{\alpha}$ to indicate the compliment to spin α . Writing out the sum over α explicitly and defining $F_{i,j} = f_{\lambda_i}(\mathbf{k}_i) f_{-\lambda_j}(\mathbf{k}_j)$ we then obtain

$$V_{\lambda_1, \lambda_2, \lambda_3, \lambda_4}(\mathbf{k}_1, \mathbf{k}_2, \mathbf{k}_3, \mathbf{k}_4) = \quad (2.A.6)$$

$$\frac{U (\lambda_2 e^{-\theta_{\mathbf{k}_2}} F_{1,2} - \lambda_1 e^{-\theta_{\mathbf{k}_1}} F_{2,1}) (\lambda_3 e^{\theta_{\mathbf{k}_3}} F_{4,3} - \lambda_4 e^{\theta_{\mathbf{k}_4}} F_{3,4})}{4N}$$

We see that V is antisymmetric under the exchange of *either* indices 1 and 2 or 3 and 4 and symmetric under the exchange of both.

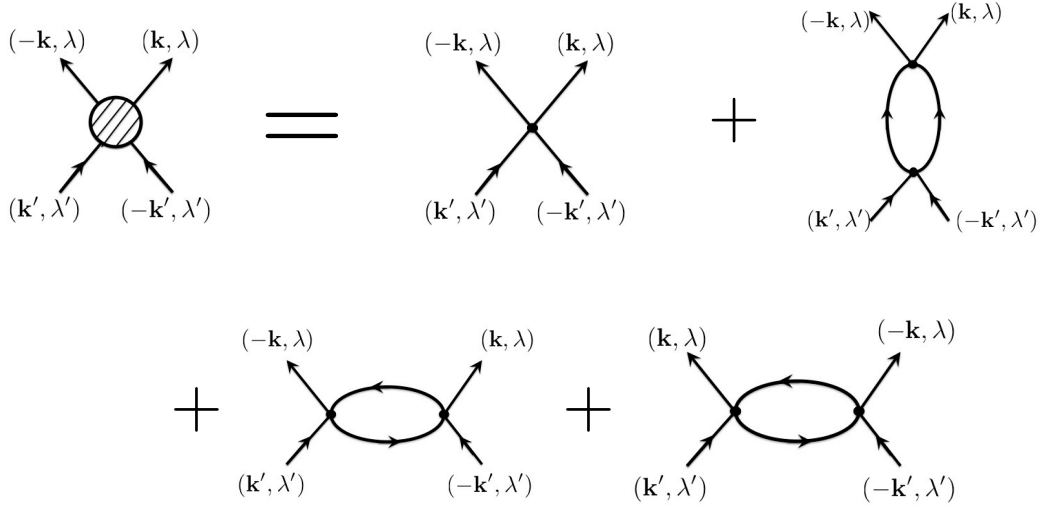


Figure 2.3: Diagrams contributing to the renormalization of the BCS coupling function up to one-loop.

2.B Three-Loop Expansion for S'_{int} on the Lattice

2.B.1 Tree Level and One-Loop

We now give expressions for the first few terms in the cumulant expansion for S'_{int} . Here we give general expressions in terms of unsolved integrals and later on we make some simplifying specializations in order to perform these integrals approximately. As we are interested in superconductivity in this model we will be invested in how the BCS channel of the original interacting action evolves under renormalization. This channel is specified by $\mathbf{k}_4 = -\mathbf{k}_3 = \mathbf{k}$, $\lambda_3 = \lambda_4 = \lambda$, $\mathbf{k}_1 = -\mathbf{k}_2 = \mathbf{k}'$ and $\lambda_2 = \lambda_1 = \lambda'$ in the original (bare) interaction S_{int} . To this end we will set all external momenta accordingly.

Let us begin our discussion with the effective interaction up to one-loop, afterwards we will extend this to three-loops. The diagrams contributing to this effective action are shown

in Fig. 2.3. We have

$$\begin{aligned}
S'_{int,1\ell} &= \delta S_{int}^{\text{tree}} + \delta S_{int}^{\text{one-loop}} \\
&= \int_0^\beta d\tau \sum_{\mathbf{k}, \mathbf{k}', \lambda, \lambda'} (V_{\lambda, \lambda'}^{\text{tree}}(\mathbf{k}, \mathbf{k}') + V_{\lambda, \lambda'}^{\text{one-loop}}(\mathbf{k}, \mathbf{k}')) \\
&\quad \times b_{\mathbf{k}, \lambda, <}^*(\tau) b_{-\mathbf{k}, \lambda, <}^*(\tau) b_{-\mathbf{k}', \lambda', <}(\tau) b_{\mathbf{k}', \lambda', <}(\tau)
\end{aligned} \tag{2.B.1}$$

where the tree level term gives the contribution $V_{\lambda, \lambda'}^{\text{tree}}(\mathbf{k}, \mathbf{k}') = \frac{U}{N} e^{i(\theta_{\mathbf{k}'} - \theta_{\mathbf{k}})} \lambda \lambda' F_{\lambda, \lambda}(\mathbf{k}, \mathbf{k}') F_{\lambda', \lambda'}(\mathbf{k}', \mathbf{k}')$ and the one-loop contribution is

$$\begin{aligned}
V_{\lambda, \lambda'}^{\text{one-loop}}(\mathbf{k}, \mathbf{k}') &= \frac{U^2}{64N} (\Pi(-\mathbf{k}, \mathbf{k}') - \Pi(\mathbf{k}, \mathbf{k}')) \\
&\quad - \frac{U}{2} V_{\lambda, \lambda'}^{\text{tree}}(\mathbf{k}, \mathbf{k}') P(\Lambda, s)
\end{aligned} \tag{2.B.2}$$

In the above we have defined the following integral

$$\begin{aligned}
\Pi_{\lambda, \lambda'}(\mathbf{k}, \mathbf{k}') &= \sum_{\lambda_5, \lambda_6} \int_{>} \frac{d^2 \mathbf{p}}{(2\pi)^2} \left(\frac{n_F(E_{\mathbf{p}, \lambda_5}) - n_F(E_{\mathbf{p} + \mathbf{k} + \mathbf{k}', \lambda_6})}{E_{\mathbf{p}, \lambda_5} - E_{\mathbf{p} + \mathbf{k} + \mathbf{k}', \lambda_6}} \right) \\
&\quad \times G_{\lambda, \lambda', \lambda_5, \lambda_6}(\mathbf{k}, \mathbf{k}', \mathbf{p})
\end{aligned} \tag{2.B.3}$$

with the function

$$\begin{aligned}
G_{\lambda, \lambda', \lambda_5, \lambda_6}(\mathbf{k}, \mathbf{k}', \mathbf{p}) &= 16 w_{\lambda_5, \lambda}(\mathbf{p}, \mathbf{k}) w_{\lambda', \lambda_6}^*(-\mathbf{k}', \mathbf{k} + \mathbf{k}' + \mathbf{p}) \\
&\quad \times w_{\lambda_6, \lambda}(\mathbf{k} + \mathbf{k}' + \mathbf{p}, -\mathbf{k}) w_{\lambda', \lambda_5}^*(\mathbf{k}', \mathbf{p})
\end{aligned} \tag{2.B.4}$$

and the $>$ on the \mathbf{p} integral is to remind us that the integral must be performed over the regions of \mathbf{p} -space satisfying both $\Lambda/s \leq |E_{\mathbf{p}, \lambda_5}| \leq \Lambda$ and $\Lambda/s \leq E_{\mathbf{p} + \mathbf{k} + \mathbf{k}', \lambda_6} \leq \Lambda$. We

have also defined the momentum independent integral P

$$\begin{aligned}
 P(\Lambda, s) &= \sum_{\lambda_5, \lambda_6} \int_{>} \frac{d^2 \mathbf{p}}{(2\pi)^2} \left(\frac{1 - n_F(E_{\mathbf{p}, \lambda_5}) - n_F(E_{\mathbf{p}, \lambda_6})}{E_{\mathbf{p}, \lambda_5} + E_{\mathbf{p}, \lambda_6}} \right) \\
 &\times |w_{\lambda_5, \lambda_6}(-\mathbf{p}, \mathbf{p})|^2
 \end{aligned} \tag{2.B.5}$$

where $n_F(\epsilon) = \frac{1}{1+e^{\beta\epsilon}}$ is the usual Fermi distribution function.

2.B.2 Two-Loop

We now move on to higher our diagrams of which we keep only diagrams with logarithmic divergences. The diagrams we sum are essentially the same as the diagrams used in Refs. [15, 16]] and we do not redraw them here.

As a two-loop contribution to our interaction we obtain

$$\begin{aligned}
 \delta S_{int}^{\text{two-loop}} &= \int_0^\beta d\tau \sum_{\mathbf{k}, \mathbf{k}', \lambda, \lambda'} V_{\lambda, \lambda'}^{\text{two-loop}}(\mathbf{k}, \mathbf{k}') \\
 &\times b_{\mathbf{k}, \lambda, <}^*(\tau) b_{-\mathbf{k}, \lambda, <}^*(\tau) b_{-\mathbf{k}', \lambda', <}(\tau) b_{\mathbf{k}', \lambda', <}(\tau)
 \end{aligned} \tag{2.B.6}$$

where we have defined

$$\begin{aligned}
 V_{\lambda, \lambda'}^{\text{two-loop}}(\mathbf{k}, \mathbf{k}') &= \frac{U^3}{4N} \lambda \lambda' e^{i(\theta_{\mathbf{k}'} - \theta_{\mathbf{k}})} F_{\lambda\lambda}(\mathbf{k}, \mathbf{k}) F_{\lambda'\lambda'}(\mathbf{k}', \mathbf{k}') P^2(\Lambda, s) \\
 &- \frac{U^3}{128N} (\lambda' e^{i\theta_{\mathbf{k}'}} F_{\lambda'\lambda'}(\mathbf{k}', \mathbf{k}') I^{2\ell}(\mathbf{k}, \lambda) \\
 &+ \lambda e^{-i\theta_{\mathbf{k}}} F_{\lambda\lambda}(\mathbf{k}, \mathbf{k}) (I^{2\ell}(\mathbf{k}', \lambda'))^*)
 \end{aligned} \tag{2.B.7}$$

where we have the integral

$$\begin{aligned}
I^{2\ell}(\mathbf{k}, \lambda) &= \sum_{\mu_1, \mu_2} \int_{>} \frac{d^2 \mathbf{p}}{(2\pi)^2} \left(\frac{1 - n_f(E_{\mathbf{p}, \mu_2}) - n_f(E_{\mathbf{p}, \mu_1})}{E_{\mathbf{p}, \mu_2} + E_{\mathbf{p}, \mu_1}} \right) \\
&\quad w_{\mu_2, \mu_1}(\mathbf{p}, -\mathbf{p}) (\hat{\Pi}_{\lambda, \mu_1, \mu_2}(-\mathbf{k}, \mathbf{p}) - \hat{\Pi}_{\lambda, \mu_1, \mu_2}(\mathbf{k}, \mathbf{p})) \\
\hat{\Pi}_{\lambda, \mu_1, \mu_2}(\mathbf{k}, \mathbf{p}) &= \sum_{\mu_3, \mu_4} \int_{>} \frac{d^2 \mathbf{p}_2}{(2\pi)^2} \left(\frac{n_f(E_{\mathbf{p}_2, \mu_3}) - n_f(E_{\mathbf{p}_2 + \mathbf{p} + \mathbf{k}, \mu_4})}{E_{\mathbf{p}_2, \mu_3} - E_{\mathbf{p}_2 + \mathbf{p} + \mathbf{k}, \mu_4}} \right) \hat{G}_{\lambda, \mu_1 \dots \mu_4}(\mathbf{k}, \mathbf{p}, \mathbf{p}_2) \\
\hat{G}_{\lambda, \mu_1 \dots \mu_4}(\mathbf{k}, \mathbf{p}, \mathbf{p}_2) &= G_{\lambda, \mu_1, \mu_3, \mu_4}(\mathbf{k}, \mathbf{p}, \mathbf{p}_2) \delta_{\mu_1, \mu_2} + \tilde{G}_{\lambda, \mu_1, \mu_3, \mu_4}(\mathbf{k}, \mathbf{p}, \mathbf{p}_2) \sigma_{\mu_1, \mu_2}^x
\end{aligned} \tag{2.B.8}$$

where $G_{\lambda, \mu_1, \mu_3, \mu_4}(\mathbf{k}, \mathbf{p}, \mathbf{p}_2)$ is defined above and

$$\begin{aligned}
\tilde{G}_{\lambda, \lambda', \lambda_5, \lambda_6}(\mathbf{k}, \mathbf{k}', \mathbf{p}) &= 16w_{\lambda_5, \lambda}(\mathbf{p}, \mathbf{k}) \\
&\quad \times w_{-\lambda', \lambda_6}^*(-\mathbf{k}', \mathbf{k} + \mathbf{k}' + \mathbf{p}) \\
&\quad \times w_{\lambda_6, \lambda}(\mathbf{k} + \mathbf{k}' + \mathbf{p}, -\mathbf{k}) w_{\lambda', \lambda_5}^*(\mathbf{k}', \mathbf{p})
\end{aligned} \tag{2.B.9}$$

2.B.3 Three-Loop

We now finally move on to fourth order. Their contribution is as follows

$$\begin{aligned}
\delta S_{int}^{\text{three-loop}} &= \int_0^\beta d\tau \sum_{\mathbf{k}, \mathbf{k}', \lambda, \lambda'} V_{\lambda, \lambda'}^{\text{three-loop}}(\mathbf{k}, \mathbf{k}') \\
&\quad \times b_{\mathbf{k}, \lambda, <}^*(\tau) b_{-\mathbf{k}, \lambda, <}^*(\tau) b_{-\mathbf{k}', \lambda', <}(\tau) b_{\mathbf{k}', \lambda', <}(\tau)
\end{aligned} \tag{2.B.10}$$

where we have defined

$$\begin{aligned}
V_{\lambda, \lambda'}^{\text{three-loop}}(\mathbf{k}, \mathbf{k}') &= -\frac{U^4 \lambda \lambda' e^{i(\theta_{\mathbf{k}'} - \theta_{\mathbf{k}})} F_{\lambda \lambda}(\mathbf{k}, \mathbf{k}) F_{\lambda' \lambda'}(\mathbf{k}', \mathbf{k}')}{2^3 N} \left(P^3(\Lambda, s) + \frac{\hat{P}(\Lambda, s)}{8} \right) \\
&\quad + \frac{U^4 P(\Lambda, s)}{2^8 N} (2\lambda' e^{i\theta_{\mathbf{k}'}} F_{\lambda' \lambda'}(\mathbf{k}', \mathbf{k}') I^{2\ell}(\mathbf{k}, \lambda) + 2\lambda e^{-i\theta_{\mathbf{k}}} F_{\lambda \lambda}(\mathbf{k}, \mathbf{k}) (I^{2\ell}(\mathbf{k}', \lambda'))^*) \\
&\quad + \frac{U^4}{2^{11} N} I^{3\ell}(\mathbf{k}, \mathbf{k}', \lambda, \lambda')
\end{aligned} \tag{2.B.11}$$

where we have the new integrals

$$I^{3\ell}(\mathbf{k}, \mathbf{k}', \lambda, \lambda') = \sum_{\mu_1, \mu_2} \int_{>} \frac{d^2 \mathbf{p}}{(2\pi)^2} \left(\frac{1 - n_f(E_{\mathbf{p}, \mu_2}) - n_f(E_{\mathbf{p}, \mu_1})}{E_{\mathbf{p}, \mu_2} + E_{\mathbf{p}, \mu_1}} \right) \quad (2.B.12)$$

$$\times (\hat{\Pi}_{\lambda, \mu_1, \mu_2}(\mathbf{k}, \mathbf{p}) - \hat{\Pi}_{\lambda, \mu_1, \mu_2}(-\mathbf{k}, \mathbf{p})) (\hat{\Pi}_{\lambda', \mu_2, \mu_1}^*(\mathbf{k}', -\mathbf{p}) - \hat{\Pi}_{\lambda', \mu_2, \mu_1}^*(-\mathbf{k}', -\mathbf{p}))$$

$$\hat{P}(\Lambda, S) = \sum_{\mu_1 \dots \mu_6} \int_{>} \frac{d^2 \mathbf{p}_1}{(2\pi)^2} \int_{>} \frac{d^2 \mathbf{p}_2}{(2\pi)^2} \int_{>} \frac{d^2 \mathbf{p}_3}{(2\pi)^2} w_{\mu_2, \mu_1}(\mathbf{p}_1, -\mathbf{p}_1) w_{\mu_5, \mu_6}^*(\mathbf{p}_3, -\mathbf{p}_3)$$

$$\times \left(\frac{1 - n_f(E_{\mathbf{p}_1, \mu_2}) - n_f(E_{\mathbf{p}_1, \mu_1})}{E_{\mathbf{p}_1, \mu_2} + E_{\mathbf{p}_1, \mu_1}} \right) \left(\frac{1 - n_f(E_{\mathbf{p}_3, \mu_6}) - n_f(E_{\mathbf{p}_3, \mu_5})}{E_{\mathbf{p}_3, \mu_6} + E_{\mathbf{p}_3, \mu_5}} \right)$$

$$\times \left(\frac{n_f(E_{\mathbf{p}_2, \mu_3}) - n_f(E_{\mathbf{p}_2 + \mathbf{p}_1 + \mathbf{p}_3, \mu_4})}{E_{\mathbf{p}_2, \mu_3} - E_{\mathbf{p}_2 + \mathbf{p}_1 + \mathbf{p}_3, \mu_4}} \right) \hat{G}_{\mu_1 \dots \mu_6}(\mathbf{p}_1, \mathbf{p}_2, \mathbf{p}_3)$$

$$\hat{G}_{\mu_1 \dots \mu_6}(\mathbf{p}_1, \mathbf{p}_2, \mathbf{p}_3) = \delta_{\mu_5, \mu_6} \hat{G}_{\mu_5, \mu_1 \mu_2 \mu_3 \mu_4}(\mathbf{p}_3, \mathbf{p}_1, \mathbf{p}_2) + \delta_{\mu_1, \mu_2} \sigma_{\mu_5, \mu_6}^x \tilde{G}_{\mu_1, \mu_5, \mu_3, \mu_4}^*(\mathbf{p}_1, \mathbf{p}_3, \mathbf{p}_2) \delta_{\mu_1, \mu_2}$$

$$+ \sigma_{\sigma_5, \sigma_6}^x \sigma_{\mu_1, \mu_2}^x \bar{G}_{\mu_5 \mu_1, \mu_3, \mu_4}(\mathbf{p}_3, \mathbf{p}_1, \mathbf{p}_2) \quad (2.B.13)$$

where

$$\bar{G}_{\lambda, \lambda', \lambda_5, \lambda_6}(\mathbf{k}, \mathbf{k}', \mathbf{p}) = 16w_{\lambda_5, \lambda}(\mathbf{p}, \mathbf{k}) \quad (2.B.14)$$

$$\times w_{-\lambda', \lambda_6}^*(-\mathbf{k}', \mathbf{k} + \mathbf{k}' + \mathbf{p})$$

$$\times w_{\lambda_6, -\lambda}(\mathbf{k} + \mathbf{k}' + \mathbf{p}, -\mathbf{k}) w_{\lambda', \lambda_5}^*(\mathbf{k}', \mathbf{p})$$

Using the above expressions for the diagrams up to fourth order in U and logarithmically enhanced we have the effective BCS channel coupling

$$V'_{\lambda, \lambda'}(\mathbf{k}, \mathbf{k}', \Lambda, s) = \frac{U}{N} e^{i(\theta_{\mathbf{k}'} - \theta_{\mathbf{k}})} \lambda \lambda' F_{\lambda, \lambda}(\mathbf{k}, \mathbf{k}) F_{\lambda', \lambda'}(\mathbf{k}', \mathbf{k}') \quad (2.B.15)$$

$$\times \left(1 - \frac{U}{2} P(\Lambda, s) + \frac{U^2}{4} P^2(\Lambda, s) - \frac{U^3}{8} P^3(\Lambda, s) - \frac{U^3}{64} \hat{P}(\Lambda, s) \right)$$

$$+ \frac{U^2}{64N} I^{1\ell}(\mathbf{k}, \mathbf{k}') + \frac{U^4}{2^{11}N} I^{3\ell}(\mathbf{k}, \mathbf{k}', \lambda, \lambda')$$

$$- \frac{U^3}{128N} (\lambda' e^{i\theta_{\mathbf{k}'}} F_{\lambda' \lambda'}(\mathbf{k}', \mathbf{k}') I^{2\ell}(\mathbf{k}, \lambda) + \lambda e^{-i\theta_{\mathbf{k}}} F_{\lambda \lambda}(\mathbf{k}, \mathbf{k}) (I^{2\ell}(\mathbf{k}', \lambda'))^*) (1 - UP(\Lambda, s))$$

where $I^{1\ell}(\mathbf{k}, \mathbf{k}') = (\Pi(-\mathbf{k}, \mathbf{k}') - \Pi(\mathbf{k}, \mathbf{k}'))$.

2.C Continuum Limit

2.C.1 Dispersions

The integrals involved in the discussion above are formidable and do not allow any further analytic progress. To make progress we focus on the continuum limit of the model above by sending $\sin k_i \rightarrow k_i$, $\cos k_i \rightarrow 1 - k_i^2/2$. This gives the dispersion

$$E_{\mathbf{k},\lambda} = tk^2 - \tilde{\mu} - 4t + \lambda\sqrt{(A^2 - 2BM)k^2 + M^2 + B^2k^4} \quad (2.C.1)$$

where $k = \sqrt{k_x^2 + k_y^2}$. To make connection with standard conventions we redefine parameters as follows and $\mu = \tilde{\mu} + 4t$. Then we have

$$\begin{aligned} E_{\mathbf{k},\lambda} &= tk^2 - \mu + \lambda\sqrt{(A^2 - 2BM)k^2 + M^2 + B^2k^4} \\ &= \epsilon_{\mathbf{k},\lambda} - \mu = E_\lambda(k) \end{aligned} \quad (2.C.2)$$

where $\epsilon_{\mathbf{k},\lambda} = tk^2 + \lambda\sqrt{(A^2 - 2BM)k^2 + M^2 + B^2k^4}$. In this limit we have the new definitions

$$\begin{aligned} e^{i\theta_{\mathbf{k}}} &= \frac{k_x + ik_y}{\sqrt{k_x^2 + k_y^2}} \\ f_\lambda(\mathbf{k}) &= f_\lambda(k) = \sqrt{\frac{d + \lambda d_3}{2d}} \end{aligned} \quad (2.C.3)$$

where $d = \sqrt{(A^2 - 2BM)k^2 + M^2 + B^2k^4}$. At $B = 0$ this is precisely the band structure considered in the work by Sau *et al.*

2.C.2 Rotational Invariance

As discussed in the main text in the continuum limit we obtain a theory which depends only on the angle between given wave vectors on the Fermi surface. In developing this result it is incredibly useful to realize that

$$\begin{aligned}
I_{\lambda,\lambda'}^{1\ell}(\mathbf{k}, \mathbf{k}', s) &= e^{i\phi} I_{\lambda,\lambda'}^{1\ell}(k, k', \phi, s) \\
I_{\lambda}^{2\ell}(\mathbf{k}, s) &= e^{-i\theta_{\mathbf{k}}} I_{\lambda}^{2\ell}(k, s) \\
I_{\lambda,\lambda'}^{3\ell}(\mathbf{k}, \mathbf{k}', s) &= -e^{i\phi} I_{\lambda,\lambda'}^{3\ell}(k, k', \phi, s)
\end{aligned} \tag{2.C.4}$$

where $\phi = \theta_{\mathbf{k}} - \theta_{\mathbf{k}'}$. The manipulations required to show this is identical to that outlined in [16]. We will give results here for $I^{1\ell}(\mathbf{k}, \mathbf{k}', s)$ first. We begin by noting the following result

$$\begin{aligned}
\Pi_{\lambda,\lambda'}(-\mathbf{k}, \mathbf{k}') &= \sum_{\lambda_5, \lambda_6} \int_{>} \frac{d^2\mathbf{p}}{(2\pi)^2} \left(\frac{n_F(E_{\lambda_5}(p)) - n_F(E_{\lambda_6}(\sqrt{p^2 + Q^2 - 2pQ \cos(\theta_{\mathbf{p}} - \theta_{\mathbf{Q}}))})}{E_{\lambda_5}(p) - E_{\lambda_6}(\sqrt{p^2 + Q^2 - 2pQ \cos(\theta_{\mathbf{p}} - \theta_{\mathbf{Q}})})} \right) \\
&\times 16w_{\lambda_5, \lambda}(\mathbf{p}, -\mathbf{k})w_{\lambda', \lambda_6}^*(-\mathbf{k}', \mathbf{p} - \mathbf{Q})w_{\lambda_6, \lambda}(\mathbf{p} - \mathbf{Q}, \mathbf{k})w_{\lambda', \lambda_5}^*(\mathbf{k}', \mathbf{p}) \tag{2.C.5}
\end{aligned}$$

where $\mathbf{Q} = \mathbf{k} - \mathbf{k}'$. By making use of the identity

$$e^{i\theta_{\mathbf{k}_1 - \mathbf{k}_2}} = \frac{k_1 e^{i\theta_{\mathbf{k}_1}} - k_2 e^{i\theta_{\mathbf{k}_2}}}{\sqrt{k_1^2 + k_2^2 - 2k_1 k_2 \cos(\theta_{\mathbf{k}_1} - \theta_{\mathbf{k}_2})}}, \tag{2.C.6}$$

shifting $\theta_{\mathbf{p}} \rightarrow \theta_{\mathbf{p}} + \theta_{\mathbf{Q}}$ and then using

$$e^{i\theta_{\mathbf{Q}}} = \left(\frac{k e^{i\theta_{\mathbf{k}}} - k' e^{i\theta_{\mathbf{k}'}}}{Q} \right) \tag{2.C.7}$$

one can show using some straightforward but tedious manipulations that if we define

$$\begin{aligned}
\mathcal{F}_{\mu_1 \dots \mu_6}(k, k', \mathbf{p}, \phi) &= \frac{16}{q^2} (\mu_5 e^{-i\theta_{\mathbf{p}}} g F_{\mu_1, \mu_5}(k, p) + \mu_1 e^{i\phi} F_{\mu_5, \mu_1}(p, k)) \\
&\times (\mu_3 F_{\mu_5, \mu_3}(p, k') - \mu_5 e^{i\theta_{\mathbf{p}}} g^* F_{\mu_3, \mu_5}(k', p)) \\
&\times (-\mu_4 q F_{\mu_6, \mu_4}(q, k') + \mu_6 g^* Q F_{\mu_4, \mu_6}(k', q) - \mu_6 g^* e^{i\theta_{\mathbf{p}}} p F_{\mu_4, \mu_6}(k', q)) \\
&\times (\mu_6 e^{-i\phi} g e^{-i\theta_{\mathbf{p}}} p F_{\mu_2, \mu_6}(k, q) - \mu_6 e^{-i\phi} g Q F_{\mu_2, \mu_6}(k, q) - \mu_2 q F_{\mu_6, \mu_2}(q, k))
\end{aligned} \tag{2.C.8}$$

where $q = \sqrt{p^2 + Q^2 - 2Qp \cos(\theta_{\mathbf{p}})}$, $\phi = \theta_{\mathbf{k}'} - \theta_{\mathbf{k}}$, $Q = \sqrt{k^2 + k'^2 - 2k' \cos(\phi)}$ and $g = \frac{ke^{i\phi} - k'}{Q}$ then it follows that

$$\begin{aligned}
\Pi_{\lambda, \lambda'}(-\mathbf{k}, \mathbf{k}') &= e^{i\phi} \sum_{\lambda_5, \lambda_6} \int_{>} \frac{d^2 \mathbf{p}}{(2\pi)^2} \left(\frac{n_F(E_{\lambda_5}(p)) - n_F(E_{\lambda_6}(q))}{E_{\lambda_5}(p) - E_{\lambda_6}(q)} \right) \\
&\times \mathcal{F}_{\lambda, \lambda', \lambda', \lambda_5, \lambda_6}(k, k', \mathbf{p}, \phi) = e^{i\phi} V_{\lambda, \lambda', \lambda'}(k, k', \phi)
\end{aligned} \tag{2.C.9}$$

Following the exact same analysis one can show that

$$\begin{aligned}
\hat{\Pi}_{\lambda, \mu_1, \mu_2}(-\mathbf{k}, \mathbf{k}') &= e^{i\phi} \sum_{\lambda_5, \lambda_6} \int_{>} \frac{d^2 \mathbf{p}}{(2\pi)^2} \left(\frac{n_F(E_{\lambda_5}(p)) - n_F(E_{\lambda_6}(q))}{E_{\lambda_5}(p) - E_{\lambda_6}(q)} \right) \\
&\times \mathcal{F}_{\lambda, \lambda, \mu_1, \mu_2, \lambda_5, \lambda_6}(k, k', \mathbf{p}, \phi) = e^{i\phi} V_{\lambda, \lambda, \mu_1, \mu_2}(k, k', \phi) \\
\tilde{\Pi}_{\mu_1, \mu_2, \mu_5, \mu_6}(-\mathbf{k}, \mathbf{k}') &= e^{i\phi} \sum_{\lambda_5, \lambda_6} \int_{>} \frac{d^2 \mathbf{p}}{(2\pi)^2} \left(\frac{n_F(E_{\lambda_5}(p)) - n_F(E_{\lambda_6}(q))}{E_{\lambda_5}(p) - E_{\lambda_6}(q)} \right) \\
&\times \mathcal{F}_{\mu_5, \mu_6, \mu_1, \mu_2, \lambda_5, \lambda_6}(k', k, \mathbf{p}, \phi) = e^{i\phi} V_{\mu_5, \mu_6, \mu_1, \mu_2}(k', k, \phi)
\end{aligned} \tag{2.C.10}$$

These three results have immediate implications for the $I^{n\ell}$ terms. First $I^{1\ell}(\mathbf{k}, \mathbf{k}', s) = e^{i\phi} I^{1\ell}(k, k', \phi, s)$ where $I^{1\ell}(k, k', \phi, s) = V_{\lambda, \lambda'}(k, k', \phi, s) + V_{\lambda, \lambda'}(k, k', \phi + \pi, s)$ and $V_{\lambda, \lambda'}(k, k', \phi) = V_{\lambda, \lambda, \lambda', \lambda'}(k, k', \phi)$. Next we have for $I^{2\ell}$

$$\begin{aligned}
I^{2\ell}(\mathbf{k}, \lambda, s) &= e^{-i\theta_{\mathbf{k}}} \sum_{\mu_1, \mu_2} \int_{>} \frac{d^2 \mathbf{p}}{(2\pi)^2} \left(\frac{1 - n_f(E_{\mathbf{p}, \mu_2}) - n_f(E_{\mathbf{p}, \mu_1})}{E_{\mathbf{p}, \mu_2} + E_{\mathbf{p}, \mu_1}} \right) |w_{\mu_2, \mu_1}(\mathbf{p}, -\mathbf{p})| \\
&\times (V_{\lambda, \lambda, \mu_1, \mu_2}(k, p, \theta_{\mathbf{p}} - \theta_{\mathbf{k}}) + V_{\lambda, \lambda, \mu_1, \mu_2}(k, p, \theta_{\mathbf{p}} - \theta_{\mathbf{k}} + \pi))
\end{aligned} \tag{2.C.11}$$

shifting $\theta_{\mathbf{p}} \rightarrow \theta_{\mathbf{p}} + \theta_{\mathbf{k}}$ above then gives $I^{2\ell}(\mathbf{k}, \lambda, s) = e^{-i\theta_{\mathbf{k}}} I_{\lambda}^{2\ell}(k, s)$. Finally we have

$$\begin{aligned}
I^{3\ell}(\mathbf{k}, \mathbf{k}', \lambda, \lambda', s) &= -e^{i(\theta_{\mathbf{k}'} - \theta_{\mathbf{k}})} \sum_{\mu_1, \mu_2} \int_{>} \frac{d^2\mathbf{p}}{(2\pi)^2} \left(\frac{1 - n_f(E_{\mathbf{p}, \mu_2}) - n_f(E_{\mathbf{p}, \mu_1})}{E_{\mathbf{p}, \mu_2} + E_{\mathbf{p}, \mu_1}} \right) \\
&\times (V_{\lambda, \lambda, \mu_1, \mu_2}(k, p, \theta_{\mathbf{p}} - \theta_{\mathbf{k}}) + V_{\lambda, \lambda, \mu_1, \mu_2}(k, p, \theta_{\mathbf{p}} - \theta_{\mathbf{k}} + \pi)) \\
&\times (V_{\lambda, \lambda, \mu_1, \mu_2}(k', p, \theta_{\mathbf{p}} - \theta_{\mathbf{k}'}) + V_{\lambda, \lambda, \mu_1, \mu_2}(k', p, \theta_{\mathbf{p}} - \theta_{\mathbf{k}'} + \pi))^*
\end{aligned} \tag{2.C.12}$$

Shifting $\theta_{\mathbf{p}} \rightarrow \theta_{\mathbf{p}} + \theta_{\mathbf{k}'}$ above then immediately gives $I^{3\ell}(\mathbf{k}, \mathbf{k}', \lambda, \lambda', s) = -e^{i(\theta_{\mathbf{k}'} - \theta_{\mathbf{k}})} I_{\lambda, \lambda'}^{3\ell}(k, k', \phi, s)$.

By using the above results we can obtain a simplified continuum limit version of Eq.

(2.B.15) which is given as follows

$$\begin{aligned}
V'_{\lambda, \lambda'}(k, k', \phi, \Lambda, s) &= \frac{U}{N} e^{i\phi} \lambda \lambda' F_{\lambda, \lambda}(k, k) F_{\lambda', \lambda'}(k', k') \\
&\times \left(1 - \frac{U}{2} P(\Lambda, s) + \frac{U^2}{4} P^2(\Lambda, s) - \frac{U^3}{8} P^3(\Lambda, s) - \frac{U^3}{64} \hat{P}(\Lambda, s) \right) \\
&- \frac{U^3 e^{i\phi}}{128N} (\lambda' F_{\lambda', \lambda'}(k', k') I_{\lambda}^{2\ell}(k) + \lambda F_{\lambda, \lambda}(k, k) (I_{\lambda'}^{2\ell}(k'))^*) (1 - UP(\Lambda, s)) \\
&+ \frac{U^2}{64N} e^{i\phi} I_{\lambda, \lambda'}^{1\ell}(k, k', \phi) - \frac{U^4}{2^{11}N} e^{i\phi} I_{\lambda, \lambda'}^{3\ell}(k, k', \phi)
\end{aligned} \tag{2.C.13}$$

We see that V' depends only on the relative angle ϕ , as is to be expected. We proceed to

write $V'_{\lambda, \lambda'}(k, k', \phi, \Lambda, s) = \frac{e^{i\phi} U}{N} v'_{\lambda, \lambda'}(k, k', \phi, \Lambda, s)$.

2.C.3 Evaluation of Integrals

We now work to evaluate, or approximately evaluate, the integrals above. The first integral

we focus on is $P(\Lambda, s)$. We have

$$\begin{aligned}
P(\Lambda, s) &= \sum_{\lambda_5, \lambda_6} \int_{>} \frac{d^2\mathbf{p}}{(2\pi)^2} \left(\frac{1 - n_F(E_{\mathbf{p}, \lambda_5}) - n_F(E_{\mathbf{p}, \lambda_6})}{E_{\mathbf{p}, \lambda_5} + E_{\mathbf{p}, \lambda_6}} \right) \\
&\times |w_{\lambda_5, \lambda_6}(-\mathbf{p}, \mathbf{p})|^2
\end{aligned} \tag{2.C.14}$$

where the ‘>’ means *both* $E_{\mathbf{p},\lambda_5}$ and $E_{\mathbf{p},\lambda_6}$ must lie in the fast mode range $\Lambda/s < |E_\lambda(p)| < \Lambda$. We set $\lambda_6 = \lambda_5$ in the above for the following reason. The \mathbf{p} integral is limited to values in \mathbf{p} -space where both bands lie in the fast mode range. For two different bands, *i.e.* $\lambda_5 \neq \lambda_6$ the small window of \mathbf{p} values for which $E_{\mathbf{p},\lambda_5}$ and $E_{\mathbf{p},\lambda_6}$ are in the fast range will in general be different. To simplify our calculation we assume that there is no overlap between these two regions and thus set $\lambda_6 = \lambda_5$. The next simplification we make has to do with what part of the above integral we are interested in. We are interested in terms that diverge as we send $s \rightarrow \infty$ [26]. The term $|w_{\lambda_5,\lambda_5}(-\mathbf{p}, \mathbf{p})|^2$ is regular as \mathbf{p} approaches a Fermi wave vector and so in order to simplify matters we set $|w_{\lambda_5,\lambda_5}(-\mathbf{p}, \mathbf{p})|^2 = |w_{\lambda_5,\lambda_6}(k_f^{\lambda_5}, k_f^{\lambda_5})|^2 = (2\lambda_5 F_{\lambda_5,\lambda_5})^2 = F_{\lambda_5}^2$ where we have defined $F_{\lambda_5} = 2\lambda_5 F_{\lambda_5,\lambda_5}$. This leaves

$$P(\Lambda, s) = \sum_{\lambda_5} F_{\lambda_5}^2 \int_{>} \frac{d^2\mathbf{p}}{(2\pi)^2} \left(\frac{1 - 2n_F(E_{\mathbf{p},\lambda_5})}{2E_{\mathbf{p},\lambda_5}} \right) \quad (2.C.15)$$

Now using the usual set of approximations for integrals of this type we set $\int_{>} \frac{d^2\mathbf{p}}{(2\pi)^2} \left(\frac{1 - 2n_F(E_{\mathbf{p},\lambda_5})}{2E_{\mathbf{p},\lambda_5}} \right) = N_{\lambda_5} \int_{>} dE \left(\frac{1 - 2n_F(E)}{2E} \right) = N_{\lambda_5} \ln(s)$ where N_{λ_5} is the density of states at the Fermi surface.

Thus

$$P(\Lambda, s) = \sum_{\lambda_5} F_{\lambda_5}^2 N_{\lambda_5} \ln(s) \equiv p \ln(s) \quad (2.C.16)$$

where $p = \sum_{\lambda_5} F_{\lambda_5}^2 N_{\lambda_5}$. Next we work on simplifying $I^{2\ell}(k, \lambda, s)$. It is given by

$$\begin{aligned} I_\lambda^{2\ell}(k, s) &= \sum_{\mu_1, \mu_2} \int_{>} \frac{d^2\mathbf{p}}{(2\pi)^2} \left(\frac{1 - n_f(E_{\mathbf{p},\mu_2}) - n_f(E_{\mathbf{p},\mu_1})}{E_{\mathbf{p},\mu_2} + E_{\mathbf{p},\mu_1}} \right) |w_{\mu_2, \mu_1}(\mathbf{p}, -\mathbf{p})|^2 \\ &\times (V_{\lambda, \lambda, \mu_1, \mu_2}(k, p, \theta_{\mathbf{p}}, s) + V_{\lambda, \lambda, \mu_1, \mu_2}(k, p, \theta_{\mathbf{p}} + \pi, s)) \end{aligned} \quad (2.C.17)$$

Again we argue that because of the restriction on the states $E_{\mathbf{p},\mu_2}$ and $E_{\mathbf{p},\mu_1}$ to be fast modes we must set $\mu_1 = \mu_2$. Further, only considering the part of the integral divergent as $s \rightarrow \infty$

while setting all other values of \mathbf{p} to lie on the Fermi surface gives

$$I_{\lambda}^{2\ell}(k, s) = \ln(s) \sum_{\mu} F_{\mu} N_{\mu} \quad (2.C.18)$$

$$\times \int_0^{2\pi} \frac{d\theta_{\mathbf{p}}}{2\pi} I_{\lambda, \mu}^{1\ell}(k, k_f^{\mu}, \theta_{\mathbf{p}}, s)$$

Taking the same steps with $I_{\lambda, \lambda'}^{3\ell}(k, k', \phi, s)$ gives us

$$I_{\lambda, \lambda'}^{3\ell}(k, k', \phi, s) = \ln(s) \sum_{\mu} N_{\mu} \int_0^{2\pi} \frac{d\theta_{\mathbf{p}}}{2\pi} \quad (2.C.19)$$

$$I_{\lambda, \mu}^{1\ell}(k, k_f^{\mu}, \theta_{\mathbf{p}} + \phi, s) (I_{\lambda', \mu}^{1\ell}(k', k_f^{\mu}, \theta_{\mathbf{p}}, s))^*$$

In order to simplify the above it becomes useful to Fourier transform $I_{\lambda, \mu}^{1\ell}(k, k', \theta)$ as follows

$$I_{\lambda, \mu}^{1\ell}(k, k', \theta, s) = \sum_{m_z} e^{im_z \theta} v_{\lambda, \mu}^{m_z}(k, k', s) \quad (2.C.20)$$

Then $I_{\lambda}^{2\ell}(k, s) = \ln(s) \sum_{\mu} F_{\mu} N_{\mu} v_{\lambda, \mu}^0(k, k', s)$ and also

$$I_{\lambda, \lambda'}^{3\ell}(k, k', \phi, s) = \ln(s) \sum_{\mu, m_z} e^{im_z \phi} N_{\mu} v_{\lambda, \mu}^{m_z}(k, k_f^{\mu}, s) (v_{\lambda', \mu}^{m_z}(k', k_f^{\mu}, s))^* \quad (2.C.21)$$

Finally we work at simplifying $\hat{P}(\Lambda, s)$. Making our usual set of simplifying assumptions we have

$$\hat{P}(\Lambda, s) = -e^{i(\theta_{\mathbf{k}'} - \theta_{\mathbf{k}})} \ln^2(s) \sum_{\mu, \nu} N_{\nu} F_{\nu} N_{\mu} F_{\mu} \int_0^{2\pi} \quad (2.C.22)$$

$$\frac{d\theta_{\mathbf{p}_1}}{2\pi} \int_0^{2\pi} \frac{d\theta_{\mathbf{p}_3}}{2\pi} V_{\mu, \nu}(k_f^{\mu}, k_f^{\nu}, \theta_{\mathbf{p}_3} - \theta_{\mathbf{p}_1} - \pi, s)$$

If we redefine the angles $\Theta = (\theta_{\mathbf{p}_1} + \theta_{\mathbf{p}_3})/2$ and $\theta = \theta_{\mathbf{p}_3} - \theta_{\mathbf{p}_1}$ we immediately obtain

$$\begin{aligned} \hat{P}(\Lambda, s) &= -\frac{1}{2} e^{i(\theta_{\mathbf{k}'} - \theta_{\mathbf{k}})} \ln^2(s) \\ &\times \sum_{\mu, \nu} N_\nu F_\nu N_\mu F_\mu v_{\mu, \nu}^0(k_f^\mu, k_f^\nu, s) \end{aligned} \quad (2.C.23)$$

Reflecting on the above we see that all of the integrals of interest in our 3-loop expansion of the effective interaction simplify to terms involving the single integral $v_{\mu, \nu}^{m_z}(k, k', s)$. The expression for this term is as follows

$$\begin{aligned} v_{\mu, \nu}^{m_z}(k, k', s) &= \sum_{\lambda_5, \lambda_6} \int_0^{2\pi} \frac{d\phi}{2\pi} e^{-im_z \phi} \int_{>} \frac{d^2 \mathbf{p}}{(2\pi)^2} \\ &\left(\frac{n_F(E_{\lambda_5}(p)) - n_F(E_{\lambda_6}(q))}{E_{\lambda_5}(p) - E_{\lambda_6}(q)} \right) \mathcal{F}_{\mu, \nu, \lambda_5, \lambda_6}(k, k', \mathbf{p}, \phi) \end{aligned} \quad (2.C.24)$$

where $\mathcal{F}_{\lambda, \lambda', \lambda_5, \lambda_6}(k, k', \mathbf{p}, \phi) = \mathcal{F}_{\lambda, \lambda, \lambda', \lambda', \lambda_5, \lambda_6}(k, k', \mathbf{p}, \phi)$. The above function is normal as we let $s \rightarrow \infty$ and so for our purposes it is sufficient to replace it with its $s \rightarrow \infty$ counterpart [15, 16, 26, 27]. Further as we are only interested in incoming/outgoing momenta on the Fermi surface(s) we set k and k' appropriately. Defining $v_{\mu, \nu}^{m_z} = v_{\mu, \nu}^{m_z}(k_f^\mu, k_f^\nu, s \rightarrow \infty)$ we have

$$\begin{aligned} v_{\mu, \nu}^{m_z} &= \sum_{\lambda_5, \lambda_6} \int_0^{2\pi} \frac{d\phi}{2\pi} e^{-im_z \phi} \int \frac{d^2 \mathbf{p}}{(2\pi)^2} \\ &\left(\frac{n_F(E_{\lambda_5}(p)) - n_F(E_{\lambda_6}(q))}{E_{\lambda_5}(p) - E_{\lambda_6}(q)} \right) \mathcal{F}_{\mu, \nu, \lambda_5, \lambda_6}(k_f^\mu, k_f^\nu, \mathbf{p}, \phi) \end{aligned} \quad (2.C.25)$$

where the restriction on the integral in V has been dropped because as $s \rightarrow \infty$ all momenta satisfy $\Lambda/s < |E_{\lambda_5}(p)| < \Lambda$.

2.C.4 Flow Equations

By using the above results we can write the following

$$\begin{aligned}
v'_{\lambda,\lambda'}(s, \phi) &= \frac{UF_\lambda F_{\lambda'}}{4} \left(1 - \frac{Up}{2} \ln(s) + \frac{U^2 p^2}{4} \ln^2(s) - \frac{U^3 p^3}{8} \ln^3(s) \right) + \frac{U^4 F_\lambda F_{\lambda'}}{256} \sum_{\mu,\nu} N_\mu F_\mu v_{\mu,\nu}^0 N_\nu F_\nu \\
&- \frac{U^3}{256} \ln(s) \left(F_\lambda \sum_{\mu} F_\mu N_\mu v_{\mu,\lambda'}^0 + F_{\lambda'} \sum_{\mu} v_{\lambda,\mu}^0 F_\mu N_\mu \right) (2 - Up \ln(s)) \\
&+ \frac{U^2}{64} \sum_{m_z} e^{im_z \phi} v_{\lambda,\lambda'}^{m_z} - \ln(s) \frac{U^4}{2^{11}} \sum_{\mu, m_z} e^{im_z \phi} N_\mu v_{\lambda,\mu}^{m_z} v_{\mu,\lambda'}^{m_z}
\end{aligned} \tag{2.C.26}$$

where in the above m_z denotes an integer value, k_f^λ is the Fermi wave vector magnitude for the λ band, and we recall that we have defined $F_\lambda = 2\lambda F_{\lambda,\lambda}(k_f^\lambda, k_f^\lambda)$, and $p = \sum_{\mu} N_\mu F_\mu^2$.

We first consider the RG flow of the $m_z \neq 0$ channel which is given by

$$v'_{\lambda,\lambda'}(s, m_z) = \frac{U^2}{64} v_{\lambda,\lambda'}^{m_z} - \ln(s) \frac{U^4}{2^{11}} \sum_{\mu} N_\mu v_{\lambda,\mu}^{m_z} v_{\mu,\lambda'}^{m_z} \tag{2.C.27}$$

To obtain a beta function from the above expression we follow the method proposed by Raghu *et al*[26] and further employed by Vafeek and Wang[15, 16]. To this end we define the g matrix $g_{\nu,\mu}(s, m_z) = \frac{U^2}{2^6} \sqrt{N_\nu N_\mu} v_{\nu,\mu}(s, m_z)$ from which we obtain

$$\begin{aligned}
g'_{\lambda,\lambda'}(s, m_z) &= g_{\lambda,\lambda'}(m_z) \\
&- 2 \ln(s) \sum_{\mu} g_{\lambda,\mu}(m_z) g_{\mu,\lambda'}(m_z)
\end{aligned} \tag{2.C.28}$$

We note that the couplings of a certain angular momentum channel is renormalized only by couplings in the same angular momentum channel. This behaviour is exact within our treatment of the continuum limit and keeping only the most divergent terms. This is rooted in the fact that our continuum limit approximation leads to an interaction term which is only

a function of the angle between the incoming and outgoing momenta (namely $\phi = \theta_{\mathbf{k}} - \theta_{\mathbf{k}'}$). After summing up diagrams we obtain only terms that are independent of ϕ , terms that only depend on one power of a function of ϕ or a convolution of functions of ϕ . This leads to a beta-function whose most divergent terms decouple in this way[15, 25–27].

The matrix $v_{\nu,\mu}(s, m_z)$ is Hermitian (as we will show in a later section of this appendix) and thus so is g . We can then diagonalize g as follows

$$g_{\nu,\mu}(m_z) = \sum_i \lambda_i^{m_z}(1) \psi_{i,\nu}^* \psi_{i,\mu} \quad (2.C.29)$$

where $\lambda^i(1)$ are the eigenvalues of $g_{\nu,\mu}(m_z)$ and $\psi_{i,\mu}$ is a vector whose columns are the (complete and orthonormal) eigenvectors of g . Using this in the above we then have

$$g'_{\lambda,\lambda'}(s, m_z) = \sum_i \psi_{i,\lambda}^* (\lambda_i^{m_z}(1) - 2 \ln(s) (\lambda_i^{m_z}(1))^2) \psi_{i,\lambda'} \quad (2.C.30)$$

The above tells that $g'_{\lambda,\lambda'}(s, m_z)$ is also diagonalized by this transformation and we obtain the result for the evolution of the eigenvalues of $g'_{\lambda,\lambda'}(m_z)$ under renormalization

$$\lambda_i^{m_z}(s) = \lambda_i^{m_z}(1) - 2 \ln(s) (\lambda_i^{m_z}(1))^2 \quad (2.C.31)$$

The beta function for λ_i is now obtained[15, 16, 26] by taking the derivative of the above with respect to $\ln(s)$ which gives

$$\frac{d\lambda_i^{m_z}(s)}{d \ln(s)} = -2(\lambda_i^{m_z}(1))^2 = -2(\lambda_i^{m_z}(s))^2 \quad (2.C.32)$$

where the second equality holds up to $\mathcal{O}(U^4)$. The solution to the above beta function is then

$$\lambda_i^{m_z}(s) = \frac{\lambda_i^{m_z}(1)}{1 + 2\lambda_i^{m_z}(1) \ln(s)} \quad (2.C.33)$$

Next we move on to the flow of the $m_z = 0$ channel. The equation for the renormalized $v'_{\lambda,\lambda'}(s, m_z = 0)$ is much more complicated than its $m_z \neq 0$ counterpart. In order to obtain a flow equation one defines the matrix $g_{\lambda,\lambda'}(0) = \sqrt{N_\lambda N_{\lambda'}} \left(\frac{UF_\lambda F_{\lambda'}}{4} + \frac{U^2}{2^6} v_{\lambda,\lambda'}(s, 0) \right)$ along with $g'_{\lambda,\lambda'}(s, 0) = \sqrt{N_\lambda N_{\lambda'}} v'_{\lambda,\lambda'}(s, 0)$ in order to find the following result which is valid up to $\mathcal{O}(U^4)$

$$\begin{aligned}
 g'_{\lambda,\lambda'}(s, 0) &= g_{\lambda,\lambda'}(0) - 2 \ln(s) \sum_{\mu} g_{\lambda,\mu}(0) g_{\mu,\lambda'}(0) & (2.C.34) \\
 &+ 4 \ln^2(s) \sum_{\mu,\nu} g_{\lambda,\mu}(0) g_{\mu,\nu}(0) g_{\nu,\lambda'}(0) \\
 &- 8 \ln^3(s) \sum_{\mu,\nu,\rho} g_{\lambda,\mu}(0) g_{\mu,\nu}(0) g_{\nu,\rho}(0) g_{\rho,\lambda'}(0)
 \end{aligned}$$

We now diagonalize $g_{\lambda,\lambda'}(0)$ and find that in the new basis $g'_{\lambda,\lambda'}(s, 0)$ is diagonal as well. This gives the result for the eigenvalues

$$\begin{aligned}
 \lambda'_i(s) &= \lambda_i^0(1) \sum_n (-2 \ln(s) (\lambda_i^0(1)))^n & (2.C.35) \\
 &\simeq \frac{\lambda_i(0)}{1 + 2\lambda_i(0) \ln(s)}
 \end{aligned}$$

Taking the derivative of the above gives the beta function

$$\frac{d\lambda_i^0(s)}{d \ln(s)} = -2(\lambda_i^0(s))^2 \quad (2.C.36)$$

the same as that for the $m_z \neq 0$ result but with a different initial condition[15, 16].

2.C.5 Hermiticity of $v_{\nu,\mu}(s, m_z)$

It is tedious but straightforward to show that $\mathcal{F}_{\mu,\nu,\lambda_5,\lambda_6}^*(k_f^\mu, k_f^\nu, \mathbf{p}, \phi) = \mathcal{F}_{\nu,\mu,\lambda_5,\lambda_6}(k_f^\nu, k_f^\mu, \mathbf{p}, -\phi)$.

From this property it follows that

$$\begin{aligned} (v_{\mu,\nu}^{m_z})^* &= \sum_{\lambda_5,\lambda_6} \int_0^{2\pi} \frac{d\phi}{2\pi} e^{im_z\phi} \int \frac{d^2\mathbf{p}}{(2\pi)^2} \\ &\times \left(\frac{n_F(E_{\lambda_5}(p)) - n_F(E_{\lambda_6}(q))}{E_{\lambda_5}(p) - E_{\lambda_6}(q)} \right) \mathcal{F}_{\nu,\mu,\lambda_5,\lambda_6}(k_f^\nu, k_f^\mu, \mathbf{p}, -\phi) \end{aligned} \quad (2.C.37)$$

We can then send $\phi \rightarrow -\phi$ and then, as everything in the integrand depends on ϕ through either $e^{i\phi}$ or $\cos(\phi)$ we can shift $\phi \rightarrow \phi + 2\pi$. From this we immediately obtain $(v_{\mu,\nu}^{m_z})^* = v_{\nu,\mu}^{m_z}$. This is important because it ensures that $v_{\nu,\mu}^{m_z}$ and thus the g 's defined above can be diagonalized by a unitary transformation.

References

- ¹A. Farrell and T. Pereg-Barnea, *Phys. Rev. B* **87**, 214517 (2013).
- ²V. Mourik, K. Zuo, S. M. Frolov, S. R. Plissard, E. P. A. M. Bakkers, and L. P. Kouwenhoven, *Science* **336**, 1003–1007 (2012).
- ³A. Das, Y. Ronen, Y. Most, Y. Oreg, M. Heiblum, and H. Shtrikman, *Nature Physics* **8**, 887–6895 (2012).
- ⁴E. J. H. Lee, X. Jiang, M. Houzet, R. Aguado, C. M. Lieber, and S. De Franceschi, *Nat Nano* **9**, 79 (2014).
- ⁵N. Read and D. Green, *Phys. Rev. B* **61**, 10267 (2000).
- ⁶V. Gurarie and L. Radzihovsky, *Phys. Rev. B* **75**, 212509 (2007).
- ⁷L. Fu and C. L. Kane, *Phys. Rev. Lett.* **100**, 096407 (2008).
- ⁸J. Alicea, *Phys. Rev. B* **81**, 125318 (2010).
- ⁹J. D. Sau, R. M. Lutchyn, S. Tewari, and S. Das Sarma, *Phys. Rev. Lett.* **104**, 040502 (2010).
- ¹⁰R. Lutchyn, J. Sau, and S. Das Sarma, *Phys. Rev. Lett.* **105**, 077001 (2010).
- ¹¹Y. Oreg, G. Refael, and F. von Oppen, *Phys. Rev. Lett.* **105**, 177002 (2010).
- ¹²A. Cook and M. Franz, *Phys. Rev. B* **84**, 201105 (2011).
- ¹³J. Klinovaja, S. Gangadharaiah, and D. Loss, *Phys. Rev. Lett.* **108**, 196804 (2012).
- ¹⁴J. Linder, Y. Tanaka, T. Yokoyama, A. Sudbø, and N. Nagaosa, *Phys. Rev. Lett.* **104**, 067001 (2010).
- ¹⁵O. Vafek and L. Wang, *Phys. Rev. B* **84**, 172501 (2011).
- ¹⁶L. Wang and O. Vafek, *Physica C: Superconductivity* **497**, 6–18 (2014).
- ¹⁷D. J. Scalapino, *Physics Reports* **250**, 329 (1995).

-
- ¹⁸D. Scalapino, *Journal of Superconductivity and Novel Magnetism* **19**, 195–200 (2006).
- ¹⁹P. Corboz, T. M. Rice, and M. Troyer, *Phys. Rev. Lett.* **113**, 046402 (2014).
- ²⁰A. Farrell and T. Pereg-Barnea, *Phys. Rev. B* **89**, 035112 (2014).
- ²¹L. P. Gor'kov and E. I. Rashba, *Phys. Rev. Lett.* **87**, 037004 (2001).
- ²²M. Sato, Y. Takahashi, and S. Fujimoto, *Phys. Rev. B* **82**, 134521 (2010).
- ²³A. Farrell, P. K. Wu, Y. J. Kao, and T. Pereg-Barnea, arXiv:1308.3724 (2014).
- ²⁴B. A. Bernevig, T. L. Hughes, and S. C. Zhang, *Science* **314**, 1757 (2006).
- ²⁵R. Shankar, *Rev. Mod. Phys.* **66**, 129–192 (1994).
- ²⁶S. Raghu, S. A. Kivelson, and D. J. Scalapino, *Phys. Rev. B* **81**, 224505 (2010).
- ²⁷S. Raghu and S. A. Kivelson, *Phys. Rev. B* **83**, 094518 (2011).
- ²⁸P. Ghosh, J. D. Sau, S. Tewari, and S. Das Sarma, *Phys. Rev. B* **82**, 184525 (2010).
- ²⁹C. L. Kane and E. J. Mele, *Phys. Rev. Lett.* **95**, 146802 (2005).
- ³⁰C. L. Kane and E. J. Mele, *Phys. Rev. Lett.* **95**, 226801 (2005).
- ³¹S. Tewari, T. D. Stanescu, J. Sau, and S. Das Sarma, *New J. Phys.* **13**, 065004 (2011).

Preface to Chapter 3

The previous manuscript concludes our study of driving a topological superconducting state. It has established that a Zeeman field may be used to create Majorana modes in a system of interacting, spin-orbit coupled electrons. We now move on to the second system of interest in this thesis, topological insulators. In particular, we take aim at topological insulators in the presence of time-periodic perturbations.

The primary motivation for this line of work comes from Lindner *et al* [1] who established that time-periodic perturbations may be used to drive a topological insulating state in a system where this phase is not occurring in equilibrium. This represents the creation of a topological state with an external field.

Our work was started by an interest in understanding how the properties of edge-states created by a time-periodic drive differ from those that occur in an equilibrium system. To begin this investigation we decided to first determine how time-periodic perturbations can be used to manipulate the edge-states in an equilibrium topological insulator. This question is the primary focus of the following manuscript.

Photon Inhibited Topological Transport in Quantum Well Heterostructures

Aaron Farrell¹ and T. Pereg-Barnea¹

¹Department of Physics and the Centre for Physics of Materials, McGill University, Montreal, Quebec, Canada H3A 2T8

This chapter has been published in Physical Review Letters. Journal Reference: Physical Review Letters, 115, 106403-106407 (2015)

Abstract

Here we provide a picture of transport in quantum well heterostructures with a periodic driving field in terms of a probabilistic occupation of the topologically protected edge states in the system. This is done by generalizing methods from the field of photon assisted tunneling. We show that the time dependent field *dresses* the underlying Hamiltonian of the heterostructure and splits the system into side-bands. Each of these sidebands is occupied with a certain probability which depends on the drive frequency and strength. This leads to a reduction in the topological transport signatures of the system because of the probability to absorb/emit a photon. Therefore when the voltage is tuned to the bulk gap the conductance is smaller than the expected $2e^2/h$. We refer to this as photon inhibited topological transport. Nevertheless, the edge modes reveal their topological origin in the robustness of the edge conductance to disorder and changes in model parameters. In this work the analogy with photon assisted tunneling allows us to interpret the calculated conductivity and explain the sum rule observed by previous authors[2]

3.1 Introduction

Topological states of matter are currently at the forefront of research in condensed matter physics. From the quantum hall effect to topological superconductors, these states are of interest for a variety of reasons. In topological insulators the in-gap edge states are of primary interest. These states are topologically protected, meaning they are insensitive to deformations of the Hamiltonian's parameters that leave the topological gap intact and the effects of disorder. The existence of such states provides a physical signature of the topology in the charge and spin conductance.

Recently, there has been a growing amount of attention paid to the generation and/or manipulation of topological states of matter through the application of a time-periodic perturbation[1–20]. Experimental progress in this direction has been made in both photonic crystals[21] and in a solid-state context in Bi_2Se_3 [22]. In the Letter we study how a time-periodic perturbation can be used to manipulate the transport properties of a quantum spin Hall insulator. For example: such a system is expected to have a two terminal conductivity of $2e^2/h$ in equilibrium. With the application of a time-periodic field, we find that this value may be reduced significantly. Despite this reduction and a deviation from quantized units of e^2/h , we find that this conductivity is still topological in the sense that it is robust to disorder, system size changes, and gap-conserving deformations of the Hamiltonian. Furthermore, we describe a method to predict the degree of these deviations quantitatively, and their dependence on the drive strength and frequency.

To understand how this reduction in the conductivity can be tuned and why it appears to be topologically robust, we have developed an understanding by generalizing the viewpoint of photon assisted tunneling[23, 24]. We find that the periodic perturbation has a two-pronged effect. First, it “dresses” the original static Hamiltonian and second, it causes the edge conductance channels to only be occupied probabilistically upon the injection of a lead electron. This is because electrons tunneling into the system can absorb/emit a photon.

In this sense, the presence of the photons inhibit the topological transport properties of the system. This description not only accounts for the reduction of the conductivity, but also explains why its values are topological in nature. This interpretation will be important for transport experiments in Floquet topological insulators. It provides an explanation of why the conductivity isn't quantized as well as shows that the conductivity can potentially be tuned predictably in the lab.

3.2 Methods

As a model system we take the quantum well heterostructures that play host to the quantum spin Hall effect. We apply a time dependent field and allow for on-site disorder. Our Hamiltonian is as follows

$$H_S = H_{QW} + H_{disorder} + H_{ext}(t) \quad (3.2.1)$$

where $H_{QW} = \sum_{\mathbf{k}} \psi_{\mathbf{k}}^\dagger \begin{pmatrix} \hat{H}(\mathbf{k}) & 0 \\ 0 & \hat{H}^*(-\mathbf{k}) \end{pmatrix} \psi_{\mathbf{k}}$ where $\psi_{\mathbf{k}}^\dagger$ is a four component creation operator for electrons at momenta \mathbf{k} in state $m_J = (1/2, 3/2, -1/2, -3/2)$ of the clean heterostructure and $\hat{H}(\mathbf{k}) = \epsilon_{\mathbf{k}} \sigma_0 + \mathbf{d}(\mathbf{k}) \cdot \boldsymbol{\sigma}$, with $\boldsymbol{\sigma}$ being a vector of Pauli matrices. In the typical language of these structures[25, 26], we take $\mathbf{d}(\mathbf{k}) = (A \sin k_x, A \sin k_y, M - 4B + 2B(\cos k_x + \cos k_y))$ and $\epsilon_{\mathbf{k}} = C - 2D(2 - \cos k_x - \cos k_y)$. In order to focus on transport without additional complications we follow Lindner and coworkers[1] and set $C = D = 0$, $A = B = 0.2|M|$. All energies are in units of M . As we are interested in a ‘‘topological’’ system we take $M = 1$ so that $\text{sgn}(M/B) = 1$ [1, 25].

Next, $H_{ext}(t) = 2(\mathbf{V} \cdot \boldsymbol{\sigma}) \cos \Omega t$ is an electromagnetic field polarized in the direction \mathbf{V} [1, 12, 27, 28]. For concreteness, we will take $\mathbf{V} = V_{ext} \hat{z}$; although this is not necessary for what follows. In short, the main results of this chapter hold regardless of the direction

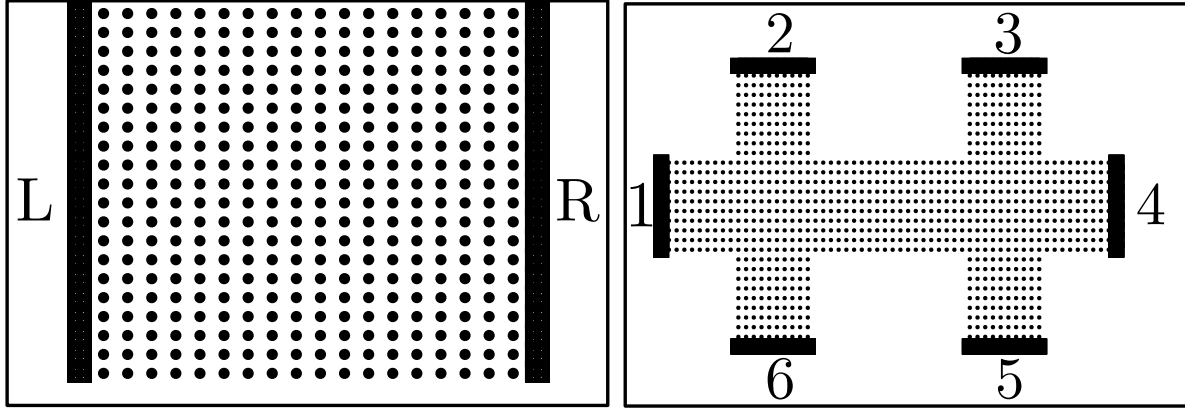


Figure 3.1: The two device geometries considered in this work. Left is a two-terminal device labeled with leads left ('L'), and right ('R'). On the right is a six terminal device labeled with leads 1 through 6. The sites coupled to leads have a solid rectangle around them.

we take for V ; it is the effective Hamiltonian that will be modified. Note $H_{ext}(t)$ obeys the periodic generalization of time-reversal invariance[1] $\mathcal{T}H_{ext}(t)\mathcal{T}^{-1} = H_{ext}(-t + \tau)$ for some τ and \mathcal{T} is the time-reversal operator. Finally, $H_{disorder} = -\sum_{i,\alpha} w_i \psi_{i,\alpha}^\dagger \psi_{i,\alpha}$ (with ψ_i^\dagger the Fourier transform of ψ_k^\dagger). This corresponds to charge impurities (disorder) changing the chemical potential on each site by w_i . We draw the $\{w_i\}$ randomly from an evenly distributed sample between $-W/2$ and $W/2$. We call W the disorder strength.

Our numerical study employs the Floquet-Landauer formalism[2, 7, 29, 30]. Here we imagine the system attached to a series of leads. The coupling strength of each lead to the system is characterized by a lead coupling Γ_λ where λ labels the lead. These couplings have a two-fold effect: (1) They add an imaginary self-energy $i\Gamma/2 = \frac{i}{2} \sum_\lambda \Gamma_\lambda$ to the system, and (2) they quantitatively determine the tunneling amplitude to/from the respective leads. Similar to Ref. [7], we consider two different device geometries (see Fig. 3.1). First, we consider a two-terminal device with the left and right end of the system attached to leads whose Fermi level lies at the "lead energy" E with a slight offset bias between the two leads [31]. In this set-up the quantity of interest is $\sigma(E)$, the differential conductivity given that the chemical potential of the leads is at energy E . For a spin Hall insulator (e.g. our model above) in equilibrium when the lead energy E in a two-terminal device

is tuned to lie in the gap (*i.e.* on the edge states), a value $\sigma(E) = 2e^2/h$ is expected[11, 34]. This is the first signature in which we are interested. For convenience, we define $\sigma_{TT} = \sigma(V \simeq 0)h/e^2$. Secondly, we consider a six-terminal device. This device allows us to probe whether the current is carried by bulk or edge modes[7, 35, 36]. In equilibrium, it is found that the only non-zero values of the transmission elements between leads λ and λ' , $T_{\lambda,\lambda'}(\epsilon)$ (with ϵ in the gap), come from tunneling between adjacent leads in the device. Thus $T_{\lambda,\lambda'}(\epsilon_F) = 0$, unless $\lambda = \lambda' \pm 1$ (where $6 + 1 \rightarrow 1$). Moreover, it is argued that $T_{\lambda,\lambda\pm 1}(\epsilon_F) = 1$ as, because of the helical edge states, a quasiparticle originating at lead λ *must* tunnel to one of the neighbouring leads. Later in this Letter we look for similar properties in the non-equilibrium system.

Before proceeding we comment on recent criticisms of Floquet states in periodically driven systems[37–40]. Floquet states are often thought of as the steady-states of a time-periodic system[41]. Refs. [37, 39, 40] argue that the long time evolution of an isolated, periodically driven system leads to an effectively infinite temperature state for some driving periods. Our formalism for calculating transport properties attaches leads to the system (*i.e.* it is not isolated anymore) and only makes assumptions about the state of the leads in the distant past, namely that the leads are in thermal equilibrium. No assumptions on the state of the system[31] in the distant past have been made. This assumption provides the state of the system at the present time and does not rely on “evolving” any particular Floquet state.

3.3 Transport Results

We begin with a clean system ($W = 0$) in a two terminal geometry. We fix $\Omega = 2.3|M|$, and tune V_{ext} . We plot σ_{TT} for $V_{ext} = 0|M|\dots|M|$ in Fig. 3.2. As V_{ext} is increased from zero, the quantization of σ_{TT} is lost. For moderately strong V_{ext} , we see that it reaches $\sigma_{TT} \sim 1.5$. This shows that for a quantum spin Hall insulator, the (bare) conductivity is

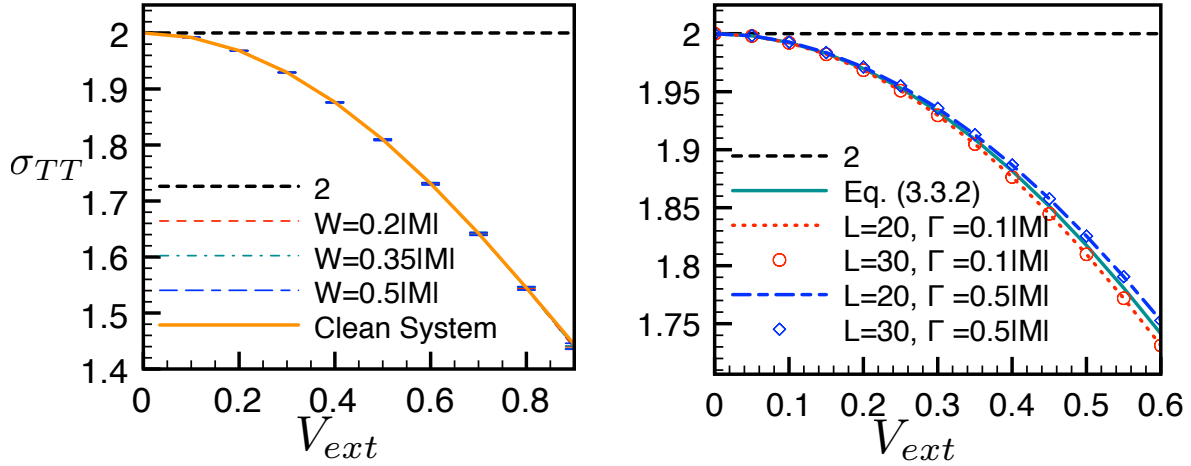


Figure 3.2: Plots of the differential two-terminal conductivity as a function of V_{ext} . Left: results for various disorder strengths, right: various values of the system size (L) and the lead coupling parameter (Γ).

not, in general, quantized to the traditional equilibrium value under the application of a periodic perturbation.

Looking again at Fig. 3.2, we see that these values are robust to the strength of the disorder potential. The deviation from the clean limit is insignificant, even up to disorder strengths of $M/2$. Additionally, these values are insensitive to the coupling strength of the system to the leads[31], Γ , and the system size. We have changed the coupling Γ over a range of values from $\Gamma \sim 0.05$ to $\Gamma \sim 1$. Breakdown on the lower bound can be attributed to the inability of electrons to enter the system from the leads, whereas breakdown at the higher bound adds a large self-energy to the system and causes a broadening of the edge-states into the bulk.

The robustness described above leaves the impression that despite the deviation of the conductivity from $\sigma_{TT} = 2$, the values it takes appear to be topologically protected. Our six-terminal calculations provide additional evidence of topological, edge conductance. With the lead energy set in the gap of the system, we find that $T_{\lambda,\lambda'} = 0$, except the off-diagonal elements $T_{\lambda,\lambda+1}$ and $T_{\lambda+1,\lambda}$. In contrast to equilibrium, we find that $T_{\lambda,\lambda+1} = T_{\lambda+1,\lambda} < 1$. In spite of this, we observe that the conduction takes place *only* between

adjacent leads suggesting that the current is only flowing on the edges.

To explain the above behavior, we borrow insight from the field of photon assisted tunneling (PAT). PAT, as first proposed by Tien and Gordon[23], was originally used to describe a superconducting-insulator-superconductor tunnel junction. When a periodic AC voltage V_{ac} is applied to one of the leads, the energy eigenstates of these leads split into sidebands at energy $E + n\hbar\Omega$ for integer n and driving frequency $\Omega = 2\pi/T$. The probability that each one of these side bands is occupied is given by $J_n^2(\alpha)$, where $\alpha = eV_{ac}/\hbar\Omega$, and J_n is the n^{th} Bessel function of the first kind. The consequence of this sideband splitting is that when a lead energy E , is applied across the tunnel junction, the electrons can tunnel into the system not just at energy E , but at $E + n\hbar\Omega$ with a probability of $J_n^2(\alpha)$. One interprets this as the electrons absorbing ($n > 0$) or emitting ($n < 0$) $|n|$ photons. As a result the conductivity in the driven system is given by $\sigma_{PAT}(E) = \sum_n J_n^2(\alpha)\sigma_0(E + n\hbar\Omega)$ [23, 24]. Here $\sigma_0(E)$ is the conductivity of the junction in the absence of the AC voltage.

Here we do not have a simple periodic modulation of the sample system, rather the modulation itself has some internal structure given by $\mathbf{V} \cdot \boldsymbol{\sigma}$. The result of this is that the system is not simply split into side-bands. The fact that $H_{ext}(t)$ does not commute with the static Hamiltonian, leads to interesting effects. In the case of off-resonant light (light where $\hbar\Omega$ does not connect parts of the clean, static spectrum), we can make some simplifying assumptions to obtain an effective description in line with PAT. We describe this simpler case here and leave the discussion of on-resonant light, where more care must be taken, for later[42].

In the field of Floquet topological insulators [2, 13–15, 30] with off-resonant light, it is known that one can think of the periodic perturbation as“dressing” the static system by modifying its underlying physical parameters to produce a new, effective *static* Hamiltonian. However, this approach is incomplete from a transport point of view. One must take into account the splitting of the states of this effective Hamiltonian into side-bands. Thus

off-resonant light has a two-sided effect: First, it dresses the static Hamiltonian to produce a new effective static Hamiltonian. Second, the eigenstates of this effective Hamiltonian are split into side-bands in a process analogous to PAT. This picture is not specific to the illustrative system we have chosen here, it is more general. It may be used, for example, to describe transport calculations in analogous systems like illuminated graphene.

To motivate this consider writing $|\psi(t)\rangle = U_V(t)|\hat{\psi}(t)\rangle$ where $i\hbar\frac{d}{dt}U_V(t) = H_{ext}(t)U_V(t)$. This transforms our problem into a new problem with the Hamiltonian $\hat{H}(t) = U_V^\dagger(t)HU_V(t)$, where H is the Hamiltonian in the absence of the time-dependent field. If $[H_{ext}(t), H] = 0$ then $\hat{H}(t) = H$ leading to an analogue of traditional PAT. Here $[H_{ext}(t), H] \neq 0$ in general and the transformation $U_V(t)$ leads to a new, time-dependent Hamiltonian. However, provided the mixing between bands is weak (off-resonant), it is possible to approximate $\hat{H}(t)$ by its time-averaged value. In the language of Floquet theory this amounts to the leading order term[30] in $\hat{H}(t)$ of the Floquet Hamiltonian $H_F = \frac{i}{T} \log \left[\mathbb{T} \left(e^{-i \int_0^T dt \hat{H}(t)} \right) \right]$, $\mathbb{T}(\cdot)$ denoting time ordering.

One can study the transport properties of this new effective Hamiltonian. This, however, will miss the unitary transformation that we have performed to get this Hamiltonian. Accounting for this transformation in a full transport calculation, in the approximation described above, we arrive at the following expression for the two-terminal conductivity of this system[31]

$$\sigma(E) = \sum_m J_m^2 \left(\frac{2V_{ext}}{\hbar\Omega} \right) \sigma_F(E + m\hbar\Omega) \quad (3.3.1)$$

where $\sigma_F(E)$ is the *static* differential conductivity of the dressed system described by H_F . For our current model, we have a finite band width and have not taken into account higher (or lower) energy bands. We assume the bands near the Fermi level are separated in energy from the other bands by a sufficient amount so that they can be neglected. Experimental validation of this comes from Ref. [22] where the experimental results can be understood by using only the bands near the Fermi level. As a result we have $\sigma_F(E + m\hbar\Omega) = \sigma_F(V)\delta_{m,0}$

for $E \simeq 0$; no states exist at $m\hbar\Omega$. Therefore, we have

$$\sigma(E) = J_0^2 \left(\frac{2V_{ext}}{\hbar\Omega} \right) \sigma_F(E) \quad (E \simeq 0) \quad (3.3.2)$$

Thus with an off resonant driving frequency, we describe the underlying system with an effective static Hamiltonian which may give rise to the signature transport properties. In the present case, we are interested in a Hamiltonian showcasing the quantum spin Hall effect. This state should have a two-terminal conductance of $2e^2/h$, and six-terminal transmission elements as described above. In the presence of a driving field, the in-gap edge states are only occupied with a certain probability due to the prospect of absorption/emission of photons. Thus, the transport property we are interested in only shows up with a certain probability. In the present case we expect $\sigma_F(V) = 2e^2/h$, and so the actual conductivity we measure will be $\sigma(E) = \frac{2e^2}{h} J_0^2 \left(\frac{2V_{ext}}{\hbar\Omega} \right)$. Plotting this against our numerical data produces excellent agreement (see Fig. 3.2). One may look at this expression as a correction to the quantized value of $2e^2/h$. One can show for in-gap energies E that $\sigma(E) \simeq \frac{2e^2}{h} \left(1 - \left(\frac{V_{ext}}{\hbar\Omega} \right)^2 \right)$, *i.e.* this correction is second order in $V_{ext}/\hbar\Omega$.

This explains our observation in the opening of this section. Despite the fact that we do not obtain the values $\sigma = 2e^2/h$, or $T_{\lambda,\lambda\pm 1} = 1$, the values that we do see are robust in the same way as the equilibrium values. The underlying system is topological in nature, with helical edge states that give rise to $2e^2/h$ conductance and $T_{\lambda,\lambda\pm 1} = 1$. However there is only a certain probability that the electrons tunneling from the leads are at the correct energy to take advantage of these channels. Thus, the presence of these photons in the system inhibits the ability of these edge channels to transport charge.

Our discussion so far has not relied on the fact that the original Hamiltonian is topological in nature, rather it is enough that the effective Hamiltonian be topological. In other systems, it is possible to drive topological states in otherwise trivial systems with off-resonant

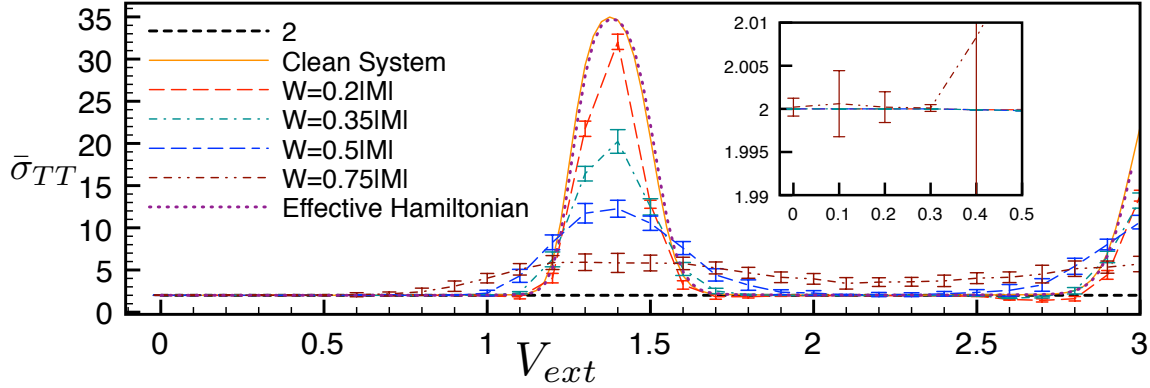


Figure 3.3: Disorder averaged summed conductivity, Eq. (3.4.1). The inset shows a zoomed in picture of the first area of conductivity quantization. Note some error bars in the insets are too small to see.

light. The most prevalent example of this is graphene, where the light produces an effective Hamiltonian with a topological mass. Thus the suppression described above may also apply to these other systems. [3–7, 11, 30]. In the present system of interest the driving of a trivial equilibrium system (*i.e.* $M = -1$ in our current language) can be driven into a topological phase. This, however, relies on the light being *on resonance*[1]. A description of this scenario inline with the discussion above is possible, but subtle and we leave it to a future communication[42].

3.4 Connection to Floquet Sum Rule

We now connect our work to a sum rule proposed recently by Kundu and Seradjeh in the context of a system with Floquet Majorana modes[2]. Similar to the current work, these authors find that in the presence of a periodic perturbation, a system with Majorana modes will not showcase the expected zero-bias quantized conductance of $2e^2/h$. Instead, the quantized conductivity is found in the sum

$$\bar{\sigma}(E) = \sum_n \sigma(E + n\hbar\Omega). \quad (3.4.1)$$

Physically, the above corresponds to performing measurements of $\sigma(E)$ not just at an in gap energy E , but for lead energies placed any number of $\hbar\Omega$'s above or below this. The results of these measurements are then summed up. Let us apply this sum rule to our system. Using Eq. (3.3.1) we have

$$\bar{\sigma}(E) = \sum_{n,m} J_m^2 \left(\frac{2V_{ext}}{\hbar\Omega} \right) \sigma_F(E + (m+n)\hbar\Omega). \quad (3.4.2)$$

Shifting $n \rightarrow n-m$, using the off resonance light conductivity $\sigma_F(E+m\hbar\Omega) = \sigma_F(E)\delta_{m,0}$ and the Bessel functions property $\sum_n J_n^2(x) = 1$ leads to $\bar{\sigma}(E) = \sigma_F(E)$. Therefore, if $\sigma_F(E)$ is quantized to $2e^2/h$, then $\bar{\sigma}(E)$ should be as well.

The above result is intuitive from a PAT point of view. At a two-terminal lead energy $E \simeq n\hbar\Omega$ the electrons must emit n photons to enter the quantized conductance channel and thus enter it with probability P_{-n} , the probability to emit n photons. This gives a conductance of $\sigma_F(0)P_{-n}$. Summing over all the lead energies is then effectively summing over all of the probabilities as $\bar{\sigma}(0) = \sigma_F(0) \sum_n P_n = \sigma_F(0)$, *i.e.* the sum rule recovers the underlying conductance.

The above derivation can be generalized to on-resonant driving under certain conditions[42]. In particular, one expects the sum rule to hold when edge states are visible in the so-called "quasi-energy" spectrum. Nonetheless, the derivation presented here contains all of the intuition required to understand the sum rule.

In Fig. 3.3 we show $\bar{\sigma}(E)$ at $E = 0$ for various different disorder strengths as well as $\sigma_F(E)$. Firstly, our data for the clean system is in excellent agreement with $\sigma_F(E)$. Secondly, the system shows noticeable deviations from $\bar{\sigma}(E \simeq 0) = 2e^2/h$ in two regimes of V_{ext} and occur in both the clean and disordered systems. Here the bulk gap in the effective Hamiltonian closes, and the topological edge states becoming washed out by bulk conduction states. This is most obvious when looking at the disorder averaged data where

the regions with $\bar{\sigma}(E) = 2e^2/h$ are insensitive to disorder, while the peaks are sensitive to disorder, as bulk conduction states should be. This result is interesting from a PAT perspective. Not only has the periodic field split the system into side bands, but it has modified the underlying system in a non-trivial way. In a traditional PAT context only the sideband splitting would take place.

3.5 Conclusions

We have developed an analogue of PAT to describe the transport signatures of topologically protected edge states in the quantum well heterostructures. Our picture entails electrons only accessing the topological edge states of the system probabilistically. The probability of the electrons to absorb/emit a photon reduces the traditional values associated with transport measurements in these systems. These reduced values are, however, still insensitive to disorder and other deformations. We refer to this phenomenon as “photon inhibited topological transport”.

By using this picture we related our system to a Floquet sum rule proposed before[2]. Our picture of PAT is able to offer a physical description of why one would expect such a rule to hold. Namely, the sum rule is adding up all of the probabilities of accessing the edge state which, by itself, should have the traditional transport signatures. This sum then reveals the underlying transport properties.

3.6 Acknowledgements

The authors are thankful for useful discussions with Jean-René Soquet, Aashish Clerk and Gil Refael. Financial support for this work was provided by the NSERC and FQRNT (TPB) and the Vanier Canada Graduate Scholarship (AF). Numerical calculations for this work were performed using McGill HPC supercomputing resources.

3.A Floquet-Landauer Formula for Transport

We begin by reviewing results for transport in a system with a time-periodic field. We review the technical aspects of deriving the Floquet-Landauer formula for the current. For additional details of this calculation we recommend Ref. [29]. We begin with a generic Hamiltonian which is given by

$$H = H_S(t) + H_L + H_C \quad (3.A.1)$$

where

$$H_S(t) = c^\dagger \mathcal{H}_S(t) c \quad (3.A.2)$$

is the Hamiltonian of the sample where $c^\dagger = (c_1^\dagger \dots c_{N_s}^\dagger)$ is a vector containing creation operators for each of the N_s degrees of freedom in the sample and $\mathcal{H}_S(t)$ is a $N_s \times N_s$ matrix coupling these degrees of freedom. This matrix contains both the static properties of the sample as well as the time dependent effects of the periodic field. Next,

$$H_L = \sum_{\lambda} b_{\lambda}^{\dagger} \mathcal{H}_{L,\lambda} b_{\lambda} \quad (3.A.3)$$

is the Hamiltonian of all of the leads where $b_{\lambda}^{\dagger} = (b_{1,\lambda}^{\dagger} \dots b_{N_{l,\lambda},\lambda}^{\dagger})$ is a vector containing creation operators for each of the N_l degrees of freedom in the lead λ and $\mathcal{H}_{l,\lambda}$ is a $N_{l,\lambda} \times N_{l,\lambda}$ matrix coupling these degrees of freedom. Finally,

$$H_C = \sum_{\lambda} \left(b_{\lambda}^{\dagger} \mathcal{K}_{\lambda} c + \text{h.c.} \right) \quad (3.A.4)$$

is the Hamiltonian coupling the sample to each of the leads. \mathcal{K}_{λ} is the $N_{l,\lambda} \times N_s$ matrix that describes these coupling strengths. The above model is completely general and makes no specification of band structure or dimension of the system.

The program for the derivation of a formula for the time averaged current, \bar{I}_λ , proceeds as follows. One writes the Heisenberg equations of motions for the sample and lead operators. The term H_C of course couples these equations. One proceeds by solving the equations for the lead operators, this can be written in terms of sample operators and the lead operators $b_\lambda(t_0)$ where t_0 is some time in the distant past.

This solution for the lead operators is now plugged into the equation for the sample operators which can, after some work, be written as

$$\begin{aligned} & \left(i\hbar \frac{d\hat{c}(t)}{dt} - \mathcal{H}_S(t)\hat{c}(t) + i \int_{t_0}^t \Gamma(t-t')\hat{c}(t')dt' \right) \\ &= i\hbar\xi(t) \end{aligned} \quad (3.A.5)$$

Where we have defined

$$\xi_\lambda(t) = -\frac{i}{\hbar}\mathcal{K}_{L,\lambda}^\dagger g_{\lambda,L}(t-t_0)\hat{b}_\lambda(t_0), \quad (3.A.6)$$

with $\xi(t) = \sum_\lambda \xi_\lambda(t)$ and also and

$$\Gamma_\lambda(t) = \frac{1}{\hbar}\mathcal{K}_{L,\lambda}^\dagger g_{\lambda,L}(t)\mathcal{K}_{L,\lambda} \quad (3.A.7)$$

and $\Gamma(t) = \sum_\lambda \Gamma_\lambda(t)$. In the above we have also defined $g_{\lambda,L}(t-t') = \exp\left[-\frac{i}{\hbar}\mathcal{H}_{L,\lambda}(t-t')\right]$, which is the temporal Green function of the isolated leads. We see that upon integrating out the leads we generate two contributions to the dynamics of the system. The first comes from $\Gamma(t)$ which acts as an imaginary self-energy in the system and will thus introduce finite lifetimes to our eigenstates. The second is to introduce the operator valued noise function $\xi(t)$. The statistics of this noise is determined by the state of the leads at a time in the distant past, $t = t_0$.

The above integro-differential equation is linear in the operators $\hat{c}(t)$ and so it can be

solved *via* a Green function method. If we define the partial transform of this Green function

$$G(t, t') = \int \frac{d\epsilon}{2\pi\hbar} e^{-i\epsilon(t-t')/\hbar} G(t, \epsilon) \quad (3.A.8)$$

Also if we define the FT's

$$\xi(\epsilon) = \int dt e^{i\epsilon t/\hbar} \xi(t) \quad \xi(t) = \int \frac{d\epsilon}{2\pi\hbar} e^{-i\epsilon t/\hbar} \xi(\epsilon) \quad (3.A.9)$$

then we can write

$$\hat{c}(t) = \frac{i}{2\pi} \int d\epsilon e^{-i\epsilon t/\hbar} G(t, \epsilon) \xi(\epsilon) \quad (3.A.10)$$

where $G(t, \epsilon)$ satisfies, upon taking $t_0 \rightarrow -\infty$

$$\begin{aligned} & \left(i\hbar \frac{d}{dt} + \epsilon - \mathcal{H}_S(t) \right) G(t, \epsilon) \\ & + i \int_0^\infty e^{i\epsilon\tau/\hbar} \Gamma(\tau) G(t - \tau, \epsilon) d\tau = I_{N_s \times N_s} \end{aligned} \quad (3.A.11)$$

where $I_{N_s \times N_s}$ is a unit matrix.

The net charge current flowing across the contact λ into the wire is given by the rate of change of the number of electrons in this lead, this is $I^\lambda(t) = e \frac{dN_\lambda}{dt}$. In other words

$$I^\lambda(t) = \frac{ei}{\hbar} [H_S(t) + H_L + H_C, N_\lambda](t) \quad (3.A.12)$$

Calculation of this commutator and using our Green function solution above shows that the current can be written entirely in terms of the noise term $\xi(\epsilon)$ which is related to $\hat{b}_\lambda(t_0)$. We then take the thermal average of $I^\lambda(t)$ assuming that the leads begin their lives at $t_0 \rightarrow -\infty$ in thermal equilibrium at some inverse temperature β_λ . This gives a general (albeit complicated) formula for $\langle I^\lambda(t) \rangle$ in terms of the $G(t, \epsilon)$. This formula is exact for any time dependence.

At this point we now use the fact that for a time-periodic system $G(t, \epsilon)$ should also be time periodic. We then define

$$G^{(n)}(\epsilon) = \frac{1}{T} \int_0^T e^{in\Omega t} G(t, \epsilon) dt \quad (3.A.13)$$

where $\Omega = 2\pi/T$. Writing the current formula in terms of this Floquet Green function shows that the current should also be periodic in T . Defining the average $\bar{I}_\lambda = \frac{1}{T} \int_0^T dt \langle I^\lambda(t) \rangle$ we then obtain the result

$$\bar{I}_\lambda = \frac{e}{\hbar} \sum_{\lambda'} \int d\epsilon (T_{\lambda, \lambda'}(\epsilon) f_{\lambda'}(\epsilon) - T_{\lambda', \lambda}(\epsilon) f_\lambda(\epsilon)) \quad (3.A.14)$$

where $f_\lambda(\epsilon) = \frac{1}{1 + \exp(\beta_\lambda(\epsilon - eV_\lambda))}$ and we have defined the transmission matrices

$$T_{\lambda, \lambda'}(\epsilon) = \sum_n \text{Tr} [\Gamma_\lambda(\epsilon + \hbar n \Omega) G^{(n)}(\epsilon) \Gamma_{\lambda'}(\epsilon) (G^{(n)}(\epsilon))^\dagger]. \quad (3.A.15)$$

The above expression has the form of the usual Landauer conductance except that the current is time averaged and the transmission matrices $T_{\lambda, \lambda'}$ are defined through the above summation. Physically, the Greens function $G_{\ell, \ell'}^{(n)}(\epsilon)$ describes the amplitude of an electron in the sample to propagate from ℓ' to ℓ at energy ϵ while absorbing ($n > 0$) or emitting ($n < 0$) $|n|$ photons. Using Floquet theory[41], this object may be expressed in terms of Floquet states[30]. Floquet states are the extension of stationary states to time-periodic systems. In the system we choose it is possible to write $G_{\ell, \ell'}^{(n)}(\epsilon)$ in terms of a matrix continued fraction expression[30, 32, 33]

In this paper we will work to simplify our discussion by employing the “wide-band” approximation. In this approximation one assumes that the density of states of the leads is constant over the energy scales in which we are interested. This amounts to assuming the lead operators, $\Gamma_\lambda(\epsilon)$, are independent of ϵ , $\Gamma_\lambda(\epsilon) \simeq \Gamma_\lambda$. Moreover, we make the

assumption of identical leads so that $(\Gamma_\lambda)_{i,j} = \Gamma \delta_{i,j} \delta_{i,\mathbf{x}_\lambda}$ where \mathbf{x}_λ are the set of all sample degrees of freedom connected to lead λ .

We are interested in devices with two different geometries. The first of these is a two-terminal device; a sample with leads attached to its left and right edges. For this type of device we label these leads as L for left and R for right. By conservation of current we must have $\bar{I}_R = -\bar{I}_L$, since the current entering the right lead must be equal to the current leaving the left lead. It is then sufficient to think only of \bar{I}_R . We now imagine biasing our sample so that we have a voltage V on the left lead and a voltage 0 on the right lead. We then define the (differential) conductance as

$$\sigma(V) = \left. \frac{d\bar{I}_R}{dV} \right|_{V=V} = \frac{e^2}{h} T_{R,L}(eV) \quad (3.A.16)$$

Thus for this geometry we have the simple result that the conductivity is simply given by the total transmission coefficient from the left lead to the right lead. For a spin Hall insulator in equilibrium when the bias voltage V is tuned to lie in the gap (*i.e.* on the edge states) the value $\sigma(V) = 2e^2/h$ is expected[11, 34].

The second type of device we are interested in is a Hall bar. This type of geometry allows us to probe whether the current is carried by bulk or edge states[7, 35, 36]. In equilibrium it is found that the only non-zero values of the transmission matrices $T_{\lambda,\lambda'}(\epsilon)$ (with ϵ in the gap) come from tunneling between adjacent leads. That is to say $T_{\lambda,\lambda'}(\epsilon_F) = 0$ unless $\lambda = \lambda' \pm 1$ where $6 + 1$ is periodically identified to 1. Moreover, it is argued that $T_{\lambda,\lambda\pm 1}(\epsilon_F) = 1$ as, because of the helical edge states, a quasiparticle originating at lead λ *must* tunnel to one of the neighboring leads.

3.B Effective Hamiltonian

Our discussion above shows that calculating the transmission elements above relies on knowledge of $G^{(n)}(\epsilon)$. This Green's function can be found by solving (in the wide-band approximation) the following equation of motion

$$\left(i\hbar \frac{d}{dt} + \epsilon - \mathcal{H}_S(t) + \frac{i}{2}\Gamma \right) G(t, \epsilon) = I \quad (3.B.1)$$

and then calculating

$$G^{(n)}(\epsilon) = \frac{1}{T} \int_0^T dt e^{in\Omega t} G(t, \epsilon) \quad (3.B.2)$$

This task is simplified by considering instead the auxiliary equation

$$\left(i\hbar \frac{d}{dt} + \epsilon - \mathcal{H}_S(t) + \frac{i}{2}\Gamma \right) \mathcal{G}(t, t', \epsilon) = \delta(t - t') \quad (3.B.3)$$

and then noting that

$$G(t, \epsilon) = \int dt' \mathcal{G}(t, t', \epsilon) \quad (3.B.4)$$

We will now focus on Eq. (3.B.3). By writing $\mathcal{H}_S(t) - \frac{i}{2}\Gamma = \hat{\mathcal{H}}_S + H_{ext}(t)$ and introducing the rotating frame picture

$$\mathcal{G}(t, t', \epsilon) = U_V(t) \check{\mathcal{G}}(t, t', \epsilon) U_V^\dagger(t') \quad (3.B.5)$$

where $i\hbar \frac{d}{dt} U_V(t) = H_{ext}(t) U_V(t)$. Then it follow that $\check{\mathcal{G}}(t, t', \epsilon)$ is a solution to

$$\left(i\hbar \frac{d}{dt} + \epsilon - \hat{\mathcal{H}}_S(t) \right) \check{\mathcal{G}}(t, t', \epsilon) = \delta(t - t') \quad (3.B.6)$$

with $\hat{\mathcal{H}}_S(t) = U_V(t)^\dagger \hat{\mathcal{H}}_S U_V(t)$ If the external, periodic potential were some potential with no internal structure coupling the degrees of freedom of the system then we would have

$\hat{\mathcal{H}}_S(t) = \hat{\mathcal{H}}_S$ as $H_{ext}(t)$ would commute with all other terms. This would immediately lead to a static system and a direct analogue of photon assisted tunneling.

For this particular problem $H_{ext}(t)$ commutes with itself at different times. As a result $U_V(t+T) = U_V(t)$ and it is useful to define

$$\begin{aligned} U_V(n) &= \frac{1}{T} \int_0^T dt e^{in\Omega t} U_V(t) \\ \hat{\mathcal{H}}_S(n) &= \frac{1}{T} \int_0^T dt e^{in\Omega t} \hat{\mathcal{H}}_S(t) \end{aligned} \quad (3.B.7)$$

Using all of these ingredients we then have

$$G^{(n)}(\epsilon) = \frac{1}{T} \int_0^T dt e^{in\Omega t} \int dt' U_V(t) \check{\mathcal{G}}(t, t', \epsilon) U_V^\dagger(t') \quad (3.B.8)$$

Our task becomes to solve Eq. (3.B.6). We do so by defining

$$\check{\mathcal{G}}(t, t', \epsilon) = \frac{1}{T} \sum_{n,m} e^{-in\Omega t} e^{im\Omega t'} \check{\mathcal{G}}_{n,m}(\epsilon) \quad (3.B.9)$$

which reduces Eq. (3.B.6) to the difference equation

$$\left(\ell \hbar \Omega + \epsilon - \hat{\mathcal{H}}_S(0) \right) \check{\mathcal{G}}_{\ell,m}(\epsilon) - \sum_{n \neq \ell} \hat{\mathcal{H}}_S(\ell - n) \check{\mathcal{G}}_{n,m}(\epsilon) = \delta_{\ell,m} \quad (3.B.10)$$

All of the Fourier expansions above when used with Eqs. (3.B.2) and (3.B.4) then give

$$G^{(n)}(\epsilon) = \sum_{\ell,m} U_V(n - \ell) \check{\mathcal{G}}_{\ell,m}(\epsilon) U_V^\dagger(-m) \quad (3.B.11)$$

We now make note of a symmetry in the difference equation for $\check{\mathcal{G}}_{\ell,m}(\epsilon)$. Namely we note that simultaneously shifting $\ell \rightarrow \ell - k$, $m \rightarrow m - k$ and $\epsilon \rightarrow \epsilon + k\hbar\Omega$ for any integer k in Eq. (3.B.10) shows that if $\check{\mathcal{G}}_{\ell,m}(\epsilon)$ is a solution than so is $\check{\mathcal{G}}_{\ell-k, m-k}(\epsilon + k\hbar\Omega)$, we thus

identify[32]

$$\check{G}_{\ell,m}(\epsilon) = \check{G}_{\ell-k,m-k}(\epsilon + k\hbar\Omega) \quad (3.B.12)$$

From the above one can conclude that all of the relevant information is contained in $\check{G}_{\ell,0}(\epsilon) \equiv G_V^{(\ell)}(\epsilon)$. The operator $G_V^{(\ell)}(\epsilon)$ solves the equation

$$\left(\ell\hbar\Omega + \epsilon - \hat{\mathcal{H}}_S(0)\right) G_V^{(\ell)}(\epsilon) - \sum_n \hat{\mathcal{H}}_S(\ell - n) G_V^{(n)}(\epsilon) = \delta_{\ell,0} \quad (3.B.13)$$

We can then write $\check{G}_{\ell,m}(\epsilon) = G_V^{(\ell-m)}(\epsilon + m\hbar\Omega)$. Plugging this in above yields

$$G^{(n)}(\epsilon) = \sum_{\ell,m} U_V(n - \ell) G_V^{(\ell-m)}(\epsilon + m\hbar\Omega) U_V^\dagger(-m) \quad (3.B.14)$$

sending $m \rightarrow -m$ and then $\ell \rightarrow \ell - m$ then gives main result of this discussion

$$G^{(n)}(\epsilon) = \sum_{\ell,m} U_V(n + m - \ell) G_V^{(\ell)}(\epsilon - m\hbar\Omega) U_V^\dagger(m) \quad (3.B.15)$$

We will use the above to find an approximate formula for the conductivity. We will develop a few other necessary relations

3.B.1 Solution for $G_V^{(\ell)}(\epsilon)$

Let us now further develop the difference equation for $G_V^{(\ell)}(\epsilon)$. To make the notation more compact let us define $\bar{H}_\ell = \hat{\mathcal{H}}_S(\ell)$ for $\ell \neq 0$ and $\bar{H}_0 = 0$. Besides being less cumbersome, this convention allows us to drop the restrictions on the sums and eventually employ Einstein summation convention. We note that we may write it as

$$\begin{aligned} G_V^{(\ell)}(\epsilon) &= \left(\ell\hbar\Omega + \epsilon - \hat{\mathcal{H}}_S(0)\right)^{-1} \delta_{\ell,0} \\ &+ \sum_n \left(\ell\hbar\Omega + \epsilon - \hat{\mathcal{H}}_S(0)\right)^{-1} \bar{H}_{\ell-n} G_V^{(n)}(\epsilon) \end{aligned} \quad (3.B.16)$$

Let us note that $g_F(\epsilon) = (\epsilon - \hat{\mathcal{H}}_S(0))^{-1}$ is the Green's function of the static system with Hamiltonian $\hat{\mathcal{H}}_S(0)$. Therefore

$$G_V^{(\ell)}(\epsilon) = g_F(\epsilon)\delta_{\ell,0} + \sum_j g_F(\epsilon + \ell\hbar\Omega)\bar{H}_{\ell-j}G_V^{(j)}(\epsilon) \quad (3.B.17)$$

We now iterate this equation. To do this let us introduce some notation to extract the useful part of the above. First, we use implied summation over repeated indices that are not ℓ . Second, we define $g_i = g_F(\epsilon + i\hbar\Omega)$. This gives

$$G_V^{(\ell)}(\epsilon) = g_0\delta_{\ell,0} + g_\ell\bar{H}_\ell g_0 + g_\ell\bar{H}_{\ell-j}g_j\bar{H}_{j-j'}G_V^{(j')}(\epsilon) \quad (3.B.18)$$

Repeated iteration of the above difference equation allows us to write

$$\begin{aligned} G_V^{(\ell)}(\epsilon) &= g_0\delta_{\ell,0} \quad (3.B.19) \\ &+ g_\ell(\bar{H}_\ell + \bar{H}_{\ell-j}g_j\bar{H}_j + \bar{H}_{\ell-j}g_j\bar{H}_{j-j'}g_{j'}\bar{H}_{j'}) \\ &+ \bar{H}_{\ell-j}g_j\bar{H}_{j-j'}g_{j'}\bar{H}_{j'-\alpha}g_\alpha\bar{H}_\alpha \\ &+ \bar{H}_{\ell-j}g_j\bar{H}_{j-j'}g_{j'}\bar{H}_{j'-\alpha}g_\alpha\bar{H}_{\alpha-\beta}g_\beta\bar{H}_{\beta-\sigma}g_\sigma\bar{H}_\sigma + \dots)g_0 \end{aligned}$$

Or

$$G_V^{(\ell)}(\epsilon) = g_F(\epsilon)\delta_{\ell,0} + g_F(\epsilon + \ell\hbar\Omega)\check{D}_\ell(\epsilon)g_F(\epsilon) \quad (3.B.20)$$

Where

$$\begin{aligned} \check{D}_\ell(\epsilon) &= \bar{H}_\ell + \bar{H}_{\ell-j}g_j\bar{H}_j + \bar{H}_{\ell-j}g_j\bar{H}_{j-j'}g_{j'}\bar{H}_{j'} \quad (3.B.21) \\ &+ \bar{H}_{\ell-j}g_j\bar{H}_{j-j'}g_{j'}\bar{H}_{j'-\alpha}g_\alpha\bar{H}_\alpha \\ &+ \bar{H}_{\ell-j}g_j\bar{H}_{j-j'}g_{j'}\bar{H}_{j'-\alpha}g_\alpha\bar{H}_{\alpha-\beta}g_\beta\bar{H}_{\beta-\sigma}g_\sigma\bar{H}_\sigma + \dots \end{aligned}$$

The above series can in turn be generated by (restoring the summation symbols)

$$\begin{aligned} \check{D}_\ell(\epsilon) &= \bar{H}_\ell + \sum_j \bar{H}_{\ell-j} g_j \bar{H}_j \\ &+ \sum_{j,j'} \bar{H}_{\ell-j} g_j \bar{H}_{j-j'} g_{j'} \check{D}_{j'}(\epsilon) \end{aligned} \quad (3.B.22)$$

Let us consider the physical implications of Eq. (3.B.20). The Greens function $G_V^{(\ell)}(\epsilon)$ is described by all possible processes starting at energy ϵ (indicated by amplitude $g_F(\epsilon)$) where the electrons absorb/emit a *net* number of photons ℓ (indicated by amplitude $\check{D}_\ell(\epsilon)$) and then end up at an energy eigenstate $\epsilon + \ell\hbar\Omega$ (hence $g_F(\epsilon + \ell\hbar\Omega)$). For a driving frequency Ω such that there are no states in the model system at $\epsilon + \ell\hbar\Omega$ no scattering can occur and we can make the approximation

$$G_V^{(\ell)}(\epsilon) \simeq g_F(\epsilon) \delta_{\ell,0} \quad (3.B.23)$$

This is precisely the case for off-resonant light.

3.B.2 Transmission Matrices

So far our discussion has been general with the only assumption being that $[H_{ext}(t), H_{ext}(t')] = 0, \forall(t, t')$ (a more general treatment in the absence of this restriction is currently a work in progress [42]). At this point we specialize to the quantum well system which has been discussed in the main text. Our first task is to define the operators $U_V(m)$. We are interested in $\mathcal{H}_{ext}(t) = 2V_{ext} \cos(\Omega t)$ where $V_{ext} = V_e \sigma_z \otimes I_L$, I_L is the identity operator on the lattice and σ_z acts on spin. This operator commutes with itself at different times and is diagonal in “spin-lattice” space. This allows us to easily define the time evolution operator as follows

$$U_V(t) = e^{-i \int_0^t dt' \mathcal{H}_{ext}(t')} = \exp \left[-i \frac{2V_e}{\hbar\Omega} \sin(\Omega t) \sigma_z \otimes I_L \right] \quad (3.B.24)$$

note that no time ordering is required in the exponential because $[H_{ext}(t), H_{ext}(t')] = 0$. Finding the Fourier series of the above periodic function is made possible by the identity $e^{-ix \sin(\Omega t)} = \sum_m J_m(x) e^{-i\Omega m t}$ where $J_m(\cdot)$ is the Bessel function of the first kind of order m . We thus have

$$U_V(t) = \sum_m J_m \left(\frac{2V_e}{\hbar\Omega} \sigma_z \otimes I_L \right) e^{-i\Omega m t} \quad (3.B.25)$$

We can then read off

$$\begin{aligned} U_V(m) &= J_m \left(\frac{2V_e}{\hbar\Omega} \sigma_z \otimes I_L \right) = J_m \left(\frac{2V_e}{\hbar\Omega} \right) S_m \otimes I_L \\ &= J_m \left(\frac{2V_{ext}}{\hbar\Omega} \right) \end{aligned} \quad (3.B.26)$$

where $S_m = \sigma_0$ if m is even and σ_z if m is odd. The second relation above comes from the Bessel function property $J_m(-x) = (-1)^m J_m(x)$. The third relation, $J_m \left(\frac{2V_{ext}}{\hbar\Omega} \right)$ is a compact form which will be useful in a derivation of the transmission elements.

With an explicit formula of $U_V(m)$ in hand we proceed to plug Eq. (3.B.15) for the Green's function into the formula for $T_{\lambda,\lambda'}(\epsilon)$ which gives

$$\begin{aligned} T_{\lambda,\lambda'}(\epsilon) &= \sum_{n,\ell,m} \sum_{\ell',m'} \text{Tr} \left[J_{n+m'-\ell'} \left(\frac{2V_{ext}}{\hbar\Omega} \right) J_{n+m-\ell} \left(\frac{2V_{ext}}{\hbar\Omega} \right) \right. \\ &\quad \left. \Gamma_\lambda G_V^{(\ell)}(\epsilon - m\hbar\Omega) J_m \left(\frac{2V_{ext}}{\hbar\Omega} \right) \Gamma_{\lambda'} J_{m'} \left(\frac{2V_{ext}}{\hbar\Omega} \right) (G_V^{(\ell')}(\epsilon - m'\hbar\Omega))^\dagger \right] \end{aligned} \quad (3.B.27)$$

where we have used the fact that the lead self energies commute with V_{ext} (the leads make no distinction between different spins of particles). The sum over Bessel functions gives a delta function. After some index relabelling we are left with

$$T_{\lambda,\lambda'}(\epsilon) = \sum_{\ell,\ell',m} \text{Tr} \left[\Gamma_{\lambda} G_V^{(\ell)}(\epsilon - (m + \ell)\hbar\Omega) \Gamma_{\lambda'} J_{m+\ell} \left(\frac{2V_{ext}}{\hbar\Omega} \right) J_{m+\ell'} \left(\frac{2V_{ext}}{\hbar\Omega} \right) (G_V^{(\ell')}(\epsilon - (m + \ell')\hbar\Omega))^{\dagger} \right] \quad (3.B.28)$$

For the driving frequency we have chosen we are dealing with off-resonant light, thus to a good approximation we take $G_V^{(\ell)}(\epsilon) = g_F(\epsilon)\delta_{\ell,0}$. Plugging into the transmission coefficient gives

$$T_{\lambda,\lambda'}(\epsilon) = \sum_m J_m^2 \left(\frac{2V_e}{\hbar\Omega} \right) \text{Tr} \left[\Gamma_{\lambda} g_F(\epsilon - m\hbar\Omega) \Gamma_{\lambda'} g_F^{\dagger}(\epsilon - m\hbar\Omega) \right] \quad (3.B.29)$$

Note the significance of this. The second term (the trace) is the *static* transmission of a dressed Hamiltonian $\hat{\mathcal{H}}_S(0)$. The pre-factor describes how this conductivity is distributed amongst different bias voltages. Thus even for off-resonant light replacement of the system Hamiltonian with an associated Floquet Hamiltonian is insufficient, one must also include the Bessel function pre-factor.

If we define

$$T_{\lambda,\lambda'}^F(\epsilon, V_e) = \text{Tr} \left[\Gamma_{\lambda} g_F(\epsilon) \Gamma_{\lambda'} g_F^{\dagger}(\epsilon) \right] \quad (3.B.30)$$

which looks like the *static* transmission matrix of a system described by the *static* Hamiltonian $\hat{\mathcal{H}}_S(0)$ (which itself depends on V_e) then we can write

$$T_{\lambda,\lambda'}(\epsilon) = \sum_m J_m^2 \left(\frac{2V_e}{\hbar\Omega} \right) T_{\lambda,\lambda'}^F(\epsilon - m\hbar\Omega, V_e) \quad (3.B.31)$$

3.B.3 Expression for the Effective Hamiltonian

We close with an expression for a derivation of the effective Hamiltonian. Recall that $\hat{\mathcal{H}}_S(t) = U_V^\dagger(t)\hat{\mathcal{H}}_S U_V(t)$ and that $\hat{\mathcal{H}}_S(n) = \frac{1}{T} \int_0^T e^{in\Omega t} \bar{H}(t)$, then by using the Fourier decomposition of $U_V(t)$ we can write

$$\hat{\mathcal{H}}_S(n) = \sum_m U_V^\dagger(m) \hat{\mathcal{H}}_S U_V(m+n) \quad (3.B.32)$$

If we now recall the relation for the U_V operators derived above, then it immediately follows that

$$\begin{aligned} \hat{\mathcal{H}}_S(n) &= \sum_m J_m \left(\frac{2V_e}{\hbar\Omega} \right) J_{m+n} \left(\frac{2V_e}{\hbar\Omega} \right) \\ &\times S_m \otimes I_L \hat{\mathcal{H}}_S S_{m+n} \otimes I_L \end{aligned} \quad (3.B.33)$$

Now let us write

$$\hat{\mathcal{H}}_S = \sum_{\alpha,\beta} \bar{\mathcal{H}}_{\alpha,\beta} \sigma_\alpha \otimes R_\beta \quad (3.B.34)$$

where R_β is a complete set of operators in the space of the lattice. Then, defining $\zeta = \frac{2V_e}{\hbar\Omega}$, noting that for $\alpha = 1$ or 2 one can show that $S_m \sigma_\alpha S_{n+m} = (-1)^m \sigma_\alpha S_n$ whereas for $\alpha = 0$ or $\alpha = 3$ they do nothing, and using the Bessel function identities $\sum_m [J_m(\zeta) J_{m+n}(\zeta)] = \delta_{n,0}$ and $\sum_m [J_m(\zeta) (-1)^m J_{m+n}(\zeta)] = \sum_m [J_m(\zeta) J_{-m+n}(\zeta)] = J_n(2\zeta)$ we have

$$\begin{aligned} \hat{\mathcal{H}}_S(m) &= \delta_{n,0} \sum_{\alpha=0,3,\beta} \bar{\mathcal{H}}_{\alpha,\beta}(\sigma_\alpha) \otimes R_\beta \\ &+ J_n(2\zeta) \sum_{\alpha=1,2,\beta} \bar{\mathcal{H}}_{\alpha,\beta}(\sigma_\alpha S_n) \otimes R_\beta \end{aligned} \quad (3.B.35)$$

It is most convenient to write this as

$$\hat{\mathcal{H}}_S(m) = \delta_{n,0} \bar{\mathcal{H}}_{03} + J_n(2\zeta) \bar{\mathcal{H}}_{12}(n) \quad (3.B.36)$$

Thus the field does not touch terms in $\hat{\mathcal{H}}_S$ proportional to σ_0 or σ_3 and “dresses” the σ_1 and σ_2 terms. Note that had we chosen the polarization $\mathbf{V}_x \neq 0$ or $\mathbf{V}_y \neq 0$ the σ_3 component of the Hamiltonian would have been renormalized as well. For this chapter this is the only difference choosing a different polarization makes.

The Green’s function g_F and the transmission matrix elements $T_{\lambda,\lambda'}^F$ are the result of calculating the Greens function and the transport properties of a system described by a static Hamiltonian $\hat{\mathcal{H}}_S(0)$. Such a Hamiltonian looks similar to our original static Hamiltonian (before periodic perturbation) but with $\bar{\mathcal{H}}_{12}$ renormalized by the Bessel function $J_0(2\zeta)$.

References

- ¹N. H. Lindner, G. Refael, and V. Galitski, *Nat Phys* **7**, 490 (2011).
- ²A. Kundu and B. Seradjeh, *Phys. Rev. Lett.* **111**, 136402 (2013).
- ³Z. Gu, H. A. Fertig, D. P. Arovas, and A. Auerbach, *Phys. Rev. Lett.* **107**, 216601 (2011).
- ⁴T. Oka and H. Aoki, *Phys. Rev. B* **79**, 081406 (2009).
- ⁵G. Usaj, P. M. Perez-Piskunow, L. E. F. Foa Torres, and C. A. Balseiro, *Phys. Rev. B* **90**, 115423 (2014).
- ⁶H. L. Calvo, H. M. Pastawski, S. Roche, and L. E. F. F. Torres, *Applied Physics Letters* **98** (2011).
- ⁷L. E. F. Foa Torres, P. M. Perez-Piskunow, C. A. Balseiro, and G. Usaj, *Phys. Rev. Lett.* **113**, 266801 (2014).
- ⁸A. Gómez-León and G. Platero, *Phys. Rev. Lett.* **110**, 200403 (2013).
- ⁹M. S. Rudner, N. H. Lindner, E. Berg, and M. Levin, *Phys. Rev. X* **3**, 031005 (2013).
- ¹⁰T. Kitagawa, E. Berg, M. Rudner, and E. Demler, *Phys. Rev. B* **82**, 235114 (2010).
- ¹¹A. Kundu, H. A. Fertig, and B. Seradjeh, *Phys. Rev. Lett.* **113**, 236803 (2014).
- ¹²Y. Tenenbaum Katan and D. Podolsky, *Phys. Rev. B* **88**, 224106 (2013).
- ¹³L. Jiang, T. Kitagawa, J. Alicea, A. R. Akhmerov, D. Pekker, G. Refael, J. I. Cirac, E. Demler, M. D. Lukin, and P. Zoller, *Phys. Rev. Lett.* **106**, 220402 (2011).
- ¹⁴D. E. Liu, A. Levchenko, and H. U. Baranger, *Phys. Rev. Lett.* **111**, 047002 (2013).
- ¹⁵C. We, J. Sun, F. Huang, Y. Li, and W. Liu, *EPL* **104**, 27004 (2013).
- ¹⁶P. Wang, Q.-f. Sun, and X. C. Xie, *Phys. Rev. B* **90**, 155407 (2014).
- ¹⁷P. Delplace, Á. Gómez-León, and G. Platero, *Phys. Rev. B* **88**, 245422 (2013).

- ¹⁸Y. Li, A. Kundu, F. Zhong, and B. Seradjeh, *Phys. Rev. B* **90**, 121401 (2014).
- ¹⁹P. Titum, N. H. Lindner, M. C. Rechtsman, and G. Refael, *Phys. Rev. Lett.* **114**, 056801 (2015).
- ²⁰K. I. Seetharam, C.-E. Bardyn, N. H. Lindner, M. S. Rudner, and G. Refael, *Phys. Rev. X* **5**, 041050 (2015).
- ²¹M. C. Rechtsman, J. M. Zeuner, Y. Plotnik, Y. Lumer, D. Podolsky, F. Dreisow, S. Nolte, M. Segev, and A. Szameit, *Nature* **496**, 196 (2013).
- ²²Y. H. Wang, H. Steinberg, P. Jarillo-Herrero, and N. Gedik, *Science* **342**, 453–457 (2013).
- ²³P. K. Tien and J. P. Gordon, *Phys. Rev.* **129**, 647–651 (1963).
- ²⁴G. Platero and R. Aguado, *Physics Reports* **395**, 1–157 (2004).
- ²⁵B. A. Bernevig, T. L. Hughes, and S.-C. Zhang, *Science* **314**, 1757–1761 (2006).
- ²⁶M. König, S. Wiedmann, C. Brune, A. Roth, H. Buhmann, L. W. Molenkamp, X.-L. Qi, and S.-C. Zhang, *Science* **318**, 766–770 (2007).
- ²⁷K.-H. Ding and G. Zhou, *Physics Letters A* **378**, 966–969 (2014).
- ²⁸X. Zhang, J. Wang, and S.-C. Zhang, *Phys. Rev. B* **82**, 245107 (2010).
- ²⁹S. Kohler, J. Lehmann, and P. Hänggi, *Physics Reports* **406**, 379–443 (2005).
- ³⁰T. Kitagawa, T. Oka, A. Brataas, L. Fu, and E. Demler, *Phys. Rev. B* **84**, 235108 (2011).
- ³¹”See the appendix of this chapter”.
- ³²D. F. Martinez, R. A. Molina, and B. Hu, *Phys. Rev. B* **78**, 045428 (2008).
- ³³D. F. Martinez, *J. Phys. A: Math. Gen.* **36**, 9827 (2003).
- ³⁴J. Tworzydło, B. Trauzettel, M. Titov, A. Rycerz, and C. Beenakker, *Phys. Rev. Lett.* **96**, 246802 (2006).
- ³⁵J.-c. Chen, J. Wang, and Q.-f. Sun, *Phys. Rev. B* **85**, 125401 (2012).

-
- ³⁶A. Roth, C. Brüne, H. Buhmann, L. W. Molenkamp, J. Maciejko, X.-L. Qi, and S.-C. Zhang, *Science* **325**, 294–297 (2009).
- ³⁷L. D’Alessio and M. Rigol, *Phys. Rev. X* **4**, 041048 (2014).
- ³⁸L. D’Alessio and M. Rigol, *Unpublished*, arXiv:1409.6319 (2014).
- ³⁹A. Lazarides, A. Das, and R. Moessner, *Phys. Rev. E* **90**, 012110 (2014).
- ⁴⁰P. Ponte, A. Chandran, Z. Papic, and D. A. Abanin, *Annals of Physics* **353**, 196–204 (2015).
- ⁴¹H. Sambe, *Phys. Rev. A* **7**, 2203–2213 (1973).
- ⁴²A. Farrell and T. Pereg-Barnea, *Phys. Rev. B* **93**, 045121 (2016).

Preface to Chapter 4

The main conclusion of the previous manuscript is that the edge-states of a topological insulator are split into side-bands by an applied time-periodic perturbation. The transport through these states was understood by developing an analogue of photon-assisted tunneling. This involves envisaging the electrons entering the sample through the leads are only accessing the topologically protected edge states of the system probabilistically. This behaviour thereby reduces the traditional values associated with transport measurement in a topological insulator.

The previous manuscript has offered a deep understanding of topological edge-states in the presence of a periodic drive. The present manuscript is now in a position to build on this understanding in order to treat a system where the edge-states are *created* by the time-periodic drive in the first place. This work will show that the intuition and tools developed in the previous manuscript are directly applicable to the strictly non-equilibrium states of the so-called Floquet topological insulator.

Edge State Transport in Floquet Topological Insulators

Aaron Farrell¹ and T. Pereg-Barnea¹

¹Department of Physics and the Centre for Physics of Materials, McGill University, Montreal, Quebec, Canada H3A 2T8

This chapter has been published in Physical Review B. Journal Reference:
Physical Review B 93, 045121 (2016)

Abstract

Floquet topological insulators are systems in which the topology emerges only when a time periodic perturbation is applied. In these systems one can define quasi-energy states which replace the equilibrium stationary states. The system exhibits its non-trivial topology by developing edge localized quasi-energy states which lie in a gap of the quasi energy spectrum. These states represent a non-equilibrium analogue of the topologically protected edge-states in equilibrium topological insulators which exhibit edge conductance of $2e^2/h$. Here we explore the transport properties of the edge-states in a Floquet topological insulator. In stark contrast to the equilibrium result, we find that the two terminal conductivity of these edge states is significantly different from $2e^2/h$. This fact notwithstanding, we find that for certain external potential strengths the conductivity is smaller than $2e^2/h$ and robust to the effects of disorder and smooth changes to the Hamiltonian's parameters. This robustness is reminiscent of the robustness found in equilibrium topological insulators. We provide an intuitive understanding of the reduction of the conductivity in terms of a picture where electrons in edge states are scattered by photons. We also consider Floquet sum rule[1] which was proposed in a different context. The summed conductivity recovers the equilibrium value of $2e^2/h$ whenever edge states are present. We show that this sum rule holds in our system using both numerical and analytic techniques.

4.1 Introduction.

Over the past decade topological insulators have become well known for their novel transport properties. The hallmark of these systems is their linearly dispersing, in-gap states. These states correspond to counter-propagating, helical edge modes. In a two dimensional geometry these edge modes represent one dimensional channels and lead to specific transport properties.

One example is a two-terminal device, where a source and drain are attached to the left and right of a sample and a bias voltage is applied across these terminals. The conductivity when these Fermi energies placed in the gap (where the edge states live) is $\sigma = 2e^2/h$ [2–4]. In a six-terminal, or Hall-bar, geometry specific values of multi-terminal resistances are expected[2–4] and these resistances are unique to counter-propagating, helical edge modes.

Although the number of confirmed topological insulators is ever increasing, materials with the correct physical parameters to support this state of matter are hard to come by. This has led many authors to consider ways in which to drive a material without any topological properties into a topological state. When a time-periodic potential is used to accomplish this task the resulting non-equilibrium topological state is called a Floquet topological insulator.

The field of Floquet topological insulators (and Floquet topological superconductors) has produced many interesting results of late[1, 5–22]. The introduction of a time-periodic potential into the system breaks continuous time-translational invariance and so one must dispense with the notion of an energy spectrum. A time-periodic field does have discrete time-translational invariance and therefore one has the ability to define an analogous concept called the “quasi-energy” spectrum[23]. In Floquet topological insulators one uses an externally applied time-periodic field of carefully chosen parameters to drive the system into its topological phase. The topology is manifest in in-gap, edge modes which are created in the quasi-energy spectrum. Such a system then represents a non-equilibrium

analogue of topological insulators, but with the added flexibility of an external periodic potential.

In this work we study the transport properties of Floquet edge-states. Our goal is to test whether transport through the edge modes of a two dimensional Floquet topological insulator is quantized and robust as in the case of equilibrium topological insulators. We initially focus on a two-terminal geometry and then move on to consider a six-terminal set-up. We expect the results and intuition developed here to be readily generalizable to other geometries. In general we find that the two-terminal conductivity of the Floquet edge-states is significantly different from the typical equilibrium value of $2e^2/h$ and can be either larger or smaller than this distinctive value depending on how the strength of the external field is tuned. The same holds true for the resistance measurements typical of a topological insulator in a six-terminal set-up.

The main results of this paper may be summarized as follows. The existence of quasi-energy edge states in the Floquet topological insulator is accompanied by a conductivity of $\sigma < 2e^2/h$, when the chemical potential lies in the quasi-energy gap. In addition, the value of $2e^2/h$ is obtained as a sum rule when the conductivity is summed over all ‘side bands’, i.e, over all energies which differ from a particular energy in the gap by an integer number of photon energies. Physically, the result $\sigma < 2e^2/h$ for non-equilibrium edge states corresponds to the presence of photons inhibiting access to the topologically protected edge states of the system.[24]

Moreover, in regions where the conductivity is smaller than $2e^2/h$, we find that the calculated values are robust to the effects of disorder, system size and changes to the Hamiltonian that maintain the energy gap. Such behavior is reminiscent of topologically protected edge states in equilibrium topological insulators and we indeed find that for the external potential strengths where we see this robustness there exist linearly dispersing, in-gap edge states in the quasi-energy spectrum. In regions where the conductivity is larger than $2e^2/h$

no robustness exists and the gap is closed, hence we are probing bulk effects.

The reduction of the topologically protected conductivity away from $2e^2/h$ can be intuitively understood by borrowing some machinery from the field of photon assisted tunneling (PAT)[25]. Namely, an electron that would normally tunnel into the edge-states of the system has a finite probability of absorbing/emitting a photon and being scattered out of the edge state. From the viewpoint of quasi-energy states this comes from understanding that the definite energy states of the leads do not perfectly overlap with the quasi-energy states of the Floquet topological insulator[15]. The heuristic description in terms of scattering of electrons by photons can be applied to observe a so-called ‘‘Floquet sum rule’’[1]. In short, the sum rule recovers all of the conductivity lost from PAT by summing over lead energies separated by photon energies $\hbar\Omega$, Ω being the frequency of the driving field. We have confirmed this sum rule using both numerics and an approximate analytic approach.

4.2 Model.

Our model Hamiltonian is that of a quantum well heterostructure[2] irradiated by linearly polarized light and subjected to a disorder potential. It is given as follows

$$H_S = \sum_{\mathbf{k}} \psi_{\mathbf{k}}^\dagger \begin{pmatrix} \hat{H}(\mathbf{k}, t) & 0 \\ 0 & \hat{H}^*(-\mathbf{k}, t) \end{pmatrix} \psi_{\mathbf{k}} - \sum_{i,\alpha} w_i \psi_{i,\alpha}^\dagger \psi_{i,\alpha} \quad (4.2.1)$$

where $\psi_{\mathbf{k}}^\dagger$ is a four component creation operator for electrons at momenta \mathbf{k} in angular momentum state $m_J = (1/2, 3/2, -1/2, -3/2)$ and ψ_i^\dagger is its Fourier transform. The first term above is the Hamiltonian of the clean, irradiated heterostructure and we have used $\hat{H}(\mathbf{k}) = \epsilon_{\mathbf{k}}\sigma_0 + \mathbf{d}(\mathbf{k}) \cdot \boldsymbol{\sigma} + 2(\mathbf{V} \cdot \boldsymbol{\sigma}) \cos \Omega t$. The second term takes into account disorder. We have used the standard definitions $\mathbf{d}(\mathbf{k}) = (A \sin k_x, A \sin k_y, M - 4B + 2B(\cos k_x + \cos k_y))$ and $\epsilon_{\mathbf{k}} = C - 2D(2 - \cos k_x - \cos k_y)$ and draw the disorder parameters, $\{w_i\}$,

randomly from an evenly distributed sample between $-W/2$ and $W/2$.

Following Lindner and coworkers[5], we set $C = D = 0$, $A = B = 0.2|M|$ and set $|M| = 1$ throughout (*i.e.* all energies are in units of $|M|$). To simulate a trivial system we set $M = -1$ so that $\text{sgn}(M/B) = -1$ [2, 5]. We take $\mathbf{V} = V_{ext}\hat{z}$ for concreteness. We note that the V_z component of \mathbf{V} is the important component from the point of view of creating Floquet edge states. It is this component that allows a gap to open and edge-states to stabilize[5]. The other components of \mathbf{V} lead to a renormalization of other components in the Hamiltonian. For a description of this renormalization see Chapter 3. Note that the field we consider here, and our subsequent observations in this paper, is assumed to always be “on”. We consider a field that was turned on in the distant past and is not switched off throughout the duration of our calculations. Furthermore, from this point forward we fix $\hbar\Omega = 2.3|M|$.

The goal of this paper will be to understand the transport properties of the non-equilibrium system described above. In order to accomplish this we must couple the system to leads/electrodes. We leave the specifics of this process to the appendix of this paper and here only discuss the matter at a high-level. We model the leads as being static (in time), *i.e.* the time-dependent field abruptly turns off at the leads. Ultimately the leads result in the system experiencing a self-energy proportional to $\Gamma(t)/2 = \sum_{\lambda} \Gamma_{\lambda}(t)/2$, where $\Gamma_{\lambda}(t)$ is the contribution of lead λ . In this paper we will work to simplify our discussion by employing the “wide-band” approximation. This phenomenological approach assumes that the density of states of the leads is constant over the energy scales in which we are interested. This amounts to assuming the Fourier transform of the lead operators, $\Gamma_{\lambda}(\epsilon)$, are independent of ϵ , *i.e.* $\Gamma_{\lambda}(\epsilon) \simeq \Gamma_{\lambda}$.

In the work in Ref. [24] we have studied a system with $\text{sgn}(M/B) > 0$. In other words, the system we were concerned with was a topological insulator, more specifically a quantum spin-Hall insulator, *before* any periodic perturbation was applied. Our work

was interested in observing the behavior of the topological edge-states in this system in the presence of a time-periodic drive. In contrast, our work here is focused on a system with trivial topology in equilibrium; there are no edge-states without the time-dependence. The system is a true Floquet topological insulator in the sense that its edge-states only develop after a time-periodic perturbation is applied. These edge-states rely crucially on band-mixing that comes from the periodic perturbation being *on-resonance*[5], i.e. the quantity $\hbar\Omega$ connects different parts of the band structure. The work in Ref. [24] only considers off-resonant light, where $\hbar\Omega$ does not join any existing eigenstates. This is in contrast to other systems, for example graphene[6–10, 26], where the Floquet topological insulator can be driven using an off-resonant perturbation[26].

Our understanding relies primarily on Floquet states[23]. Floquet states are the extension of stationary states to time-periodic systems. In a time-periodic system one deals with (Floquet) states that solve the Schrödinger equation and are characterized by a definite quasi-energy. These states are traditionally written as $|\psi_{\tilde{\eta}}(t)\rangle = e^{-i\tilde{\eta}t/\hbar}|\phi_{\tilde{\eta}}(t)\rangle$, which leads to the eigenvalue equation $(H(t) - i\hbar\partial_t)|\phi_{\tilde{\eta}}(t)\rangle = \tilde{\eta}|\phi_{\tilde{\eta}}(t)\rangle$ where $H(t)$ is the full Hamiltonian of the system, $\tilde{\eta}$ are the quasi-energies and $|\phi_{\tilde{\eta}}(t+T)\rangle = |\phi_{\tilde{\eta}}(t)\rangle$. We note that if $|\phi_{\tilde{\eta}}(t)\rangle$ is an eigenstate with quasi-energy $\tilde{\eta}$, then $e^{i\Omega t}|\phi_{\tilde{\eta}}(t)\rangle$ is also an eigenstate but with quasi-energy $\tilde{\eta} + \hbar\Omega$. Therefore the quasi-energy spectrum is only unique up to integer multiples of $\hbar\Omega$. This allows us to define a “Brillouin zone” for the quasi-energies, we will call this the Floquet zone. For this work we consider $0 \leq \eta < \hbar\Omega$, we will use the convention η to denote quasi-energies confined to this zone while $\tilde{\eta}$ above is unconfined. This reflects the fact that energy in a time periodic system is only conserved modulo $\hbar\Omega$; an electron in a quasi-energy state $|\phi_{\eta}(t)\rangle$ can always absorb or emit a photon.

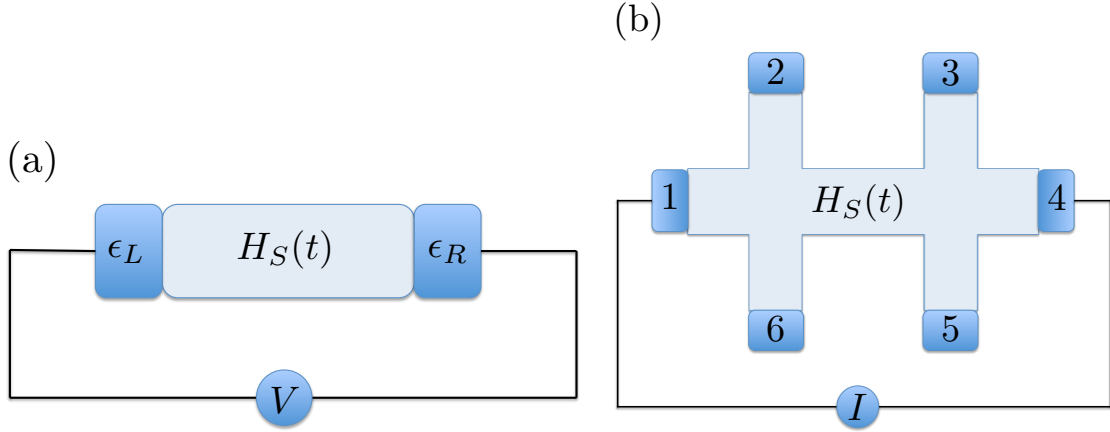


Figure 4.1: Two geometries considered in this work. On the left we have the two-terminal set-up with a bias voltage V/e offsetting the two Fermi energies ϵ_L and ϵ_R . On the right we have the six terminal set-up with a current I being driven between leads 1 and 4

4.3 Two Terminal Conductivity.

Let us begin with our results for the two-terminal conductivity of this system. We calculate the conductivity numerically using Floquet-Landauer theory[10, 26]. In this two-terminal setup, shown in Fig. 4.1a, we consider the leads to be kept at a voltage such that the Fermi level of both leads, which we will refer to as the lead energies, takes a value E . We then apply a (vanishingly) small bias voltage V/e so that the Fermi energies of the two leads are $\epsilon_L = E + V$ and $\epsilon_R = E$. We study the differential conductivity at a lead energy of $E = \Omega/2$ which is where the edge states are expected to be found[5]. Referring to our results in Fig. 4.2a we see that, with the exception of a small area near $V_{ext} = 0.3|M|$, the two-terminal conductivity generally decreases with V_{ext} in the range of parameters considered. We note that nowhere do we see a saturation to a value of $\sigma = 2e^2/h$, nor any other constant value. This fact notwithstanding, our results do have the striking feature that after a certain value of V_{ext} the conductivity becomes insensitive to the effects of disorder; in that region all of the curves overlap. In Fig. 4.2b we see that in this same region our results are insensitive to system length L and to the parameter Γ which describes the strength of the coupling to the leads. Thus we note our second result, for some values of V_{ext} the calculated

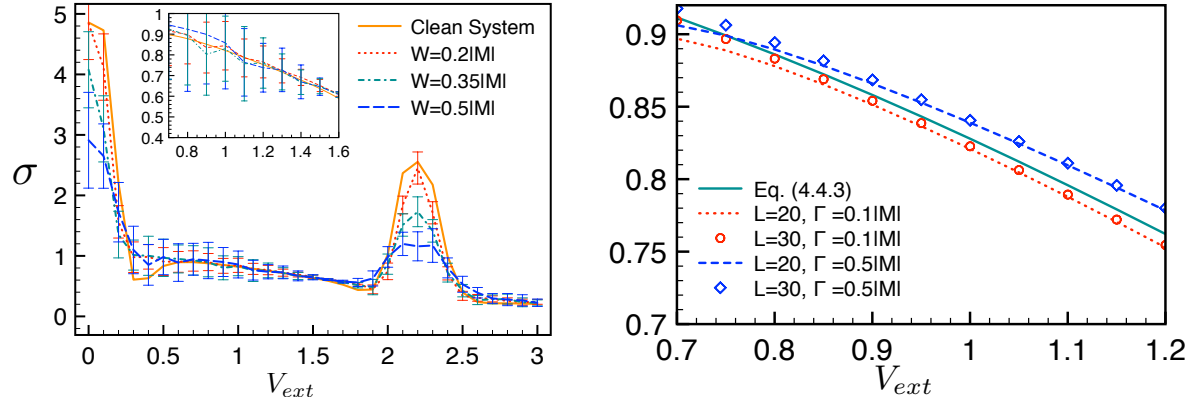


Figure 4.2: Two terminal conductivity in units of e^2/h . The left shows the conductivity at $E = \Omega/2$ in a two terminal set up as a function of external potential strength for various disorder strengths W and system size $L = 20$. The right is the conductivity for various values of the system size, L , and the lead coupling parameter Γ over a region where edge states are present.

conductivity is robust in the same way as for an equilibrium topological insulator.

The robustness in the conductivity coexists with the presence of edge-states in the quasi-energy spectrum. To show this we consider the system in the absence of leads and in a semi-infinite cylindrical geometry. By semi-infinite geometry we mean a system with open boundary conditions in the y direction and periodic boundary conditions in the x direction. The quasi-energy for our model appears in Fig. 4.3 for several values of the external potential strength V_{ext} . For small driving strength the gap remains closed, but as the strength is increased the gap opens up leaving linearly dispersing states. Further inspection of these states reveals that they reside on the edge of the system[5]. In general we have found that when this gap is open and large enough to withstand the effects of disorder or coupling to the leads, the value calculated for the conductivity is robust in the same sense as edge states in a topological insulator.

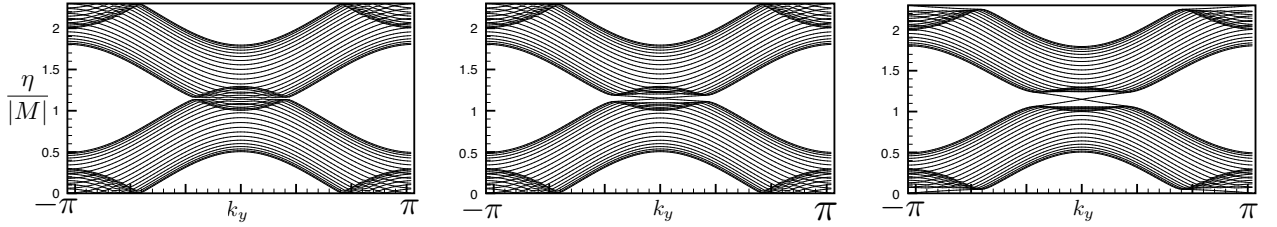


Figure 4.3: Quasi-energy spectrum of a topologically trivial sample at different driving amplitudes in a semi-infinite cylindrical geometry. The left plot is for $V_{ext} = 0.1|M|$, the middle $V_{ext} = 0.3|M|$, and the right $V_{ext} = 0.9|M|$.

4.4 Photon Inhibited Transport and Floquet Sum Rule.

Thus far we have shown that when this system plays host to edge states the conductivity we find appears to be topologically robust. We now address the question of why it does not have the hallmark value of $2e^2/h$. For this we further generalize a technique inspired by photon-assisted tunnelling[25, 27] and used in Ref. [24]. In this work it was shown that for a topological heterostructure the presence of an external time-periodic field reduces the conductivity away from $2e^2/h$. This reduction and other subsequent results can be accounted for by understanding that the external potential not only “dresses” the quantum well Hamiltonian, but also splits this dressed system into side-bands[25, 27]. The splitting means that the edge states of the system are only populated probabilistically, accounting for the reduction in the standard transport quantities. The specific application of Ref. [24] relied crucially on the driving potential being *off-resonance*, *i.e.* that it did not mix portions of the equilibrium band structure. The current system requires *on-resonance* light in order to drive the system into a topological state. In spite of this, our results are conducive to a similar interpretation in that we see topologically robust results in Fig. 4.2 that are different from $2e^2/h$.

To put this discussion on more general grounds we appeal to Floquet theory. As discussed previously, in a time-periodic system the states of interest are the steady state solutions $|\psi_\eta(t)\rangle = e^{-i\eta t/\hbar}|\phi_\eta(t)\rangle$, where η is the quasi-energy and $(H(t) - i\hbar\partial_t)|\phi_\eta(t)\rangle =$

$\eta|\phi_\eta(t)\rangle$. For periodic dependence in t we are free to define the following decomposition

$$|\phi_\eta(t)\rangle = \sum_n e^{-in\Omega t} |\phi_n\rangle \quad (4.4.1)$$

In the literature the states $|\phi_n\rangle$ are commonly called sideband states[28] and are determined as solutions to the eigenvalue equation $\sum_n \bar{H}_{n,m} |\phi_m\rangle = (\eta + n\hbar\Omega) |\phi_n\rangle$ where $\bar{H}_{n,m} = \frac{1}{T} \int_0^T dt e^{i(n-m)\Omega t} H(t)$.

We now calculate the time-averaged expectation value of the energy in the steady state $|\psi_\eta(t)\rangle$ which we define as $\bar{E} = \frac{1}{T} \int_0^T dt \langle \psi_\eta(t) | H(t) | \psi_\eta(t) \rangle$. Using the side-band decomposition in equation (4.4.1) and the fact that $|\psi_\eta(t)\rangle$ solves the Schrödinger equation immediately gives

$$\bar{E} = \sum_n (\eta + \hbar\Omega n) \langle \phi_n | \phi_n \rangle \quad (4.4.2)$$

Noting that $\langle \phi_n | \phi_n \rangle \geq 0$ and $\sum_n \langle \phi_n | \phi_n \rangle = 1$ (the latter property follows from the normalization of $|\phi_\eta(t)\rangle$) allows us to interpret the above average as follows. In the quantum state $|\psi_\eta(t)\rangle$ the energies $\eta + \hbar\Omega n$ occur with probability $\langle \phi_n | \phi_n \rangle$.

We now tie the above statistical interpretation to our observations of the transport in the Floquet topological insulators. For the system of interest one can calculate the appropriate quasi-energies $0 \leq \eta < \hbar\Omega$ and their corresponding wave functions $|\phi_\eta(t)\rangle$, these are the steady states of our sample. Now, when electrons from the lead are injected into the system at some definite energy E , as opposed to an equilibrium case, only a portion of the sample state overlaps with the definite energy lead state[15]. Physically, we envision this in terms of electrons being able to absorb or emit photons once they enter the sample. For lead electrons at an energy $E = \eta + N\hbar\Omega$ there is only a probability $\langle \phi_N | \phi_N \rangle$ that the electron will absorb/emit enough photons to access the sample state with quasi energy η . This quasi-energy spectrum may contain topologically protected edge states[12–16]. Now, when we try to access these states from a charge transport point of view we can only access the

state at a certain probability, because of the possibility to absorb/emit photons. Therefore expected signatures of these edge states, *e.g.* $\sigma = 2e^2/h$ conductance, are probabilistically suppressed.

Note that this argument *does not* rely on the periodic perturbation being on or off resonance, it is simply a consequence of the discrete time-translational invariance. Therefore, when one is dealing with Floquet edge-states it should be kept in mind that the weight of these edge states is distributed into sidebands as discussed above. Indeed in the current system one can approximately obtain a description of the conductivity at specific lead energies $E + n\hbar\Omega$ (where the edge-states live). Quoting only the result here (for a detailed derivation please see the appendix)

$$\begin{aligned} \sigma(E + N\hbar\Omega) &\simeq \frac{1}{2} \left(J_N^2 \left(\frac{2V_{ext}}{\hbar\Omega} \right) + J_{N+1}^2 \left(\frac{2V_{ext}}{\hbar\Omega} \right) \right) \\ &\times \tilde{\sigma}(E, V_{ext}) \end{aligned} \quad (4.4.3)$$

where the relevant energy E is chosen to be in the vicinity of $\hbar\Omega/2$ where the localized quasi-energy states appear. $\tilde{\sigma}(E, V_{ext})$ is a complicated function of the model parameters and, interestingly, *cannot* be thought of as the conductivity of some effective static system. We find numerically that $\tilde{\sigma}(E, V_{ext}) \simeq 2e^2/h$ when edge-states are present in the quasi-energy spectrum. The important implication of the above formula is that the conductivity can be thought of as an overall probabilistic factor times a conductivity expression. The above approximate result compares very well to our numerical calculations. A plot of this function appears in Fig. 4.2b.

With the intuition for why the conductivity is suppressed in Floquet topological edge-states, let us move on to present results for how the value of $2e^2/h$ can be recovered. In short, by setting lead energies at $\hbar\Omega/2 + n\hbar\Omega$ and summing over all n we should be able to recollect the lost statistical weight from the photon scattering. Towards this end we

consider the quantity[1]

$$\bar{\sigma}(E, V_{ext}) = \sum_n \sigma(E + n\hbar\Omega) = \tilde{\sigma}(E, V_{ext}). \quad (4.4.4)$$

We calculate $\bar{\sigma}(E \simeq \Omega/2)$ for various different values of V_{ext} and also at different disorder strengths. Our results are presented in Fig. 4.4. What we see is quite satisfying: for a window of V_{ext} values we see that $\bar{\sigma} = 2e^2/h$. Moreover, this window corresponds to the same parameter regime where there are in-gap quasi-energy edge states, and insensitivity of the system to disorder, system size and other parameters in Figs. 4.2, 4.3.

We understand the plot in Fig. 4.4 as follows. For smaller V_{ext} the external field is not strong enough to open a gap and “expose” the edge states. Therefore the conduction σ is a result of bulk processes and thus sensitive to disorder strength. As V_{ext} gets large enough to open a sufficiently stable gap the edge states appear in this gap and are unobscured by bulk states. Here we see $\bar{\sigma} = 2e^2/h$ and an *insensitivity* to disorder strength. Eventually V_{ext} becomes so strong that the gap closes again and bulk states dominate. In this case $\bar{\sigma}(\hbar\Omega/2) > 2e^2/h$ representing bulk conductivity. When the gap opens again at a larger external potential we see a reversion back to $\bar{\sigma} = 2e^2/h$.

4.5 Hall Bar Geometry and Edge States

Up to now we have presented our findings in a two-terminal device geometry. We now move on to study a six-terminal device in an effort to further illustrate that the conductivity discussed above is indeed a result of conduction along the edge of the sample, and not some coincidental edge effect. Our set-up is motivated by experiments on Hall Bar systems[3, 10, 29]. An illustration of the set-up that we have in mind appears in Fig. 4.1b.

In the absence of a periodic driving potential the six terminal geometry is used as follows. Assuming all voltages are close to the Fermi level and that all leads are identical so

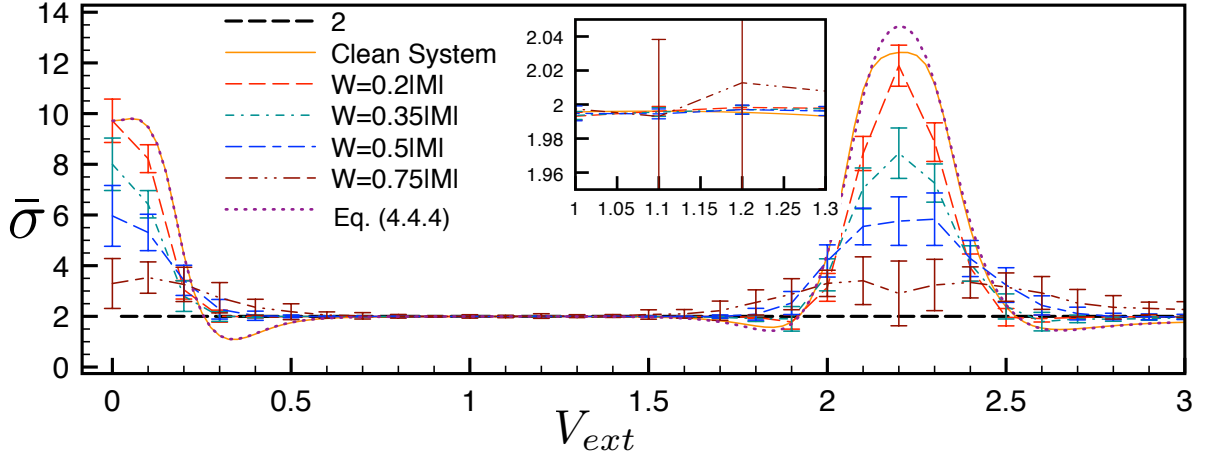


Figure 4.4: Results for disorder averaged summed conductivity, *i.e.* Eq. (4.4.4) in the text, with $M = -1$ and $E = \Omega/2$ and in units of e^2/h for various disorder strengths W . The inset shows a zoomed in picture of the first area of conductivity quantization. The disorder plots are constructed by averaging over 40 randomly drawn collection of disorder potentials while the error bars represent one standard deviation of this data. Note some error bars in the insets are too small to see. This data has been obtained from a calculation on a 20×20 lattice.

we can drop the pumped current[10] one approximates Eq. (4.A.5) as

$$\bar{I}_\lambda = -\frac{e^2}{h} \sum_{\lambda'} (T_{\lambda,\lambda'}(E_f)V_{\lambda'} - T_{\lambda',\lambda}(E_f)V_\lambda) \quad (4.5.1)$$

where λ labels each of the side terminals. For a spin-Hall insulator dissipationless edge states exist and so one expects $T_{i,i+1} = T_{i+1,i} = 1$ where we periodically identify $6 + 1 \rightarrow 1$. Now one imagines driving a current I from contact 1 to contact 4. We then have $\mathbf{I} = (I, 0, 0, -I, 0, 0)^T$ where we have defined $\mathbf{I}_i = \bar{I}_i$. Inverting Eq. (4.5.1) one can find the voltages required to drive such a current. Doing so gives $V_1 - V_4 = \frac{3h}{2e^2}I$ and $V_2 - V_3 = \frac{h}{2e^2}I$. Defining $R_{i,j} = (V_i - V_j)/I$ as the resistance between terminals i and j we find $R_{1,4} = \frac{3}{2}h/e^2$ and $R_{2,3} = \frac{1}{2}h/e^2$. These values are unique to transport from dissipationless, helical edge states

Here we will discuss a generalization of this concept to the effect which we have dis-

cussed so far. For our insulator in the topological regime we find that $T_{i,j} = 0$ except the off-diagonal elements $T_{i,i+1}$ and $T_{i+1,i}$ where again we periodically identify $6 + 1 \rightarrow 1$. In contrast to the equilibrium observation we find that $T_{i,i+1} = T_{i+1,i} = T^{(n)} \neq 1$ where $T^{(n)}$ is the tunneling value for the lead Fermi energies near the gap in the n^{th} Floquet zone. We now again imagine driving a current I from contact 1 to contact 4 with the bias voltages set near the middle of the gap in the n^{th} Floquet zone. Defining $R_{i,j}^{(n)} = (V_i - V_j)/I$ as the resistance between terminals i and j in this case we find $R_{1,4}^{(n)} = \frac{3}{2T^{(n)}}h/e^2$ and $R_{2,3}^{(n)} = \frac{1}{2T^{(n)}}h/e^2$. Note that the signature results in terms of rational fractions of h/e^2 are lost, they've been reduced by a factor of $T^{(n)}$.

Using the above result we can realize two interesting properties of these Floquet devices. The first is the following

$$\frac{R_{1,4}^{(n)}}{R_{2,3}^{(n)}} \simeq 3 \quad \forall n \quad (4.5.2)$$

That is, taking the ratio of these two resistances gives 3 regardless of which Floquet zone the Fermi energies are set in. Finally, in analogy with how we can retain the quantized value of σ in the two-terminal device considered above we can retain the equilibrium result here as follows

$$\bar{R}_{1,4}^F = \left(\sum_n \frac{1}{R_{1,4}^{(n)}} \right)^{-1} = \frac{3}{2}h/e^2 \quad (4.5.3)$$

and

$$\bar{R}_{2,3}^F = \left(\sum_n \frac{1}{R_{2,3}^{(n)}} \right)^{-1} = \frac{1}{2}h/e^2 \quad (4.5.4)$$

These results are consistent with the picture developed above of edge-states that are only occupied in a probabilistic way. The fact that $T_{i,j \neq i \pm 1} = 0$ reflects the edge conductance. The fact that $T_{i,i \pm 1} < 1$ reflects the fact that in a periodically driven system electrons entering lead i has a probability to absorb or emit a photon before reaching terminal $i \pm 1$. Thus $T_{i,j}$ is reduced. By summing over all Floquet zones we again effectively sum over all of these probabilities and retain the expected equilibrium result.

As a numerical test of the above we calculate T_{ij} for lead energies $(n + 1/2)\hbar\Omega$ for $V_{ext} = 0.675|M|$, i.e. where we expect to see in gap edge-states. In our calculation we find $T_{ij} = 0$ for $i \neq j$ except when $j = i \pm 1$. We observe that $T_{i,i\pm 1}(n = 0) = T_{i,i\pm 1}(n = -1) \simeq 0.46$, $T_{i,i\pm 1}(n = 1) = T_{i,i\pm 1}(n = -2) \simeq 0.04$ and zero for all other n 's. These numerical values satisfy $\sum_n T_{i,i\pm 1}(n) = 1$ and therefore satisfy the results established in this section.

4.6 Conclusions.

We have explored the transport properties of Floquet topological edge-states in a quantum well heterostructure. At first we took a numerical approach which showed that in the presence of Floquet edge states in the quasi-energy spectrum the two-terminal conductivity is topologically robust, albeit *not* quantized to $2e^2/h$.

To explain the reduction of the two-terminal conductivity compared to the equilibrium value of $2e^2/h$ we appealed to an intuitive description in terms of electrons being scattered by photons. This picture consists of viewing the Floquet edge states in the quasi-energy spectrum as having their weight distributed into side-bands of energies $\eta + n\hbar\Omega$. The result of this side-band distribution is that as we attempt to inject an electron from a lead at some energy E there is a certain probability that it will absorb/emit enough photons to find the Floquet edge state.

The heuristic picture in terms of scattering by photons motivated us to propose a means to salvage the equilibrium conductivity of $2e^2/h$. This can be done using a recently proposed Floquet sum rule[1], which in our formalism has a natural interpretation. In our picture the topological Floquet states represent a superposition of states in various side bands. The different coefficients in the superposition $\langle \phi_n | \phi_\eta \rangle$ determine the overlap. Our Floquet edge states nicely obey this sum rule showing a summed conductivity value of

$\bar{\sigma} = 2e^2/h$ is found when the external field is such that edge states in the quasi-energy spectrum exist. Moreover, the result $\bar{\sigma} = 2e^2/h$ is robust to disorder even up to very large disorder strengths.

Finally, we have extended our results to study a six-terminal, or Hall-bar, set-up. Here the equilibrium signatures of the quantum spin-Hall effect are several characteristic resistance measurements. We have shown that these resistances are increased relative to the equilibrium case. This fact notwithstanding, following our intuition from the two-terminal results we have suggested a sum rule for the six-terminal resistance measurements that recovers the equilibrium result. This sum rule is also intuitively explained in terms of photon-inhibition of edge-states.

4.7 Acknowledgments

The authors are thankful for useful discussions with Jean-René Soquet, Aashish Clerk and Gil Refael. Financial support for this work was provided by the NSERC and FQRNT (TPB) and the Vanier Canada Graduate Scholarship (AF). Numerical calculations for this work were performed using McGill HPC supercomputing resources.

4.A Floquet-Landauer Formalism for Transport

Here we present only the essential aspects of the Floquet-Landauer formalism. A more detailed description of our specific approach to this problem can be found in the Supplemental material of [24]. Moreover, an excellent review can be found in Ref. [28].

We begin with a generic Hamiltonian which is given by

$$H = H_S(t) + H_L + H_C \tag{4.A.1}$$

where

$$H_S(t) = c^\dagger \mathcal{H}_S(t) c \quad (4.A.2)$$

is the Hamiltonian of the sample where $c^\dagger = (c_1^\dagger \dots c_{N_s}^\dagger)$ is a vector containing creation operators for each of the N_s degrees of freedom in the sample and $\mathcal{H}_S(t)$ is a $N_s \times N_s$ matrix coupling these degrees of freedom. This matrix contains both the static properties of the sample as well as the time dependent effects of the periodic field. Next,

$$H_L = \sum_{\lambda} b_{\lambda}^{\dagger} \mathcal{H}_{L,\lambda} b_{\lambda} \quad (4.A.3)$$

is the Hamiltonian of all of the leads where $b_{\lambda}^{\dagger} = (b_{1,\lambda}^{\dagger} \dots b_{N_{l,\lambda},\lambda}^{\dagger})$ is a vector containing creation operators for each of the N_l degrees of freedom in the lead λ and $\mathcal{H}_{l,\lambda}$ is a $N_{l,\lambda} \times N_{l,\lambda}$ matrix coupling these degrees of freedom. Finally,

$$H_C = \sum_{\lambda} \left(b_{\lambda}^{\dagger} \mathcal{K}_{\lambda} c + \text{h.c.} \right) \quad (4.A.4)$$

is the Hamiltonian coupling the sample to each of the leads. \mathcal{K}_{λ} is the $N_{l,\lambda} \times N_s$ matrix that describes these coupling strengths. The above model is completely general and makes no specification of band structure or dimension of the system.

The time-averaged current flowing through the sample out of lead λ can be shown to read as follows

$$\bar{I}_{\lambda} = \frac{e}{h} \sum_{\lambda'} \int d\epsilon (T_{\lambda,\lambda'}(\epsilon) f_{\lambda'}(\epsilon) - T_{\lambda',\lambda}(\epsilon) f_{\lambda}(\epsilon)) \quad (4.A.5)$$

where $f_{\lambda}(\epsilon) = \frac{1}{1 + \exp(\beta_{\lambda}(\epsilon - eV_{\lambda}))}$ and we have defined the transmission matrices

$$T_{\lambda,\lambda'}(\epsilon) = \sum_n \text{Tr} \left[\Gamma_{\lambda}(\epsilon + \hbar n \Omega) G^{(n)}(\epsilon) \Gamma_{\lambda'}(\epsilon) (G^{(n)}(\epsilon))^{\dagger} \right]. \quad (4.A.6)$$

where

$$G^{(n)}(\epsilon) = \frac{1}{T} \int_0^T e^{in\Omega t} G(t, \epsilon) dt \quad (4.A.7)$$

and $G(t, \epsilon)$ solves

$$\begin{aligned} & \left(i\hbar \frac{d}{dt} + \epsilon - \mathcal{H}_S(t) \right) G(t, \epsilon) \\ & + i \int_0^\infty e^{i\epsilon\tau/\hbar} \Gamma(\tau) G(t - \tau, \epsilon) d\tau = I_{N_s \times N_s} \end{aligned} \quad (4.A.8)$$

In the above $\Gamma(t)$ can be thought of as the self-energy obtained from integrating out the leads in the system. From our microscopic Hamiltonian above it is given by

$$\Gamma_\lambda(t) = \frac{1}{\hbar} \mathcal{K}_{L,\lambda}^\dagger g_{\lambda,L}(t) \mathcal{K}_{L,\lambda} \quad (4.A.9)$$

and $\Gamma(t) = \sum_\lambda \Gamma_\lambda(t)$. In the above we have also defined $g_{\lambda,L}(t-t') = \exp[-\frac{i}{\hbar} \mathcal{H}_{L,\lambda}(t-t')]$, which is the temporal Green function of the isolated leads. In this paper we will work to simplify our discussion by employing the “wide-band” approximation. This phenomenological approach assumes that the density of states of the leads is constant over the energy scales in which we are interested. This amounts to assuming the lead operators, $\Gamma_\lambda(\epsilon)$, are independent of ϵ , $\Gamma_\lambda(\epsilon) \simeq \Gamma_\lambda$. Moreover, we make the assumption of identical leads so that $(\Gamma_\lambda)_{i,j} = \Gamma \delta_{i,j} \delta_{i,\mathbf{x}_\lambda}$ where \mathbf{x}_λ are the set of all sample degrees of freedom connected to lead λ . We note that as we are dealing with topological transport properties none of these details should change our results.

In a two-terminal device the sample has leads attached to its left and right edges. For this type of device we label these leads as L for left and R for right. By conservation of current we must have $\bar{I}_R = -\bar{I}_L$, since the current entering the right lead must be equal to the current leaving the left lead. It is then sufficient to think only of \bar{I}_R . We now imagine biasing our sample so that we have a voltage $E/e + V/e$ on the left lead and a voltage

$E/e + 0$ on the right lead, where E is the Fermi level of both leads. We then define the (differential) conductance as

$$\sigma(E) = \left. \frac{d\bar{I}_R}{dV} \right|_{V=0} = \frac{e^2}{h} T_{R,L}(E) \quad (4.A.10)$$

Thus for this geometry we have the simple result that the conductivity is simply given by the total transmission coefficient from the left lead to the right lead.

4.B Approximate Result for the Conductivity

Here we detail the steps taken to derive the approximate result for the conductivity presented in Eq. (4). We begin (in the wide band approximation) with the equation of motion for $G(t, \epsilon)$

$$\left(i\hbar \frac{d}{dt} + \epsilon - \mathcal{H}_S(t) + \frac{i}{2}\Gamma \right) G(t, \epsilon) = I \quad (4.B.1)$$

We note the fact that $G(t, \epsilon)$ explicitly depends on time. This is in contrast to equilibrium where $G(t, \epsilon) \rightarrow G(\epsilon)$ has no time dependence (as $\mathcal{H}_S(t) = \mathcal{H}_S$) and the above simplifies to $(\epsilon - \mathcal{H}_S + \frac{i}{2}\Gamma) G(\epsilon) = I$. The remaining time index can be shown to be periodic in time[28] and therefore we are free to define.

$$G^{(n)}(\epsilon) = \frac{1}{T} \int_0^T dt e^{in\Omega t} G(t, \epsilon) \quad (4.B.2)$$

It is the above object that we ultimately need to find.

This task is simplified by considering instead the auxiliary equation

$$\left(i\hbar \frac{d}{dt} + \epsilon - \mathcal{H}_S(t) + \frac{i}{2}\Gamma \right) \mathcal{G}(t, t', \epsilon) = \delta(t - t') \quad (4.B.3)$$

and then noting that

$$G(t, \epsilon) = \int dt' \mathcal{G}(t, t', \epsilon) \quad (4.B.4)$$

We will now focus on Eq. (4.B.3). By writing $\mathcal{H}_S(t) - \frac{i}{2}\Gamma = \hat{\mathcal{H}}_S + H_{ext}(t)$ and introducing the rotating frame picture

$$\mathcal{G}(t, t', \epsilon) = U_V(t) \check{\mathcal{G}}(t, t', \epsilon) U_V^\dagger(t') \quad (4.B.5)$$

where $i\hbar \frac{d}{dt} U_V(t) = H_{ext}(t) U_V(t)$. Then it follow that $\check{\mathcal{G}}(t, t', \epsilon)$ is a solution to

$$\left(i\hbar \frac{d}{dt} + \epsilon - \hat{\mathcal{H}}_S(t) \right) \check{\mathcal{G}}(t, t', \epsilon) = \delta(t - t') \quad (4.B.6)$$

with the “rotating” version of $\hat{\mathcal{H}}_S$ being $\hat{\mathcal{H}}_S(t) = U_V(t)^\dagger \hat{\mathcal{H}}_S U_V(t)$. If the external, periodic potential were some potential with no internal structure coupling the degrees of freedom of the system then we would have $\hat{\mathcal{H}}_S(t) = \hat{\mathcal{H}}_S$ as $H_{ext}(t)$ would commute with all other terms. This would immediately lead to a static system and a direct analogue of photon assisted tunneling.

For this particular problem $H_{ext}(t)$ commutes with itself at different times. As a result $U_V(t+T) = U_V(t)$ and it is useful to define

$$\begin{aligned} U_V(n) &= \frac{1}{T} \int_0^T dt e^{in\Omega t} U_V(t) \\ \hat{\mathcal{H}}_S(n) &= \frac{1}{T} \int_0^T dt e^{in\Omega t} \hat{\mathcal{H}}_S(t) \end{aligned} \quad (4.B.7)$$

Using all of these ingredients we then have

$$G^{(n)}(\epsilon) = \frac{1}{T} \int_0^T dt e^{in\Omega t} \int dt' U_V(t) \check{\mathcal{G}}(t, t', \epsilon) U_V^\dagger(t') \quad (4.B.8)$$

Our task becomes to solve Eq. (4.B.6). We do so by defining

$$\check{G}(t, t', \epsilon) = \frac{1}{T} \sum_{n,m} e^{-in\Omega t} e^{im\Omega t'} \check{G}_{n,m}(\epsilon) \quad (4.B.9)$$

which reduces Eq. (4.B.6) to the difference equation

$$\left(\ell \hbar \Omega + \epsilon - \hat{\mathcal{H}}_S(0) \right) \check{G}_{\ell,m}(\epsilon) - \sum_{n \neq \ell} \hat{\mathcal{H}}_S(\ell - n) \check{G}_{n,m}(\epsilon) = \delta_{\ell,m} \quad (4.B.10)$$

Where $\hat{\mathcal{H}}_S(\ell)$ is defined in equation (4.B.7). All of the Fourier expansions above when used with Eqs. (4.B.2) and (4.B.4) then give

$$G^{(n)}(\epsilon) = \sum_{\ell,m} U_V(n - \ell) \check{G}_{\ell,m}(\epsilon) U_V^\dagger(-m) \quad (4.B.11)$$

We now make note of a symmetry in the difference equation for $\check{G}_{\ell,m}(\epsilon)$. Namely we note that simultaneously shifting $\ell \rightarrow \ell - k$, $m \rightarrow m - k$ and $\epsilon \rightarrow \epsilon + k\hbar\Omega$ for any integer k in Eq. (4.B.10) shows that if $\check{G}_{\ell,m}(\epsilon)$ is a solution than so is $\check{G}_{\ell-k,m-k}(\epsilon + k\hbar\Omega)$, we thus identify[30]

$$\check{G}_{\ell,m}(\epsilon) = \check{G}_{\ell-k,m-k}(\epsilon + k\hbar\Omega) \quad (4.B.12)$$

From the above one can conclude that all of the relevant information is contained in $\check{G}_{\ell,0}(\epsilon) \equiv G_V^{(\ell)}(\epsilon)$. The operator $G_V^{(\ell)}(\epsilon)$ solves the equation

$$\left(\ell \hbar \Omega + \epsilon - \hat{\mathcal{H}}_S(0) \right) G_V^{(\ell)}(\epsilon) - \sum_n \hat{\mathcal{H}}_S(\ell - n) G_V^{(n)}(\epsilon) = \delta_{\ell,0} \quad (4.B.13)$$

We can then write $\check{G}_{\ell,m}(\epsilon) = G_V^{(\ell-m)}(\epsilon + m\hbar\Omega)$. Plugging this in above yields

$$G^{(n)}(\epsilon) = \sum_{\ell,m} U_V(n - \ell) G_V^{(\ell-m)}(\epsilon + m\hbar\Omega) U_V^\dagger(-m) \quad (4.B.14)$$

sending $m \rightarrow -m$ and then $\ell \rightarrow \ell - m$ then gives main result of this discussion

$$G^{(n)}(\epsilon) = \sum_{\ell, m} U_V(n + m - \ell) G_V^{(\ell)}(\epsilon - m\hbar\Omega) U_V^\dagger(m) \quad (4.B.15)$$

We will use the above to find an approximate formula for the conductivity. We will develop a few other necessary relations

So far our discussion has been general with the only assumption being that $[H_{ext}(t), H_{ext}(t')] = 0, \forall(t, t')$ (a more general treatment in the absence of this restriction is currently a work in progress [31]). At this point we specialize to the quantum well system which has been discussed in the main text. Our first task is to define the operators $U_V(m)$. We are interested in $\mathcal{H}_{ext}(t) = 2V_{ext} \cos(\Omega t)$ where $V_{ext} = V_e \sigma_z \otimes I_L$, I_L is the identity operator on the lattice and σ_z acts on spin. This operator commutes with itself at different times and is diagonal in “spin-lattice” space. This allows us to easily define the time evolution operator as follows

$$U_V(t) = e^{-i \int_0^t dt' \mathcal{H}_{ext}(t')} = \exp \left[-i \frac{2V_e}{\hbar\Omega} \sin(\Omega t) \sigma_z \otimes I_L \right] \quad (4.B.16)$$

note that no time ordering is required in the exponential because $[H_{ext}(t), H_{ext}(t')] = 0$. Finding the Fourier series of the above periodic function is made possible by the identity $e^{-ix \sin(\Omega t)} = \sum_m J_m(x) e^{-i\Omega m t}$ where $J_m(\cdot)$ is the Bessel function of the first kind of order m . We thus have

$$U_V(t) = \sum_m J_m \left(\frac{2V_e}{\hbar\Omega} \sigma_z \otimes I_L \right) e^{-i\Omega m t} \quad (4.B.17)$$

We can then read off

$$\begin{aligned} U_V(m) &= J_m \left(\frac{2V_e}{\hbar\Omega} \sigma_z \otimes I_L \right) = J_m \left(\frac{2V_e}{\hbar\Omega} \right) S_m \otimes I_L \\ &= J_m \left(\frac{2V_{ext}}{\hbar\Omega} \right) \end{aligned} \quad (4.B.18)$$

where $S_m = \sigma_0$ if m is even and σ_z if m is odd and the second and third equality can be established using a series expansion of the Bessel function. The second relation above comes from the Bessel function property $J_m(-x) = (-1)^m J_m(x)$. The third relation, $J_m\left(\frac{2V_{ext}}{\hbar\Omega}\right)$ is a compact form which will be useful in a derivation of the transmission elements. With an explicit formula of $U_V(m)$ in hand we proceed to plug Eq. (4.B.15) for the Green's function into the formula for $T_{\lambda,\lambda'}(\epsilon)$ which gives

$$T_{\lambda,\lambda'}(\epsilon) = \sum_{n,\ell,m} \sum_{\ell',m'} \text{Tr} \left[J_{n+m'-\ell'} \left(\frac{2V_{ext}}{\hbar\Omega} \right) J_{n+m-\ell} \left(\frac{2V_{ext}}{\hbar\Omega} \right) \right. \quad (4.B.19)$$

$$\left. \Gamma_\lambda G_V^{(\ell)}(\epsilon - m\hbar\Omega) J_m \left(\frac{2V_{ext}}{\hbar\Omega} \right) \Gamma_{\lambda'} J_{m'} \left(\frac{2V_{ext}}{\hbar\Omega} \right) (G_V^{(\ell')}(\epsilon - m'\hbar\Omega))^\dagger \right]$$

where we have used the fact that the lead self energies commute with V_{ext} (the leads make no distinction between different spins of particles). The sum over Bessel functions gives a delta function. After some index relabelling we are left with

$$T_{\lambda,\lambda'}(\epsilon) = \sum_{\ell,\ell',m} \text{Tr} \left[\Gamma_\lambda G_V^{(\ell)}(\epsilon - (m+\ell)\hbar\Omega) \Gamma_{\lambda'} J_{m+\ell} \left(\frac{2V_{ext}}{\hbar\Omega} \right) J_{m+\ell'} \left(\frac{2V_{ext}}{\hbar\Omega} \right) (G_V^{(\ell')}(\epsilon - (m+\ell')\hbar\Omega))^\dagger \right] \quad (4.B.20)$$

We see that knowledge of $G_V^{(\ell)}(\epsilon - (m+\ell)\hbar\Omega)$ will allow us to find the tunnelling matrices and hence the two terminal conductivity. Towards this end we now write a formal solution of the difference equation for $G_V^{(\ell)}(\epsilon)$.

To make the notation more compact let us define

$$\bar{H}_\ell = \begin{cases} \hat{\mathcal{H}}_S(\ell) & : \ell \neq 0 \\ 0 & : \ell = 0 \end{cases} \quad (4.B.21)$$

Besides being less cumbersome, this convention allows us to drop the restrictions on the

sums and eventually employ Einstein summation convention. Starting from Eq. (4.B.10) and acting on both sides with $\left(\ell\hbar\Omega + \epsilon - \hat{\mathcal{H}}_S(0)\right)^{-1}$ then gives

$$G_V^{(\ell)}(\epsilon) = \left(\ell\hbar\Omega + \epsilon - \hat{\mathcal{H}}_S(0)\right)^{-1} \delta_{\ell,0} \quad (4.B.22)$$

$$+ \sum_n \left(\ell\hbar\Omega + \epsilon - \hat{\mathcal{H}}_S(0)\right)^{-1} \bar{H}_{\ell-n} G_V^{(n)}(\epsilon)$$

Let us note that $g_F(\epsilon) = \left(\epsilon - \hat{\mathcal{H}}_S(0)\right)^{-1}$ is the Green's function of the static system with Hamiltonian $\hat{\mathcal{H}}_S(0)$. Therefore

$$G_V^{(\ell)}(\epsilon) = g_F(\epsilon)\delta_{\ell,0} + \sum_j g_F(\epsilon + \ell\hbar\Omega)\bar{H}_{\ell-j}G_V^{(j)}(\epsilon) \quad (4.B.23)$$

We now iterate this equation. To do this let us introduce some notation to extract the useful part of the above. First, we use implied summation over repeated indices that are not ℓ . Second, we define $g_i = g_F(\epsilon + i\hbar\Omega)$. This gives

$$G_V^{(\ell)}(\epsilon) = g_0\delta_{\ell,0} + g_\ell\bar{H}_\ell g_0 + g_\ell\bar{H}_{\ell-j}g_j\bar{H}_{j-j'}G_V^{(j')}(\epsilon) \quad (4.B.24)$$

Repeated iteration of the above difference equation allows us to write

$$G_V^{(\ell)}(\epsilon) = g_0\delta_{\ell,0} \quad (4.B.25)$$

$$+ g_\ell(\bar{H}_\ell + \bar{H}_{\ell-j}g_j\bar{H}_j + \bar{H}_{\ell-j}g_j\bar{H}_{j-j'}g_{j'}\bar{H}_{j'})$$

$$+ \bar{H}_{\ell-j}g_j\bar{H}_{j-j'}g_{j'}\bar{H}_{j'-\alpha}g_\alpha\bar{H}_\alpha$$

$$+ \bar{H}_{\ell-j}g_j\bar{H}_{j-j'}g_{j'}\bar{H}_{j'-\alpha}g_\alpha\bar{H}_{\alpha-\beta}g_\beta\bar{H}_{\beta-\sigma}g_\sigma\bar{H}_\sigma + \dots)g_0$$

Or

$$G_V^{(\ell)}(\epsilon) = g_F(\epsilon)\delta_{\ell,0} + g_F(\epsilon + \ell\hbar\Omega)\check{D}_\ell(\epsilon)g_F(\epsilon) \quad (4.B.26)$$

Where

$$\begin{aligned}
\check{D}_\ell(\epsilon) &= \bar{H}_\ell + \bar{H}_{\ell-j}g_j\bar{H}_j + \bar{H}_{\ell-j}g_j\bar{H}_{j-j'}g_{j'}\bar{H}_{j'} \\
&+ \bar{H}_{\ell-j}g_j\bar{H}_{j-j'}g_{j'}\bar{H}_{j'-\alpha}g_\alpha\bar{H}_\alpha \\
&+ \bar{H}_{\ell-j}g_j\bar{H}_{j-j'}g_{j'}\bar{H}_{j'-\alpha}g_\alpha\bar{H}_{\alpha-\beta}g_\beta\bar{H}_{\beta-\sigma}g_\sigma\bar{H}_\sigma + \dots
\end{aligned} \tag{4.B.27}$$

The above series can in turn be generated by (restoring the summation symbols)

$$\begin{aligned}
\check{D}_\ell(\epsilon) &= \bar{H}_\ell + \sum_j \bar{H}_{\ell-j}g_j\bar{H}_j \\
&+ \sum_{j,j'} \bar{H}_{\ell-j}g_j\bar{H}_{j-j'}g_{j'}\check{D}_{j'}(\epsilon)
\end{aligned} \tag{4.B.28}$$

Physically, the Greens function $G_V^{(\ell)}(\epsilon)$ is described by all possible processes starting at energy ϵ (indicated by amplitude $g_F(\epsilon)$) where the electrons absorb/emit a *net* number of photons ℓ (indicated by amplitude $\check{D}_\ell(\epsilon)$) and then end up at an energy eigenstate $\epsilon + \ell\hbar\Omega$ (hence $g_F(\epsilon + \ell\hbar\Omega)$).

We are interested in energies $E + N\hbar\Omega$ where $E \simeq \hbar\Omega/2$. Near such energies the Greens functions we need are then given by

$$\begin{aligned}
G_V^{(\ell)}(E + (N - m - \ell)\hbar\Omega) &= g_F(E + (N - m)\hbar\Omega)\delta_{\ell,0} \\
&+ g_F(E + (N - m)\hbar\Omega)\check{D}_\ell(E + (N - m - \ell)\hbar\Omega)g_F(E + (N - m - \ell)\hbar\Omega)
\end{aligned} \tag{4.B.29}$$

We now assume that for the parameters we are interested in the unit of energy $\hbar\Omega$ connects two (and not more) points on the spectrum of $\hat{\mathcal{H}}_S(0)$. Namely an energy $-\Omega\hbar$ can move us from $\Omega/2$ to $-\Omega/2$. Any other photon processes are not possible though. Plotting the spectrum of $\hat{\mathcal{H}}_S(0)$ reveals this to be true for the parameters we have considered in the main text.

The above discussion leads us to make the approximation

$$g_F(E + K\hbar\Omega) = \delta_{K,0}g_F(E) + \delta_{K,-1}g_F(-E) \quad (4.B.30)$$

The motivation for the above approximation is as follows. $g_F(\epsilon)$ is the Greens function for the system with Hamiltonian $\hat{\mathcal{H}}_S(0)$. We are interested in energies $\epsilon = E \simeq \hbar\Omega/2$, where Ω is the driving frequency. Now, owing to the finite bandwidth of the dressed Hamiltonian $\hat{\mathcal{H}}_S(0)$, there are no energy eigenstates at $E + N\hbar\Omega$ for $N > 0$. There are states at $E - \hbar\Omega \simeq -\Omega/2$ but none for any $\hbar\Omega$ below this. Thus the above approximation ignores values of K for which $\hat{\mathcal{H}}_S(0)$ has no states at $E + K\hbar\Omega$.

Let us now define

$$\tilde{g}_F(E) = g_F(E) + g_F(E)\check{D}_0(E)g_F(E) \quad (4.B.31)$$

and use the fact that $E - \hbar\Omega \simeq -E$ we immediately find

$$\begin{aligned} & G_V^{(\ell)}(E + (N - m - \ell)\hbar\Omega) \\ &= \delta_{N,m} (\tilde{g}_F(E)\delta_{\ell,0} + g_F(E)\check{D}_1(-E)g_F(-E)\delta_{\ell,1}) \\ &+ \delta_{N+1,m} (\tilde{g}_F(-E)\delta_{\ell,0} + g_F(-E)\check{D}_{-1}(E)g_F(E)\delta_{\ell,-1}) \end{aligned} \quad (4.B.32)$$

Plugging this into the transmission matrix formula gives

$$\begin{aligned}
T_{\lambda,\lambda'}(E + N\hbar\Omega) &= J_N^2 \left(\frac{2V_{ext}}{\hbar\Omega} \right) \left(\text{Tr} \left(\Gamma_\lambda \tilde{g}_F(E) \Gamma_{\lambda'} \tilde{g}_F^\dagger(E) \right) \right) \\
&+ \text{Tr} \left(\Gamma_\lambda g_F(-E) \check{D}_{-1}(E) g_F(E) \Gamma_{\lambda'} (g_F(-E) \check{D}_{-1}(E) g_F(E))^\dagger \right) \\
&+ J_{N+1}^2 \left(\frac{2V_{ext}}{\hbar\Omega} \right) \left(\text{Tr} \left(\Gamma_\lambda \tilde{g}_F(-E) \Gamma_{\lambda'} \tilde{g}_F^\dagger(-E) \right) \right) \\
&+ \text{Tr} \left(\Gamma_\lambda g_F(E) \check{D}_1(-E) g_F(-E) \Gamma_{\lambda'} (g_F(E) \check{D}_1(-E) g_F(-E))^\dagger \right) \\
&+ J_{N+1} \left(\frac{2V_{ext}}{\hbar\Omega} \right) J_N \left(\frac{2V_{ext}}{\hbar\Omega} \right) \left(\text{Tr} \left(\Gamma_\lambda \tilde{g}_F(E) \Gamma_{\lambda'} S_1(g_F(E) \check{D}_1(-E) g_F(-E))^\dagger \right) \right) \\
&+ \text{Tr} \left(\Gamma_\lambda g_F(E) \check{D}_1(-E) g_F(-E) \Gamma_{\lambda'} S_1 \tilde{g}_F^\dagger(E) \right) \\
&+ J_{N+1} \left(\frac{2V_{ext}}{\hbar\Omega} \right) J_N \left(\frac{2V_{ext}}{\hbar\Omega} \right) \left(\text{Tr} \left(\Gamma_\lambda \tilde{g}_F(-E) \Gamma_{\lambda'} S_1(g_F(-E) \check{D}_{-1}(E) g_F(E))^\dagger \right) \right) \\
&+ \text{Tr} \left(\Gamma_\lambda g_F(-E) \check{D}_{-1}(E) g_F(E) \Gamma_{\lambda'} S_1 \tilde{g}_F^\dagger(-E) \right)
\end{aligned} \tag{4.B.33}$$

where $S_1 = \sigma_z \otimes I_L$. Let us now consider $D_{-1}(E)$. Using our generating function we have

$$\check{D}_\ell(E) = \bar{H}_\ell + \bar{H}_{\ell-j} g_j \bar{H}_j + \bar{H}_{\ell-j} g_j \bar{H}_{j-j'} g'_j \check{D}_{j'}(E) \tag{4.B.34}$$

This equation can be solved for both $D_{-1}(E)$ and $D_1(-E)$, the results are

$$D_{-1}(E) = - \left(I + \bar{H}_1 g_F(E) \bar{H}_1 g_F(-E) \right)^{-1} \bar{H}_1 \tag{4.B.35}$$

and

$$D_1(-E) = \left(I + \bar{H}_1 g_F(-E) \bar{H}_1 g_F(E) \right)^{-1} \bar{H}_1 \tag{4.B.36}$$

Further let us note that

$$D_0(E) = \left(I - \bar{H}_1 g_F(-E) \bar{H}_{-1} g_F(E) \right)^{-1} \bar{H}_1 g_F(-E) \bar{H}_{-1} \tag{4.B.37}$$

Using this one can show that

$$\tilde{g}_F(E) = g_F(E) + g_F(E)\check{D}_0(E)g_F(E) = \frac{1}{E - (\bar{H}_0 + \bar{H}_1 g_F(-E)\bar{H}_{-1})} \quad (4.B.38)$$

So $\tilde{g}_F(E)$ is the Green's function of a system with an effective Hamiltonian $\bar{H}_0 + \bar{H}_1 g_F(-E)\bar{H}_{-1}$.

Now let us define

$$F_{up}(E) = g_F(E)\check{D}_1(-E)g_F(-E) = g_F(E)H_1\tilde{g}_F(-E) \quad (4.B.39)$$

and

$$F_{down}(E) = g_F(-E)\check{D}_{-1}(E)g_F(E) = -F_{up}(-E) \quad (4.B.40)$$

Using these definitions the tunnelling elements can be written

$$\begin{aligned} T_{\lambda,\lambda'}(E + N\hbar\Omega) &= J_N^2 \left(\frac{2V_{ext}}{\hbar\Omega} \right) \left(\text{Tr} \left(\Gamma_\lambda \tilde{g}_F(E) \Gamma_{\lambda'} \tilde{g}_F^\dagger(E) \right) + \text{Tr} \left(\Gamma_\lambda F_{up}(-E) \Gamma_{\lambda'} F_{up}^\dagger(-E) \right) \right) \\ &+ J_{N+1}^2 \left(\frac{2V_{ext}}{\hbar\Omega} \right) \left(\text{Tr} \left(\Gamma_\lambda \tilde{g}_F(-E) \Gamma_{\lambda'} \tilde{g}_F^\dagger(-E) \right) + \text{Tr} \left(\Gamma_\lambda F_{up}(E) \Gamma_{\lambda'} F_{up}^\dagger(E) \right) \right) \quad (4.B.41) \\ &+ J_{N+1} \left(\frac{2V_{ext}}{\hbar\Omega} \right) J_N \left(\frac{2V_{ext}}{\hbar\Omega} \right) \left(\text{Tr} \left(\Gamma_\lambda \tilde{g}_F(E) \Gamma_{\lambda'} S_1 F_{up}^\dagger(E) \right) + \text{Tr} \left(\Gamma_\lambda F_{up}(E) \Gamma_{\lambda'} S_1 \tilde{g}_F^\dagger(E) \right) \right) \\ &- J_{N+1} \left(\frac{2V_{ext}}{\hbar\Omega} \right) J_N \left(\frac{2V_{ext}}{\hbar\Omega} \right) \left(\text{Tr} \left(\Gamma_\lambda \tilde{g}_F(-E) \Gamma_{\lambda'} S_1 F_{up}^\dagger(-E) \right) + \text{Tr} \left(\Gamma_\lambda F_{up}(-E) \Gamma_{\lambda'} S_1 \tilde{g}_F^\dagger(-E) \right) \right) \end{aligned}$$

We now note that in our numerical calculations our system has energy eigenstates distributed symmetrically around $E = 0$ (as we have taken $C = D = 0$). In such a system we must have $WH_S W^\dagger = -H_S$ where W is some operator. From this it follows that $W\tilde{g}_F(-E)W^\dagger = -\tilde{g}_F(E)$ and also $WF_{up}(-E)W^\dagger = -F_{up}(-E)$. Using the fact that the leads (and $\Gamma_{\lambda'} S_1$) also obey this symmetry and inserting the identity in the form $W^\dagger W = I$ in strategic places above leaves

$$\begin{aligned}
T_{\lambda,\lambda'}(E + N\hbar\Omega) &= \left(J_N^2 \left(\frac{2V_{ext}}{\hbar\Omega} \right) + J_{N+1}^2 \left(\frac{2V_{ext}}{\hbar\Omega} \right) \right) \\
&\times \left(\text{Tr} \left(\Gamma_\lambda \tilde{g}_F(E) \Gamma_{\lambda'} \tilde{g}_F^\dagger(E) \right) + \text{Tr} \left(\Gamma_\lambda F_{up}(E) \Gamma_{\lambda'} F_{up}^\dagger(E) \right) \right)
\end{aligned} \tag{4.B.42}$$

which we write as

$$\begin{aligned}
&T_{\lambda,\lambda'}(E + N\hbar\Omega) \\
&= \frac{1}{2} \left(J_N^2 \left(\frac{2V_{ext}}{\hbar\Omega} \right) + J_{N+1}^2 \left(\frac{2V_{ext}}{\hbar\Omega} \right) \right) \hat{T}_{\lambda,\lambda'}(E, V_{ext})
\end{aligned} \tag{4.B.43}$$

where

$$\begin{aligned}
&\hat{T}_{\lambda,\lambda'}(E, V_{ext}) \\
&= 2 \left(\text{Tr} \left(\Gamma_\lambda \tilde{g}_F(E) \Gamma_{\lambda'} \tilde{g}_F^\dagger(E) \right) + \text{Tr} \left(\Gamma_\lambda F_{up}(E) \Gamma_{\lambda'} F_{up}^\dagger(E) \right) \right)
\end{aligned} \tag{4.B.44}$$

We note that in a two-terminal geometry when there are edge-states in the quasi energy spectrum we find that $\hat{T}_{\lambda,\lambda'}(E, V_{ext}) = 2$. Each of the two terms above looks reminiscent of a conductivity. The first term looks like a contribution coming from edge-states at an energy E , while the second term looks like a contribution coming from the edge-states at $-E$ transitioning to E .

4.B.1 Expression for the Effective Hamiltonian

We close with an expression for a derivation of the effective Hamiltonian. Recall that $\hat{\mathcal{H}}_S(t) = U_V^\dagger(t) \hat{\mathcal{H}}_S U_V(t)$ and that $\hat{\mathcal{H}}_S(n) = \frac{1}{T} \int_0^T e^{in\Omega t} \bar{H}(t)$, then by using the Fourier

decomposition of $U_V(t)$ we can write

$$\hat{\mathcal{H}}_S(n) = \sum_m U_V^\dagger(m) \hat{\mathcal{H}}_S U_V(m+n) \quad (4.B.45)$$

If we now recall the relation for the U_V operators derived above, then it immediately follows that

$$\begin{aligned} \hat{\mathcal{H}}_S(n) &= \sum_m J_m \left(\frac{2V_e}{\hbar\Omega} \right) J_{m+n} \left(\frac{2V_e}{\hbar\Omega} \right) \\ &\times S_m \otimes I_L \hat{\mathcal{H}}_S S_{m+n} \otimes I_L \end{aligned} \quad (4.B.46)$$

Now let us write

$$\hat{\mathcal{H}}_S = \sum_{\alpha,\beta} \bar{\mathcal{H}}_{\alpha,\beta} \sigma_\alpha \otimes R_\beta \quad (4.B.47)$$

where R_β is a complete set of operators in the space of the lattice. Then, defining $\zeta = \frac{2V_e}{\hbar\Omega}$, noting that for $\alpha = 1$ or 2 one can show that $S_m \sigma_\alpha S_{n+m} = (-1)^m \sigma_\alpha S_n$ whereas for $\alpha = 0$ or $\alpha = 3$ they do nothing, and using the Bessel function identities $\sum_m [J_m(\zeta) J_{m+n}(\zeta)] = \delta_{n,0}$ and $\sum_m [J_m(\zeta) (-1)^m J_{m+n}(\zeta)] = \sum_m [J_m(\zeta) J_{-m+n}(\zeta)] = J_n(2\zeta)$ we have

$$\begin{aligned} \hat{\mathcal{H}}_S(m) &= \delta_{n,0} \sum_{\alpha=0,3,\beta} \bar{\mathcal{H}}_{\alpha,\beta}(\sigma_\alpha) \otimes R_\beta \\ &+ J_n(2\zeta) \sum_{\alpha=1,2,\beta} \bar{\mathcal{H}}_{\alpha,\beta}(\sigma_\alpha S_n) \otimes R_\beta \end{aligned} \quad (4.B.48)$$

It is most convenient to write this as

$$\hat{\mathcal{H}}_S(m) = \delta_{n,0} \bar{\mathcal{H}}_{03} + J_n(2\zeta) \bar{\mathcal{H}}_{12}(n) \quad (4.B.49)$$

Thus the field does not touch terms in $\hat{\mathcal{H}}_S$ proportional to σ_0 or σ_3 and “dresses” the σ_1 and σ_2 terms.

The Green's function g_F and the transmission matrix elements $T_{\lambda,\lambda'}^F$ are the result of calculating the Greens function and the transport properties of a system described by a static Hamiltonian $\hat{\mathcal{H}}_S(0)$. Such a Hamiltonian looks similar to our original static Hamiltonian (before periodic perturbation) but with $\bar{\mathcal{H}}_{12}$ renormalized by the Bessel function $J_0(2\zeta)$. Moreover, σ is not simply the static conductivity of $\bar{\mathcal{H}}_{03}$.

References

- ¹A. Kundu and B. Seradjeh, *Phys. Rev. Lett.* **111**, 136402 (2013).
- ²B. A. Bernevig, T. L. Hughes, and S.-C. Zhang, *Science* **314**, 1757–1761 (2006).
- ³A. Roth, C. Brüne, H. Buhmann, L. W. Molenkamp, J. Maciejko, X.-L. Qi, and S.-C. Zhang, *Science* **325**, 294–297 (2009).
- ⁴M. König, S. Wiedmann, C. Brune, A. Roth, H. Buhmann, L. W. Molenkamp, X.-L. Qi, and S.-C. Zhang, *Science* **318**, 766–770 (2007).
- ⁵N. H. Lindner, G. Refael, and V. Galitski, *Nat Phys* **7**, 490 (2011).
- ⁶Z. Gu, H. A. Fertig, D. P. Arovas, and A. Auerbach, *Phys. Rev. Lett.* **107**, 216601 (2011).
- ⁷T. Oka and H. Aoki, *Phys. Rev. B* **79**, 081406 (2009).
- ⁸G. Usaj, P. M. Perez-Piskunow, L. E. F. Foa Torres, and C. A. Balseiro, *Phys. Rev. B* **90**, 115423 (2014).
- ⁹H. L. Calvo, H. M. Pastawski, S. Roche, and L. E. F. F. Torres, *Applied Physics Letters* **98**, 232103 (2011).
- ¹⁰L. E. F. Foa Torres, P. M. Perez-Piskunow, C. A. Balseiro, and G. Usaj, *Phys. Rev. Lett.* **113**, 266801 (2014).
- ¹¹Y. H. Wang, H. Steinberg, P. Jarillo-Herrero, and N. Gedik, *Science* **342**, 453–457 (2013).
- ¹²A. Gómez-León and G. Platero, *Phys. Rev. Lett.* **110**, 200403 (2013).
- ¹³M. S. Rudner, N. H. Lindner, E. Berg, and M. Levin, *Phys. Rev. X* **3**, 031005 (2013).
- ¹⁴T. Kitagawa, E. Berg, M. Rudner, and E. Demler, *Phys. Rev. B* **82**, 235114 (2010).
- ¹⁵A. Kundu, H. A. Fertig, and B. Seradjeh, *Phys. Rev. Lett.* **113**, 236803 (2014).
- ¹⁶Y. Tenenbaum Katan and D. Podolsky, *Phys. Rev. B* **88**, 224106 (2013).

-
- ¹⁷L. Jiang, T. Kitagawa, J. Alicea, A. R. Akhmerov, D. Pekker, G. Refael, J. I. Cirac, E. Demler, M. D. Lukin, and P. Zoller, *Phys. Rev. Lett.* **106**, 220402 (2011).
- ¹⁸D. E. Liu, A. Levchenko, and H. U. Baranger, *Phys. Rev. Lett.* **111**, 047002 (2013).
- ¹⁹C. We, J. Sun, F. Huang, Y. Li, and W. Liu, *EPL* **104**, 27004 (2013).
- ²⁰P. Wang, Q.-f. Sun, and X. C. Xie, *Phys. Rev. B* **90**, 155407 (2014).
- ²¹P. Delplace, Á. Gómez-León, and G. Platero, *Phys. Rev. B* **88**, 245422 (2013).
- ²²Y. Li, A. Kundu, F. Zhong, and B. Seradjeh, *Phys. Rev. B* **90**, 121401 (2014).
- ²³H. Sambe, *Phys. Rev. A* **7**, 2203–2213 (1973).
- ²⁴A. Farrell and T. Pereg-Barnea, *Phys. Rev. Lett.* **115**, 106403 (2015).
- ²⁵P. K. Tien and J. P. Gordon, *Phys. Rev.* **129**, 647–651 (1963).
- ²⁶T. Kitagawa, T. Oka, A. Brataas, L. Fu, and E. Demler, *Phys. Rev. B* **84**, 235108 (2011).
- ²⁷G. Platero and R. Aguado, *Physics Reports* **395**, 1–157 (2004).
- ²⁸S. Kohler, J. Lehmann, and P. Hänggi, *Physics Reports* **406**, 379–443 (2005).
- ²⁹J.-c. Chen, J. Wang, and Q.-f. Sun, *Phys. Rev. B* **85**, 125401 (2012).
- ³⁰D. F. Martinez, R. A. Molina, and B. Hu, *Phys. Rev. B* **78**, 045428 (2008).
- ³¹A. Farrell and T. Pereg-Barnea, *Work in progress on topological systems* (2015).

Preface to Chapter 5

The main formalism and interpretation in Chapters 3 and 4 has been built upon an understanding in terms of the topological edge-states being split into sidebands. A deeper understanding of these states, as well as connecting them to a different system of interest, is desirable. In addition to this, there are several experimental hurdles to overcome given the assumptions of the previous two manuscripts. One of these is understanding the turn-on of the time periodic field, as the field in these previous works has always assumed to be on for a long time. Second, these chapters have worked in the large frequency limit. Most of experimental tools available (e.g. terahertz laser spectroscopy) exist at smaller energies/frequencies. The purpose of the following manuscript is to address all of the above issues as well as to connect to recent experimental work by the group of Nu Gedik [1] at MIT. We develop results for ARPES measurements of a 3D topological insulator in the presence of terahertz electromagnetic radiation. We do this by allowing for the field to have a finite width envelope and treating the turn-on explicitly. We also assume the frequency to be small (terahertz) and build up an understanding of this system using the side-band language of the previous two chapters, all while connecting our results to experiment.

Time-dependent population of sidebands in a Dirac system

Aaron Farrell¹ and T. Pereg-Barnea¹

¹Department of Physics and the Centre for Physics of Materials, McGill University, Montreal, Quebec, Canada H3A 2T8

The manuscript has been accepted for publication in Physical Review B.
arXiv reference: arXiv:1603.09718

Abstract

Pump-probe techniques with high temporal resolution allow one to drive a system of interest out of equilibrium and at the same time, probe its properties. Recent advances in these techniques open the door to studying new, non-equilibrium phenomena such as Floquet topological insulators and superconductors. These advances also necessitate the development of theoretical tools for understanding the experimental findings and predicting new ones.

In the present work, we provide a theoretical foundation to understand the non-equilibrium behaviour of a Dirac system. We present detailed numerical calculations and simple analytic results for the evolution of a Dirac system irradiated by light. These results are framed intuitively by appealing to the recently revitalized notion of sidebands[2, 3]. We find that, under the application of circularly polarized light, a Dirac point only ever splits into two copies of sidebands. Meanwhile, the application of linearly polarized light leaves the Dirac point intact while producing sidebands. Our immediate interest in this work is in connection to time and angle resolved photoemission experiments, where we find excellent qualitative agreement between our results and those in the literature[1]. However, our results are general and may prove useful beyond this particular application and should be relevant to other pump-probe experiments.

5.1 Introduction

One of the greatest triumphs in the last decade of condensed matter research has been the theoretical prediction[4–6] and subsequent experimental realization[7–9] of the topological insulator (TI). These materials are insulating in the bulk, while their edge plays host to topologically protected metallic modes with energies lying in the band gap of bulk states. The existence of these edge-states makes TIs of great fundamental and practical interest with applications ranging from quantum computation to spintronics. Moreover, the discovery of topological systems leads to a new classification of possible states of matter.

While many of the topological systems can be understood by non-interacting, clean systems at equilibrium the study of topological states is not limited to those. The effects of disorder, for example may drive a system in and out of a topological state.[10, 11] It is therefore interesting to ask whether there is a knob that can be tuned to alter the topological properties of a system.

One auspicious route towards the generation of a TI comes from considering time-periodic perturbations[1–3, 12–31]. In these systems, a time-periodic perturbation, is applied to a topologically trivial system and drives it into a non-equilibrium topological state. As continuous time translational invariance is broken, it is no longer appropriate to discuss energy eigenstates. One must instead talk about their quasi-energy spectrum, which is the closest analogue to an energy spectrum for a system with discrete time-translational invariance[32]. The topological state created with an external, time-periodic perturbation is called a Floquet topological insulator (FTI) and it exhibits edge-states in the gap of its quasi-energy spectrum[12].

The notion of a FTI has garnered much attention lately, and has enjoyed experimental validation in the field of photonic crystals, where Floquet states can be simulated in the laboratory[33]. However, a solid state verification of a Floquet topological state and several issues regarding feasibility have been raised[34]. The first of these is that most

available periodic perturbations are not perfectly periodic, but have an envelope function in addition to the periodic signal. The second, perhaps more pressing, issue has to do with the experimentally available frequencies. Present discussions in the literature are valid in the large frequency limit $\Omega \gg \Omega_{BW}$, Ω being the applied frequency and Ω_{BW} being the frequency of the band-width of the system. However, available technology in terahertz is sub-bandwidth. This small frequency is believed to be problematic as it will lead to a complicated quasi-energy structure which may obscure any potential topological effects.

Given the above complications, our goal in the present paper is to understand the behaviour of a topological system in the presence of a non-periodic and sub-bandwidth external perturbation. We will work with Dirac cone dispersion, typical for a three dimensional topological insulator surface, in order to develop a fundamental understanding and will not discuss a Floquet topological insulator at this point. Our work is inspired by measurements of Wang *et al* in Ref. [1]. This group used time resolved-angle resolve photoemission spectroscopy (TR-ARPES) to view the evolution of surface states of Bi_2Se_3 , a three dimensional topological insulator. We find excellent qualitative agreement with these results.

We employ the language of sidebands recently used in Refs. [2, 3]. This language allows us to develop the three main results of this work. The first of these is that even though applying a sub-bandwidth perturbation to a system may “fold” many states into the Floquet zone, only a few of these states have any spectral weight and contribute to physical processes. In the present example, we consider a Dirac cone, which has effectively an infinite band-width. We find that only states within a couple $\hbar\Omega$ from the Fermi surface have any statistical weight in our side-band picture. Second, we work in a regime where the time scale over which the pump pulse envelope is changing is much longer than the period time of the drive. In this regime we develop simple, analytic expressions. Finally, we show that the structure of a Dirac cone colludes with circularly polarized light to produce *only two* sidebands for momenta near the Dirac point. This is quite remarkable; the spectral

weight of the equilibrium Dirac point states is entirely shared between two sidebands. It therefore behaves as two massive Dirac points, with different masses. These two cones share the spectral weight of the original Dirac cone.

The intuition developed here, as well as the satisfactory results in view of recent experiments[1], will add to a current ongoing discussion in the literature regarding the stability of Floquet-states[31, 35–38]. Our side-band interpretation in concert with an understanding of Floquet states and the results of Ref. [Wang] provide an intuitive physical picture. Sidebands develop over the lifetime of the pump pulse; their eigenstates can be found from the system’s quasi energy states and their weight in the time-dependent wave function can be viewed as probabilistic occupation.

The rest of this paper is organized as follows. In the following section we discuss some fundamentals of the Floquet formalism in order to introduce the side-band intuition of Refs. [2, 3]. We move on to present our model and methods. In Section 5.3 we present our results and discussion for two polarizations of light. The appendices detail various technical aspects of the work.

5.2 Preliminaries

5.2.1 Sidebands

We begin with a brief discussion of Floquet theory as it pertains to the language of sidebands. Consider the time-dependent Schrödinger equation

$$i\hbar\partial_t|\psi(t)\rangle = H(t)|\psi(t)\rangle \quad (5.2.1)$$

where $H(t+T) = H(t)$ is a Hamiltonian with period T . Defining $\Omega = 2\pi/T$ the principle result of Floquet theory is that the steady states of the above system can be written as[32]

$$|\psi(t)\rangle = e^{-i\eta t/\hbar}|\phi(t)\rangle \quad (5.2.2)$$

where $(H(t) - i\hbar\partial_t)|\phi(t)\rangle = \eta|\phi(t)\rangle$ and $|\phi(t+T)\rangle = |\phi(t)\rangle$. The eigenvalues η are typically called the quasi-energies. The quasi-energies are only unique up to integer multiples of $\hbar\Omega$, as can be seen by noting that $e^{in\Omega t}|\phi(t)\rangle$ is an eigenvalue of $(H(t) - i\hbar\partial_t)$ with quasi-energy $\eta + n\hbar\Omega$ and also meets the boundary condition $|\phi(t+T)\rangle = |\phi(t)\rangle$. Thus all quasi-energies are defined within a first "Floquet zone", an interval of energies of width $\hbar\Omega$. The center of this zone is, of course, arbitrary. The quasi-energy spectrum in the first Floquet zone can be copied at intervals of $\hbar\Omega$ above and below to generate the full quasi-energy spectrum.

We now introduce the sidebands. Since $|\phi(t)\rangle$ is periodic, we are free to express it as a discrete Fourier series $|\phi(t)\rangle = \sum_n e^{-in\Omega t}|n\rangle$. The full wave function reads

$$|\psi(t)\rangle = \sum_n e^{-i(\eta+n\hbar\Omega)t/\hbar}|n\rangle \quad (5.2.3)$$

The states $|n\rangle$ are determined by solving the eigenvalue equation $\sum_m (H_{n-m} - n\hbar\Omega\delta_{n,m})|m\rangle = \eta|n\rangle$ where $H_n = \int_0^T \frac{dt}{T} e^{in\Omega t} H(t)$.

The intuitive picture we wish to take away from Eq. (5.2.3) is the following. In a time periodic system the steady states are a linear combination of definite energy states with energies $\eta + n\hbar\Omega$ and probability $\langle n|n\rangle$. This follows from either inspecting Eq. (5.2.3) or by noting that the average energy over one cycle of the period reads

$$\bar{E} = \int_0^T \frac{dt}{T} \langle \psi(t) | H(t) | \psi(t) \rangle = \sum_n \langle n | n \rangle (\eta + n\hbar\Omega) \quad (5.2.4)$$

For pedagogical reasons we now consider the application of the above theory to a time-independent system. To be more concrete, let's say we have an applied perturbation with frequency Ω but a vanishingly small amplitude. In this limit $H_n = \delta_{n,0}H$ and the eigenvalue equation becomes $(H - n\hbar\Omega)|n\rangle = \eta|n\rangle$. The solution to this system is $|n\rangle = \delta_{N,n}|\zeta\rangle$ with $\eta = E - N\hbar\Omega$, where $H|\zeta\rangle = E|\zeta\rangle$ and N is an integer that takes E and moves it into the first Floquet zone we have chosen for our problem. Thus when the time periodic fields are turned off the system is, of course, found in eigenstates of the static Hamiltonian. These eigenstates can, of course, be defined in a first Floquet zone, but if this first Floquet zone does not contain E (i.e. if $N \neq 0$ in the language above) then there exists a quasi-energy $E - N\hbar\Omega$, but this state has *zero* probability of being occupied in the first Floquet zone because $\langle n|n\rangle = \delta_{n,N}$. One must move to the N^{th} Floquet zone where this state is occupied with unit probability. The moral of this exercise is the following. When working in the Floquet zone the quasienergy spectrum might be dense with folded bands. However, the 'occupation' of a given state (its weight in the time dependent wavefunction) may be zero in the first Floquet zone, leaving only a few relevant states.

Starting from the above limit, as we turn on the time dependence there are two effects that take place. First, electrons beginning in the original eigenstates develop some probability to absorb or emit photons and thus their unit probability of being found in one Floquet zone gets smeared into other, adjacent Floquet zones. This creates "copies" of the original band structure analogous to those proposed by Tien and Gordon several decades ago[39]. Second, unlike the physics of Ref. [39], in our present system these sidebands can also be modified in a non-trivial way. This occurs when states corresponding to absorbing/emitting different number of photons hybridize. This can lead to important effects such as gaps in these sidebands opening.

The above interpretation is important when applying a probe of well defined energy to a time periodic system. Examples of this situation are the studies in Refs. [2, 3] where

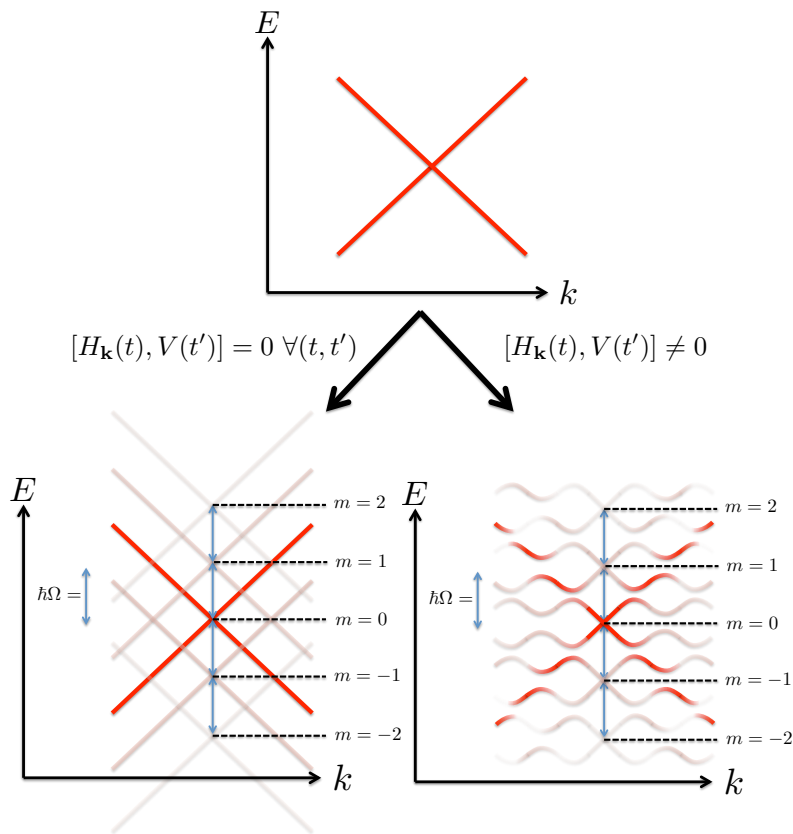


Figure 5.1: Schematic picture of the main results of this paper. The original Dirac cone is split into sidebands, with sidebands further away from the original cone receiving less "weight". In the figure this is signified using lighter colours for less probable sidebands. Now, if the operator describing the time periodic field, $V(t)$, commutes with the original Hamiltonian, $H_{\mathbf{k}}(t)$, then this splitting is all that happens. If these two operators do not commute sidebands hybridize and the band structure becomes modified by, e.g., having gaps opened.

we calculate the transport properties of periodically driven quantum well heterostructures. Namely, the edge-states in these systems, whether naturally occurring or driven, are split into sidebands. As a result, certain transport signatures of these edge states, for example $2e^2/h$ conductance, are fragmented. In Refs. [2, 3] we have discussed how a sum rule[24] can be used to salvage these transport signatures. This sum rule is rooted in the understanding that systems in a time-periodic field have their energy bands modified by the time-periodic perturbation and also that these bands are split into sidebands. Crucially, these sidebands are only occupied with a certain probability, and, for reasonable field strengths, this probability decreases with the separation in energy between the original energy eigenvalue and the side-band eigenvalue that we're interested in. Thus it is usually appropriate to treat only eigenstates within several multiples of $\hbar\Omega$ from the Fermi level.

The above observations are important to keep in mind when applying Floquet theory to look at the quasi-energies by themselves. When the energy scale $\hbar\Omega$ is small compared to the band-width of the equilibrium model, the quasi-energy spectrum becomes very convoluted as *many* eigenstates are “folded” back into the Floquet zone. Making predictions based on this spectrum alone then becomes an arduous task. The discussion above, and the results to follow, illustrate that one must keep in mind that even though the quasi-energy spectrum may become complicated in this limit, only quasi-energies resulting from folding of energies within a few $\hbar\Omega$ of the Fermi energy contribute significantly to observables. The information about these probabilities is contained in the often ignored side-band states $|n\rangle$ and their statistical weight.

Our model is a generic Dirac cone and no cut-off is considered, thus our effective bandwidth is infinite. We subject this system to terahertz frequency light $\hbar\Omega \sim 30\text{meV}$. Looking only at the quasi-energy spectrum of this system the Dirac cone will be folded back into the Floquet zone infinitely many times and would thus be meaningless. We therefore approach the system in a slightly different manner, while keeping in mind the side-band language

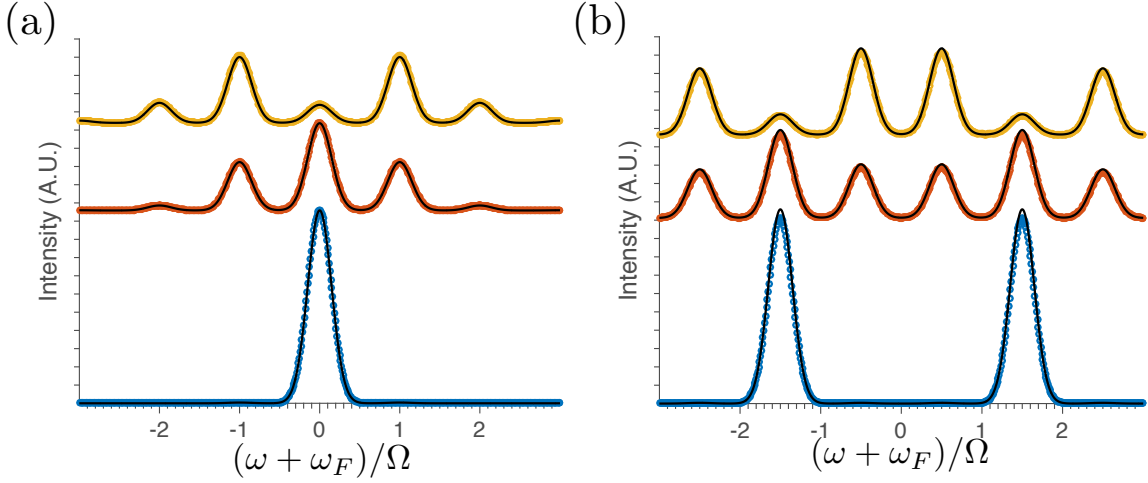


Figure 5.2: Comparison of numerical results found by integrating the time dependent Dirac equation and the analytic approximation in Eq. (5.3.6) for $I(k_x, 0, \omega, t_{\mathcal{O}})$. The left plots $I(0, 0, \omega, t_{\mathcal{O}})$ for different delay times $t_{\mathcal{O}}$ while the right plots $I(0.05\text{\AA}^{-1}, 0, \omega, t_{\mathcal{O}})$ also for different delay times. In these plots the bottom plot is for $t_{\mathcal{O}} = -500\text{fs}$, the middle for $t_{\mathcal{O}} = -100\text{fs}$ and the top is for $t_{\mathcal{O}} = 0\text{fs}$. In all plots the solid line is the approximation in Eq. (5.3.6) while the circles are numerical results. There is excellent agreement between the numerics and our approximation for all three delay times.

discussed above. Provided that the field is turned on slowly compared to the frequency of the light, the system evolves into a state described by a splitting of its original bands into sidebands. In cases where the operator describing the external field commutes with the static Hamiltonian *at all times*, this side-band splitting is the only effect of the light, i.e. we see no hybridization and no gap opening. In all other cases there are additional modifications of the sidebands. In either case, we see that for physical field strengths only the first couple of sidebands carry any spectral weight in these simulations, in spite of the fact that the system is subjected to low-frequency light. These central results of our work are summarized in the schematic in Fig. 5.1. This intuition should be relevant to related experiments on time-dependent systems and will be crucial in driving a topological state with externally applied light.

5.2.2 Model Hamiltonian

We begin with the following Dirac Hamiltonian

$$h_{\mathbf{k}} = \hbar v_F (\mathbf{k} \times \vec{\sigma}) \cdot \hat{z} - \mu \sigma_0 \quad (5.2.5)$$

where v_F is the Fermi velocity, $\vec{\sigma}_i = \sigma_i$ is a vector of Pauli matrices and μ the Fermi energy. The above Hamiltonian is immediately applicable to the surface of a three dimensional topological insulator (TI) and should also be relevant to graphene in the limit where any applied field doesn't induce intervalley scattering.

We now envisage the above system irradiated by an electromagnetic field. To keep our theoretical model simple we assume this field is spatially constant over the sample size. This should be approximately true for the terahertz type radiation considered here where the wavelength of the light should be tens of microns[1]. We model this electromagnetic field as follows

$$\mathbf{E}_{pump}(t) = E_0 e^{-\frac{t^2}{2T_{pump}^2}} \mathbf{E}_{\Omega}(t) \quad (5.2.6)$$

where E_0 is the amplitude of this pump pulse, T_{pump} is the width of the pulse and $\mathbf{E}_{\Omega}(t)$ is the monochromatic component of the field. In this paper we consider two scenarios: (1) Linearly polarized light, with $\mathbf{E}_{\Omega}(t) = \sin \Omega t \hat{x}$ and (2) circularly polarized light in which case $\mathbf{E}_{\Omega}(t) = \sin \Omega t \hat{x} - \cos \Omega t \hat{y}$.

We introduce the above field via minimal coupling, ignoring the Zeeman effect, as we expect the dominant contribution to come from the electron's orbital motion. We choose a Gauge such that the electric scalar potential $\Phi = 0$ and $\mathbf{E}_{pump}(t) = -\partial_t \mathbf{A}_{pump}(t)$, see appendix C for more details. Thus we have $\mathbf{A}_{pump}(t) = -\int_{-\infty}^t dt' \mathbf{E}_{pump}(t')$ where we have chosen in initial condition such that $\mathbf{A}_{pump}(t) \rightarrow 0$ for $t \rightarrow -\infty$. This choice of initial condition is, of course, immaterial and represents the gauge freedom of the problem. We show in the appendix that within the formalism we use in this paper[34, 40, 41] this

choice of initial condition does not change any of our observations.

Let us define the frequency scale associated with the pump pulse envelope $\Omega_{pump} = 2\pi/T_{pump}$. We work in the limit $\Omega_{pump} \ll \Omega$ in which case it is appropriate to write (see Appendix 5.A for more details)

$$\mathbf{A}_{pump}(t) = \frac{E_0}{\Omega} e^{-\frac{t^2}{2T_{pump}^2}} \tilde{\mathbf{E}}_{\Omega}(t) \quad (5.2.7)$$

where $\tilde{\mathbf{E}}_{\Omega}(t)$ is defined through $\frac{d}{dt} \tilde{\mathbf{E}}_{\Omega}(t) = -\Omega \mathbf{E}_{\Omega}(t)$. The evolution of our time-dependent system is now described through a minimal coupling of the above pump field to our Dirac Hamiltonian via $\hbar\mathbf{k} \rightarrow \hbar\mathbf{k} - e\mathbf{A}_{pump}(t)$. Thus the (time-dependent) Hamiltonian we work with is as follows

$$H_{\mathbf{k}}(t) = v_F [(\hbar\mathbf{k} - e\mathbf{A}_{pump}(t)) \times \vec{\sigma}] \cdot \hat{z} - \mu\sigma_0 \quad (5.2.8)$$

To complete our discussion of the models we must define the probe pulse profile. For this we take the envelope function $s(t, t_{\mathcal{O}}) = e^{-\frac{(t-t_{\mathcal{O}})^2}{2T_{probe}^2}}$ where T_{probe} is the width of the probe, assumed to be much shorter than the width of the pump, $T_{probe} \ll T_{pump}$, and $t_{\mathcal{O}}$ is the delay time between the pump and probe peaks. $t_{\mathcal{O}}$ is effectively the time at which we are “viewing” the system. In the above model we have (arbitrarily) assigned $t = 0$ to be the time at which the pump pulse is maximal.

In our simulation we take experimentally relevant values for the parameters from Ref. [1]. Namely, we estimate $\hbar v_F \simeq 3.6 \text{ eV}\text{\AA}$, $\mu \simeq 300\text{meV}$, $\hbar\Omega \simeq 120\text{meV}$. For convenience we define $\omega_F = \mu/\hbar$. We take a pump-pulse with a full width half-max (FWHM) of 250fs ($T_{pump} \simeq 106.16\text{fs}$) and a probe-pulse with [34] $T_{probe} = 26\text{fs}$. Finally, to fully illustrate the conceptual power of our findings we take $E_0 \simeq 7.5 \times 10^{-3} \text{ V/\AA}$, slightly exaggerated from the estimates of Ref. [1].

5.2.3 Photocurrent

A simplified picture of the technology involved in ARPES is to think of the experimental set-up as measuring the particle current of electrons ejected from the sample at a wave vector \mathbf{k} , energy $\hbar\omega$ and time $t_{\mathcal{O}}$ (relative to the pump maximum time). This measurement is called the photocurrent, $I(k_x, k_y, \omega, t_{\mathcal{O}})$. Typically this quantity involves complicated momentum, orbital, and time dependent matrix elements. To develop a solid understanding for this problem we will work under the assumption that these matrix elements are the same for all orbitals, momenta and times. Under this approximation the relevant quantity to calculate is [34, 40, 41]

$$I(k_x, k_y, \omega, t_{\mathcal{O}}) = \text{Im} \left[\int dt_1 \int dt_2 s(t_1, t_{\mathcal{O}}) s(t_2, t_{\mathcal{O}}) e^{i\omega(t_1 - t_2)} \text{Tr} (G_{\mathbf{k}}^<(t_1, t_2)) \right] \quad (5.2.9)$$

In the above $G_{\mathbf{k}}^<(t_1, t_2)$ is the 2×2 lesser Green's function matrix of the system in spin space. It is obtained by evolving the equilibrium states of the original Dirac cone from the distant past to the present. It is defined as follows

$$G_{\mathbf{k}\sigma\sigma'}^<(t, t') \equiv i \langle c_{\mathbf{k}\sigma}^\dagger(t) c_{\mathbf{k}\sigma'}(t') \rangle \quad (5.2.10)$$

where $c_{\mathbf{k}\alpha}^\dagger$ creates an electron with momenta \mathbf{k} and spin α .

Our theory relies on knowing the solutions to the Dirac equation at all times, as these states can be used to construct the above Green's function. We therefore define the states

$$i\hbar\partial_t |\psi_{\mathbf{k},\alpha}(t)\rangle = H_{\mathbf{k}}(t) |\psi_{\mathbf{k},\alpha}(t)\rangle \quad (5.2.11)$$

subject to the initial condition $|\psi_{\mathbf{k},\alpha}(t \rightarrow -\infty)\rangle = |\phi_{\mathbf{k},\alpha}\rangle$ where $|\phi_{\mathbf{k},\alpha}\rangle$ are the eigenstates

of the equilibrium system satisfying $h_{\mathbf{k}}|\phi_{\mathbf{k},\alpha}\rangle = E_{\mathbf{k}\alpha}|\phi_{\mathbf{k},\alpha}\rangle$, with $E_{\mathbf{k}\alpha} = \alpha\hbar v_F|\mathbf{k}| - \mu$ with $\alpha = \pm 1$ labeling the chirality of the state.

Once these wave functions are known the lesser Green's function of the system can be constructed (see Appendix 5.B)

$$G_{\mathbf{k}\sigma\sigma'}^<(t, t') = i \sum_{\alpha} |\psi_{\mathbf{k},\alpha}^{\sigma}(t)\rangle \langle \psi_{\mathbf{k},\alpha}^{\sigma'}(t')| f(E_{\mathbf{k}\alpha}) \quad (5.2.12)$$

where $f(E_{\mathbf{k}\alpha})$ is a Fermi function and $|\psi_{\mathbf{k},\alpha}^{\sigma}(t)\rangle$ is the spin σ component of the state $|\psi_{\mathbf{k},\alpha}(t)\rangle$.

The theory described in the rest of this paper involves determining $G_{\mathbf{k}}^<(t, t')$ either analytically or numerically and then making use of Eq. (5.2.9) to estimate the results of a TR-ARPES experiment.

5.3 Results and Discussion

Using the methodology outlined above, we present our results and interpretation of calculations relevant to TR-ARPES measurements. For the sake of clarity, we divide our discussion into two categories. First, we consider light polarized along the x direction of the sample. Next, we allow for circularly polarized light. Certain limits of these two set-ups can be solved analytically and crucial insight can be gained into the distribution of states in a non-equilibrium system. We begin with linearly polarized light.

5.3.1 Linearly Polarized Light

We consider an electric field along the x direction only. In this case a closed form solution to the Dirac equation can be found along the $k_y = 0$ cut of the Brillouin zone:

$$H_{k_x, k_y=0}(t) = v_F(\hbar k_x - eA_x(t))\sigma_y - \mu\sigma_0 \quad (5.3.1)$$

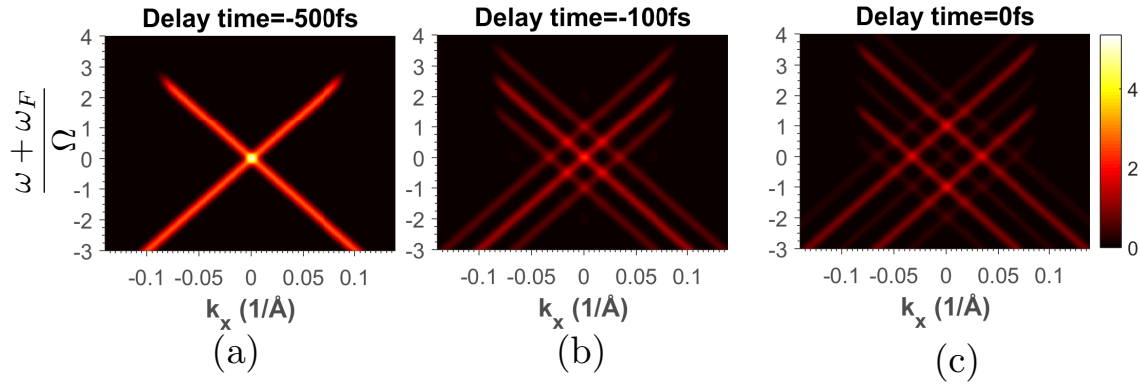


Figure 5.3: Plot of the photocurrent $I(k_x, 0, \omega, t_{\mathcal{O}})$ at various values of the delay time $t_{\mathcal{O}}$ for linearly polarized light. In the distant past we see only the Dirac cone, as the pump field starts to turn on we see copies of this cone (sidebands) begin to develop. As the field envelope becomes larger weight of the original Dirac cone is shifted into other sidebands.

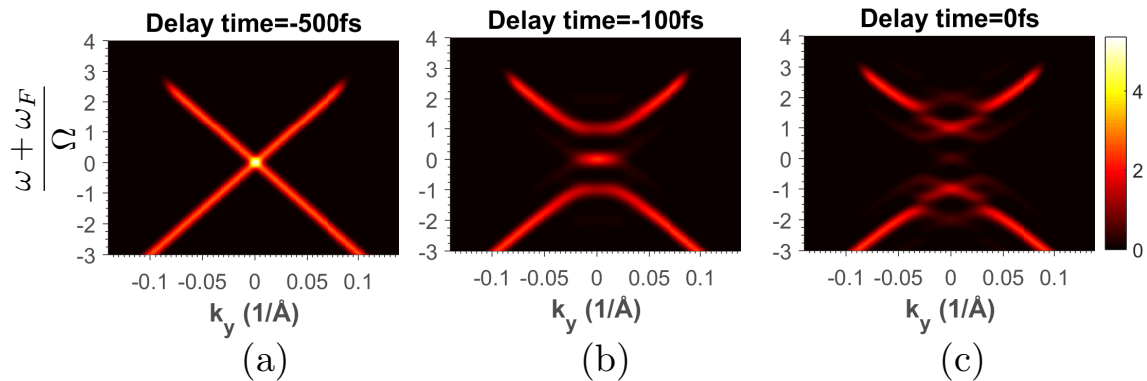


Figure 5.4: Plot of the photocurrent $I(0, k_y, \omega, t_{\mathcal{O}})$ at various values of the delay time $t_{\mathcal{O}}$ for linearly polarized light. In the distant past we again only see the Dirac cone, as the pump field starts to turn on we see copies of this cone (sidebands) begin to develop and these copies develop avoided crossings. As the field becomes fully turned on the weight of the original Dirac cone is shifted into other sidebands and these gaps become more evident.

In this case the time dependent field commutes with the Hamiltonian for the chosen momenta and the wave functions can be written as

$$\begin{aligned} |\psi_{k_x,0,\alpha}(t)\rangle &= e^{-i(\alpha v_F k_x - \mu/\hbar)(t-t_r)} \\ &\times e^{i e \alpha v_F \int_{t_r}^t dt' A_x(t')/\hbar} |\phi_{k_x,0,\alpha}\rangle \end{aligned} \quad (5.3.2)$$

where $t_r \rightarrow -\infty$ is the “turn-on” time for the field. This gives the Green’s function

$$\begin{aligned} G_{k_x,0'}^<(t,t') &= i \sum_{\alpha} e^{-i(\alpha v_F k_x - \mu/\hbar)(t-t')} \\ &\times \exp\left(i \frac{e \alpha v_F}{\hbar} \int_{t'}^t dt'' A_x(t'')\right) f(E_{k_x,0\alpha}) \\ &\times |\phi_{k_x,0,\alpha}\rangle \langle \phi_{k_x,0,\alpha}| \end{aligned} \quad (5.3.3)$$

note that the above is independent of t_r . We eventually need $\text{Tr}(G_{k_x,0'}^<(t,t'))$, where the trace is over spin degrees of freedom. This trace can be performed in any complete basis and becomes particularly simple when we choose the states $|\phi_{k_x,0,\alpha}\rangle$, which leaves

$$\begin{aligned} \text{Tr}[G_{k_x,0'}^<(t,t')] &= i \sum_{\alpha} e^{-i(\alpha v_F k_x - \mu/\hbar)(t-t')} \\ &\times \exp\left(i \frac{e \alpha v_F}{\hbar} \int_{t'}^t dt'' A_x(t'')\right) f(E_{\mathbf{k}\alpha}) \end{aligned} \quad (5.3.4)$$

Our discussion has been exact until this point. We would now like to make an approximation to simplify the above trace. We recall that $A_x(t) = \frac{E_0}{\Omega} e^{-t^2/2T_{pump}^2} \cos \Omega t$ and expand it in the limit $T_{pump} \gg 2\pi/\Omega$. Integration by parts may be used to show that to leading order in $1/T_{pump}\Omega$

$$\begin{aligned} \int_{t'}^t dt'' A_x(t'') &= \\ \frac{E_0}{\Omega^2} \left(e^{-t^2/2T_{pump}^2} \sin \Omega t - e^{-t'^2/2T_{pump}^2} \sin \Omega t' \right) \end{aligned} \quad (5.3.5)$$

Using the above, the identity $e^{ix \sin \Omega t} = \sum_m J_m(x) e^{im\Omega t}$ and assuming the probe pulse is much shorter than the pump pulse gives the following result for the photocurrent (for technical details see Appendix 5.D)

$$I(k_x, 0, \omega, t_{\mathcal{O}}) = 2\pi T_{probe}^2 \sum_{\alpha, m} f(E_{k_x, 0, \alpha}) J_m^2(A_{eff}(t_{\mathcal{O}})) \exp \left[-(\omega - \alpha v_F k_x + \frac{\mu}{\hbar} - m\Omega)^2 T_{probe}^2 \right] \quad (5.3.6)$$

where

$$A_{eff}(t_{\mathcal{O}}) \simeq \frac{\int dt e^{-\frac{(t-t_{\mathcal{O}})^2}{2T_{probe}^2}} \mathcal{A}(t)}{\int dt e^{-\frac{(t-t_{\mathcal{O}})^2}{2T_{probe}^2}}} \quad (5.3.7)$$

with $\mathcal{A}(t) = \frac{eE_0 v_F}{\hbar \Omega^2} e^{-t^2/2T_{pump}^2}$. The above formula is our main analytic result for this part of the paper. It provides a nice picture of the sideband splitting that occurs in the presence of a periodic field. Owing to the nature of the applied field, which commutes with the Hamiltonian, none of the original bands are dressed. The exponent describes peaks not just at energy eigenvalues $v_F \hbar k_x - \mu$, but also at integer values of $\hbar \Omega$ above and below this value. This indicates that there are copies of the original band structure at multiples of $\hbar \Omega$ above and below the original pattern.

The Bessel function pre-factor gives the weights of these sideband peaks. These weights depend on the probe time due to the time dependence of the driven system. Owing to the simple structure at $k_y = 0$ there is no interference/avoided crossing of sidebands. Thus in the limit of a wide pump pulse the system is split into sidebands and the population of these sidebands is given by the instantaneous weighted average of the pump envelope function.

We now turn to numerics in order to test the validity of our analytic results and to extend our analysis to finite k_y . For this we integrate the Dirac equation numerically. We begin by fixing $k_y = 0$ and comparing our analytic treatment to exact numerics. Fig. 5.2 shows $I(k_x, 0, \omega, t_{\mathcal{O}})$ for $k_x = 0$ and $k_x = 0.05 \text{ \AA}^{-1}$ for several values of $t_{\mathcal{O}}$. As can be seen

in the figure, there is excellent agreement between our approximate formula above and the numerics. Fig. 5.2 also nicely illustrates the sideband interpretation discussed above. We see that all of the spectral weight associated with the original peaks in the distant past (before the pump pulse hits the system) gets redistributed into sidebands separated by $\hbar\Omega$.

Next we move on to present results going beyond the scope of the analytic results. We plot $I(k_x, 0, \omega, t_{\mathcal{O}})$ and $I(0, k_y, \omega, t_{\mathcal{O}})$ in Figs. 5.3 and 5.4. First, the results for $I(k_x, 0, \omega, t_{\mathcal{O}})$ (within the purview of the analytic approach above) nicely confirm the intuition developed above; we see *no* renormalization of the energy bands and a simple development of sidebands. These sidebands are evident by the copies of the Dirac cone seen in the above plots. Second, $I(0, k_y, \omega, t_{\mathcal{O}})$ goes beyond our analytic approach above. We see a twofold effect as the pump-pulse hits the system. The primary effect is a splitting of the system into sidebands. The secondary effect is a renormalization of the sideband structure, this opens gaps at energies where level crossing occurs in equilibrium.

5.3.2 Circularly Polarized Light

We now shift our focus to the more involved problem of circularly polarized light. Circularly polarized light makes even the $k_y = 0$ cut along momentum space intractable analytically. We can, however, make progress right at the equilibrium Dirac point $k_x = k_y = 0$, the Γ -point. Here we have

$$H_{\Gamma}(t) = -\hbar\Omega\mathcal{A}(t) [\cos \Omega t\sigma_y - \sin \Omega t\sigma_x] - \mu\sigma_0 \quad (5.3.8)$$

The above can be written as

$$H_{\Gamma}(t) = -\hbar\Omega\mathcal{A}(t)e^{-i\Omega t\sigma_z/2}\sigma_y e^{i\Omega t\sigma_z/2} - \mu\sigma_0 \quad (5.3.9)$$

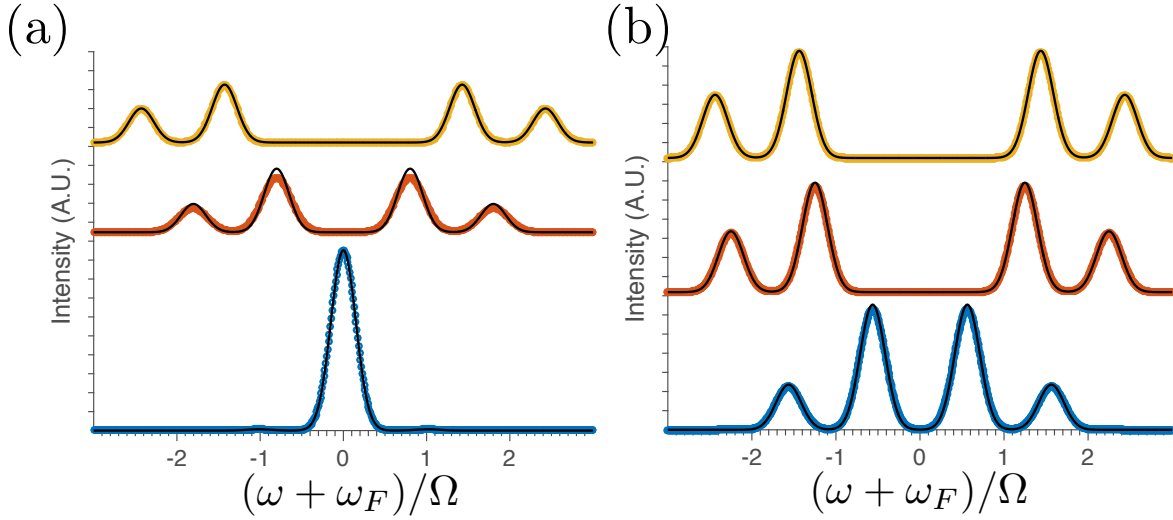


Figure 5.5: Comparison of numerical results found by integrating the time dependent Dirac equation and the analytic approximation in Eq. (5.3.15) for $I(0, 0, \omega, t_{\mathcal{O}})$. The left shows $I(0, 0, \omega, t_{\mathcal{O}})$ for different delay times $t_{\mathcal{O}}$ while the right shows $I(0, 0, \omega, t_{\mathcal{O}})$ also for different delay times but this time with a pulse FWHM of 500fs instead of 250fs. In these plots the bottom plot is for $t_{\mathcal{O}} = -500$ fs, the middle for $t_{\mathcal{O}} = -100$ fs and the top is for $t_{\mathcal{O}} = 0$ fs. In all plots the solid line is the approximation in Eq. (5.3.15) while the circles are numerical results. On the top row we see reasonable agreement between numerics and our approximation for all three delay times. When we turn up the pulse width, which effectively makes the "turn-on" time slower, we see that the agreement becomes excellent.

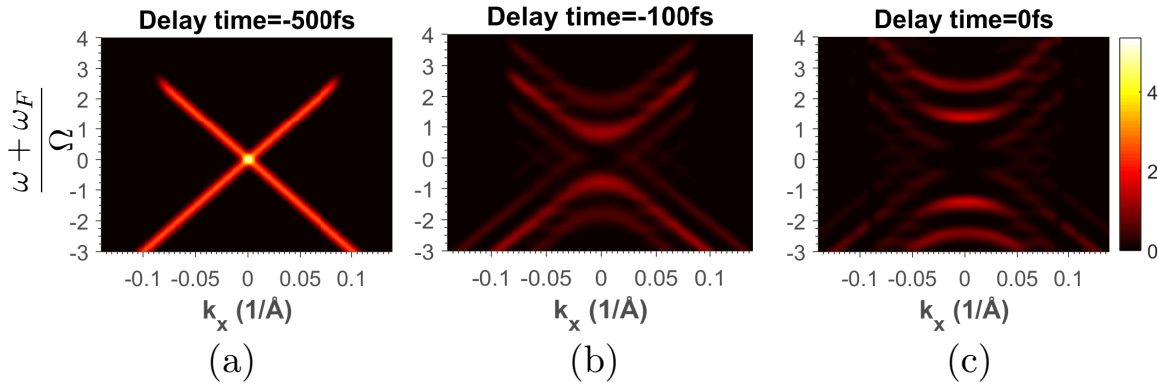


Figure 5.6: Plot of the photocurrent $I(k_x, 0, \omega, t_{\mathcal{O}})$ at various values of the delay time $t_{\mathcal{O}}$ for circularly polarized light. In the distant past we see only the Dirac cone, as the pump field starts to turn on we see copies of this cone (sidebands) begin to develop and the Dirac cone becomes gapped out. At $t_{\mathcal{O}} = 0$ we can plainly see only two sidebands through the cut $k_x = 0$.

To solve for the evolution under this Hamiltonian we transform to a rotating frame by letting $|\psi_{\Gamma\alpha}(t)\rangle = e^{i\mu(t-t_r)/\hbar} e^{i\Omega t\sigma_z/2} |\hat{\psi}_{\Gamma\alpha}(t)\rangle$. Our equation of motion for the wave function then reads

$$i\hbar\partial_t|\hat{\psi}_{\Gamma\alpha}(t)\rangle = \left(-\hbar\Omega\mathcal{A}(t)\sigma_y + \frac{\hbar\Omega}{2}\sigma_z\right)|\hat{\psi}_{\Gamma\alpha}(t)\rangle \quad (5.3.10)$$

Our purpose in finding $|\psi_{\Gamma\alpha}(t)\rangle$ is to build the Green's function $G_{\Gamma}^{\leq}(t, t')$ and ultimately convolve this Green's function with the probe pulse envelope. Therefore, a good first approximation would be to find the wave function in the vicinity of $t_{\mathcal{O}}$, the peak time of the probe-pulse. We therefore make the somewhat crude approximation $\mathcal{A}(t) \rightarrow A_{eff}(t_{\mathcal{O}})$ in the above equation of motion, Eq. 5.3.10. This yields an effective (rotating frame) Hamiltonian which is time independent. The above equation of motion can be therefore solved to give:

$$\begin{aligned} |\psi_{\Gamma\alpha}(t)\rangle &= e^{i\mu(t-t_r)/\hbar} e^{i\Omega t\sigma_z/2} \\ &\times e^{-iH_{eff}(t-t_r)/\hbar} |\hat{\psi}_{\Gamma\alpha}(t_r)\rangle \end{aligned} \quad (5.3.11)$$

where

$$H_{eff} = -\hbar\Omega A_{eff}(t_{\mathcal{O}})\sigma_y + \frac{\hbar\Omega}{2}\sigma_z \quad (5.3.12)$$

is an effective, time-independent, Hamiltonian in the vicinity of $t_{\mathcal{O}}$. $|\hat{\psi}_{\Gamma\alpha}(t_r)\rangle$ is the rotating frame wave function in the distant past. By requiring that the wavefunction $|\psi_{\Gamma\alpha}(t)\rangle$ at $t \rightarrow t_r$ be a simple spinor (whose direction can be arbitrarily chosen due to the degeneracy at the Dirac point) we find

$$|\hat{\psi}_{\Gamma\alpha}(t_r)\rangle = e^{-i\Omega t_r\sigma_z/2} |\phi_{\Gamma\alpha}\rangle \quad (5.3.13)$$

where $\{|\phi_{\Gamma\alpha}\rangle\}$ are the eigenstates at the Dirac point in the distant past. Using the above, noting that the eigenvalues of H_{eff} are $\pm E_{eff}(t_{\mathcal{O}}) = \pm\sqrt{(\hbar v_F A_{eff}(t_{\mathcal{O}}))^2 + (\frac{\hbar\Omega}{2})^2}$, and performing some additional manipulations which are left for Appendix 5.E we arrive at the following approximation for the photocurrent

$$I(0, 0, \omega, t_{\mathcal{O}}) = 2\pi T_{probe}^2 \text{Im} \left[\sum_{\alpha\beta, s, s'} f(\epsilon_{\Gamma\alpha}) e^{-i(s-s')E_{eff}(t_{\mathcal{O}})t_r/\hbar} A_{\alpha,\beta}^s (A_{\alpha,\beta}^{s'})^* \right] \quad (5.3.14)$$

$$\times \exp \left[-(\omega + \mu/\hbar - \beta\Omega/2 - sE_{eff}(t_{\mathcal{O}})/\hbar)^2 T_{probe}^2/2 \right] \exp \left[-(\omega + \mu/\hbar - \beta\Omega/2 - s'E_{eff}(t_{\mathcal{O}})/\hbar)^2 T_{probe}^2/2 \right]$$

where α, β, s, s' all run over ± 1 and $A_{\alpha,\beta}^s = (\delta_{\alpha,\beta} - s\hat{a} \cdot \langle \phi_{\beta} | \vec{\sigma} | \phi_{\alpha} \rangle) / 2$, $|\phi_{+}\rangle = (1, 0)^T$, $|\phi_{-}\rangle = (0, 1)^T$ and $\mathbf{a} = a\hat{a} = -\hbar\Omega A_{eff}(t_{\mathcal{O}})\hat{y} + \frac{\hbar\Omega}{2}\hat{z}$. We now note that $E_{eff}(t_{\mathcal{O}}) = \sqrt{(\hbar v_F A_{eff}(t_{\mathcal{O}}))^2 + (\frac{\hbar\Omega}{2})^2} \geq \hbar\Omega/2 \gg 1/T_{probe}$. Thus the distance separating the peaks in the Gaussians above (which is $2E_{eff}(t_{\mathcal{O}})/\hbar$) is much larger than the width of the peaks. We therefore discard terms where $s \neq s'$. Further, we note that the eigenvalues in the distant past $\epsilon_{\Gamma\alpha} = -\mu$ are independent of α (as we're at the Dirac point). These two observations along with some additional straightforward, but tedious, algebra lead to the simplified result

$$I(0, 0, \omega, t_{\mathcal{O}}) \quad (5.3.15)$$

$$= 2\pi T_{probe}^2 f(-\mu) \sum_{\beta, s} \left(\frac{1 - s\beta\hat{a}_z}{2} \right) \exp \left[-(\omega + \mu/\hbar - \beta\Omega/2 - sE_{eff}(t_{\mathcal{O}})/\hbar)^2 T_{probe}^2 \right]$$

Examining the above shows that the ARPES spectrum from the Γ point shows the following features at energies E (measured from μ) with weights P

$$\begin{aligned}
 E_1 &= -E_{eff}(t_{\mathcal{O}}) + \hbar\Omega/2 & P_1 &= \left(\frac{1 + \hat{a}_z}{2}\right) \\
 E_2 &= E_{eff}(t_{\mathcal{O}}) - \hbar\Omega/2 & P_2 &= \left(\frac{1 + \hat{a}_z}{2}\right) \\
 E_3 &= -E_{eff}(t_{\mathcal{O}}) - \hbar\Omega/2 & P_3 &= \left(\frac{1 - \hat{a}_z}{2}\right) \\
 E_4 &= E_{eff}(t_{\mathcal{O}}) + \hbar\Omega/2 & P_4 &= \left(\frac{1 - \hat{a}_z}{2}\right)
 \end{aligned} \tag{5.3.16}$$

where $\hat{a}_z = \frac{\hbar\Omega}{2E_{eff}(t_{\mathcal{O}})}$. It is obvious from the above that there is no additional spectral weight in any other energy. When the amplitude $A(t)$ is shut off $\hat{a}_z \rightarrow 1$ and we see $E_1, E_2 \rightarrow 0$ with weights going to unity. At the same time $E_3, E_4 \rightarrow \pm\hbar\Omega$, albeit with zero weight.

Our interpretation of the above is as follows. As the pump probe is turned on, the original two-fold degeneracy at the Dirac point is lifted and a gap is opened up with width

$$G(t_{\mathcal{O}}) = \sqrt{(2\hbar v_F A_{eff}(t_{\mathcal{O}}))^2 + (\hbar\Omega)^2} - \hbar\Omega \tag{5.3.17}$$

the weight of these states is $\left(\frac{1+\hat{a}_z}{2}\right)$ which decreases with field strength. The peaks at the other two energies correspond to single sidebands of the states E_1 and E_2 . Put another way, $E_3 = E_1 - \Omega\hbar$ while $E_4 = E_2 + \hbar\Omega$. The weights of these sidebands increase with field strength. Interestingly, unlike our treatment of the linearly polarized light, there is no statistical weight given to any other sidebands, all of the spectral weight is found within two sidebands. Note that the same approximations were made in both cases. We would like to point out that these results should hold when multiple Dirac cones are present in the system. This effect may however be obscured by the side-bands of higher energy bands. Therefore

it should be visible provided the driving field is not strong enough for these side-bands to have a large weight in the vicinity of the Dirac point.

With the above analytic analysis let us move on to numerical methods in an effort to validate the above description and further explore momenta where an approximate solution is not tractable. We do this with the side-band language discussed above in mind.

We begin with a simulation at the Gamma point. Fig. 5.5 shows $I(0, 0, \omega, t_{\mathcal{O}})$ as a function of ω for various different values of $t_{\mathcal{O}}$. Both our approximate analytic expression as well as our numerics are displayed in this plot. We see that the approximation provided above is in good agreement with the numerics with respect to both the size of the gap and the position of the sidebands, it also shows that this approximation becomes better when the width of the pump-pulse gets larger.

Let us now move on to explore a wider range of momentum using our numerical protocol. Fig. 5.6 shows the time-evolution of the ARPES spectrum for a cut such that $k_y = 0$. A cut along $k_x = 0$ looks very similar and such plots would not add to the present discussion. In the figure we see effects common to all results in this work. As the field strength is turned on the original Dirac cone is copied into sidebands, each of which is populated only with a certain weight. States in these sidebands then hybridize with each other leading to gaps. Most notable, our analytic result for the Γ point is verified at the center of the momentum cut.

5.4 Conclusions

We have provided both simple analytic results and rigorous numerical simulations of TR-ARPES in a Dirac system. Our results show that the time-evolution of an ARPES spectrum can be understood using the language of probabilistic occupation of sidebands in a time periodic system[2, 3]. In this interpretation, the amplitude of the envelope of the externally

applied field is replaced by a weighted average over the pulse-width of the ARPES probe waveform. We see the original band structure of the system split into sidebands and these sidebands are then modified by the presence of the light. Our results are in qualitative agreement with those of the experimental work in Ref. [1].

Our work also highlights the fact that not all sidebands are equally important. We showed that despite the repeated folding of the Dirac cone into the Floquet zone only a few sidebands, which are displaced by a few $\hbar\Omega$ s from the equilibrium energy, contribute to the time resolved ARPES signal. This point pertains not only to the results of Ref. [1] but also to other measurements on Floquet topological systems such as transport[2, 3].

Finally, we have explored an interesting interplay between a Dirac point and circularly polarized light. Our results suggest that under the application of circularly polarized light the Dirac point is gapped and copied into two side-bands *only*. This is in contrast to other systems, and other points in the Brillouin zone, where many sidebands can be seen.

5.5 Acknowledgements

The authors are thankful for useful discussions with Nuh Gedik. Financial support for this work was provided by the NSERC and FQRNT (TPB) and the Vanier Canada Graduate Scholarship (AF). Numerical calculations for this work were performed using McGill HPC supercomputing resources.

5.A Integrals Involving the Pump Envelope

As discussed above, we choose to describe this electric field in a gauge where the scalar potential is zero. Thus we have

$$\begin{aligned} \mathbf{A}_{pump}(t) &= - \int_{-\infty}^t dt' \mathbf{E}_{pump}(t') \\ &= -E_0 \int_{-\infty}^t dt' e^{-\frac{t'^2}{2T_{pump}^2}} \mathbf{E}_{\Omega}(t') \end{aligned} \quad (5.A.1)$$

where we have chosen in initial condition such that $\mathbf{A}_{pump}(t) \rightarrow 0$ for $t \rightarrow -\infty$.

Let us define the frequency scale associated with the pump pulse $\Omega_{pump} = 2\pi/T_{pump}$.

We work in the limit

$$\Omega_{pump} \ll \Omega \quad (5.A.2)$$

such that there are many oscillations within the pump field envelope. We now define $\mathbf{E}_{\Omega}(t) = -\frac{\tilde{\mathbf{E}}'_{\Omega}(t)}{\Omega}$ and integrate by parts to obtain

$$\begin{aligned} \mathbf{A}_{pump}(t) &= \frac{E_0}{\Omega} e^{-\frac{t^2}{2T_{pump}^2}} \tilde{\mathbf{E}}_{\Omega}(t) \Big|_{-\infty}^t \\ &+ \frac{E_0}{\Omega T_{pump}^2} \int_{-\infty}^t dt' t' e^{-\frac{t'^2}{2T_{pump}^2}} \tilde{\mathbf{E}}_{\Omega}(t') \\ &= \frac{E_0}{\Omega} e^{-\frac{t^2}{2T_{pump}^2}} \tilde{\mathbf{E}}_{\Omega}(t) + \mathcal{O}\left(\frac{\Omega_{pump}}{\Omega}\right) \end{aligned} \quad (5.A.3)$$

The above process could in principle be iterated to produce a perturbative expansion in $\frac{\Omega_{pump}}{\Omega}$, although we stop here for practicality. We could alternatively write $\frac{\Omega_{pump}}{\Omega} = \frac{T}{T_{pump}}$, which tells us this expression is valid in the limit $T \ll T_{probe}$; i.e. the amplitude changes on a much longer time scale than the period of oscillation. We neglect all but the leading order terms. Continuing the procedure above shows that the next to leading order term is

of order $\left(\frac{\Omega_{pump}}{\Omega}\right)^2$. Thus we work in a regime where

$$\mathbf{A}_{pump}(t) \simeq \frac{E_0}{\Omega} e^{-\frac{t^2}{2T_{pump}^2}} \tilde{\mathbf{E}}_{\Omega}(t) \quad (5.A.4)$$

5.B Green's Function

We now consider the quantity

$$G_{\mathbf{k},\alpha\beta}^<(t, t') = i\langle c_{\mathbf{k}\beta}^{\dagger}(t')c_{\mathbf{k}\alpha}(t) \rangle \quad (5.B.1)$$

In order to define a useful quantity we consider the equation of motion for the electronic operators:

$$\dot{c}_{\mathbf{k}\alpha}(t) = i[\mathcal{H}(t), c_{\mathbf{k}\alpha}(t)] \quad (5.B.2)$$

where the over-dot denotes differentiation with respect to time and $\mathcal{H}(t) = \sum_{\mathbf{k},\alpha,\beta} c_{\mathbf{k}\alpha}^{\dagger} H_{\mathbf{k},\alpha\beta}(t) c_{\mathbf{k}\beta}$.

Using the Hamiltonian defined above and calculating the commutator gives

$$\dot{c}_{\mathbf{k}\alpha}(t) = -iH_{\mathbf{k},\alpha\beta}(t)c_{\mathbf{k}\beta}(t) \quad (5.B.3)$$

where summation over repeated indices is implied. The above equation is linear in electron operators. We thus try a solution of the form $c_{\mathbf{k}\alpha}(t) = U_{\mathbf{k}\alpha\alpha'}(t, t_r)c_{\mathbf{k}\alpha'}(t_r)$ where the $U_{\mathbf{k}\alpha\alpha'}(t, t_r)$ are complex numbers. Plugging this in gives

$$\dot{U}_{\mathbf{k}\alpha\alpha'}(t, t_r)c_{\mathbf{k}\alpha'}(t_r) = -iH_{\mathbf{k},\alpha\beta}(t)U_{\mathbf{k}\beta\alpha'}(t, t_r)c_{\mathbf{k}\alpha'}(t_r) \quad (5.B.4)$$

Which implies

$$i\dot{U}_{\mathbf{k}\alpha\alpha'}(t, t_r) = H_{\mathbf{k},\alpha\beta}(t)U_{\mathbf{k}\beta\alpha'}(t, t_r) \quad (5.B.5)$$

promoting U and H to matrices gives

$$i\partial_t U_{\mathbf{k}}(t, t_r) = H_{\mathbf{k}}(t)U_{\mathbf{k}}(t, t_r) \quad (5.B.6)$$

The formal solution to the above equation is

$$U_{\mathbf{k}}(t, t_r) = T \left(e^{-i \int_{t_r}^t d\tau H_{\mathbf{k}}(\tau)} \right) \quad (5.B.7)$$

and it obeys $U_{\mathbf{k}}(t, t')U_{\mathbf{k}}(t', t_r) = U_{\mathbf{k}}(t, t_r)$ and $(U_{\mathbf{k}}(t, t_r))^\dagger = U_{\mathbf{k}}(t_r, t)$, where T is the time ordering operator. Using this solution we can write

$$\begin{aligned} G_{\mathbf{k}, \alpha\beta}^<(t, t') &= iU_{\mathbf{k}\alpha\alpha'}(t, t_r)U_{\mathbf{k}\beta\beta'}^*(t', t_r)\langle c_{\mathbf{k}\beta'}^\dagger(t_r)c_{\mathbf{k}\alpha'}(t_r) \rangle \\ &= U_{\mathbf{k}\alpha\alpha'}(t, t_r)G_{\mathbf{k}, \alpha'\beta'}^<(t_r, t_r)U_{\mathbf{k}\beta\beta'}^*(t', t_r) \end{aligned} \quad (5.B.8)$$

Writing the above in matrix form gives

$$G_{\mathbf{k}}^<(t, t') = U_{\mathbf{k}}(t, t_r)G_{\mathbf{k}}^<(t_r, t_r)U_{\mathbf{k}}^\dagger(t', t_r) \quad (5.B.9)$$

or

$$G_{\mathbf{k}}^<(t, t') = U_{\mathbf{k}}(t, t_r)G_{\mathbf{k}}^<(t_r, t_r)U_{\mathbf{k}}(t_r, t') \quad (5.B.10)$$

Which is conceptually appealing. We begin at t' , propagate back to t_r where we know the Green's function and then propagate forward to t . We now assume that the system begins at time t_r in equilibrium in a system obeying the unperturbed Hamiltonian. Thus we write $G_{\mathbf{k}}^<(t_r, t_r) = i \sum_{\alpha} |\phi_{\mathbf{k}\alpha}\rangle\langle\phi_{\mathbf{k}\alpha}|f(E_{\mathbf{k}\alpha})$. Noting that $|\psi_{\mathbf{k}\alpha}(t)\rangle = U_{\mathbf{k}}(t, t_r)|\phi_{\mathbf{k}\alpha}\rangle$ then immediately leads to the expression for the Green's function used in the main text, Eq. 5.2.12 .

5.C Gauge Choice

In considering the effects of electromagnetic fields we must ensure that our theory is gauge invariant. A general gauge transformation is applied as follows

$$\mathbf{A}(\mathbf{r}, t) \rightarrow \mathbf{A}(\mathbf{r}, t) + \nabla\chi(\mathbf{r}, t) \quad (5.C.1)$$

$$\Phi(\mathbf{r}, t) \rightarrow \Phi(\mathbf{r}, t) - \partial_t\chi(\mathbf{r}, t)$$

$$c_{j\sigma} \rightarrow e^{ie\chi(\mathbf{r}_j, t)/\hbar} c_{j\sigma}$$

Within the so called ‘‘Hamiltonian gauge’’ used above we take $\Phi = 0$ and $\mathbf{E}(t) = -\partial_t\mathbf{A}(t)$. Therefore, to remain within this choice of Gauge and not change our problem in a non-trivial way by for example, introducing a spatial dependence, we must be free to introduce a Gauge change $\chi = \mathbf{r} \cdot \mathbf{f}$ where \mathbf{f} is an arbitrary, *constant* vector. This amounts to the Gauge change $\mathbf{A}(t) \rightarrow \mathbf{A}(t) + \mathbf{f}$, $\Phi(\mathbf{r}, t) \rightarrow \Phi(\mathbf{r}, t)$ and $c_{j\sigma} \rightarrow e^{ie\mathbf{r}_j \cdot \mathbf{f}/\hbar} c_{j\sigma}$. Fourier transforming the electron annihilation operator leads to the result that the Gauge change makes the modification $c_{\mathbf{k}\sigma} \rightarrow c_{\mathbf{k}-e\mathbf{f},\sigma}$. Note also that $H_{\mathbf{k}}(t) \rightarrow H_{\mathbf{k}-e\mathbf{f}}(t)$ under this transformation. Thus our time evolution operators change as $U_{\mathbf{k}}(t, t') \rightarrow U_{\mathbf{k}-e\mathbf{f}}(t, t')$ and therefore all of the Greens functions defined above transform as $G_{\mathbf{k}}(t, t') \rightarrow G_{\mathbf{k}-e\mathbf{f}}(t, t')$ and are thus not Gauge invariant.

It is useful to note conceptually where this Gauge freedom comes from. We require $\mathbf{E}(t) = -\partial_t\mathbf{A}(t)$ which in turn gives

$$\mathbf{A}(t) = - \int_{\mathcal{O}}^t dt' \mathbf{E}(t') + \mathbf{A}(\mathcal{O}) \quad (5.C.2)$$

where the initial condition $\mathbf{A}(\mathcal{O})$ is *unfixed* by the electric field. Thus the freedom we have lies in our choice of the reference $\mathbf{A}(\mathcal{O})$. Recall the turn on procedure we have in mind: the pump field is off for $t < t_r$ and is switched on after-wards. Therefore, for this choice

of set-up it is convenient to express \mathbf{A} as follows

$$\begin{aligned}\mathbf{A}(t) &= -\Theta(t - t_0) \int_{t_r}^t dt' \mathbf{E}(t') + \mathbf{A}(t_0) \\ &= \mathbf{A}_{physical}(t) + \mathbf{A}(t_r)\end{aligned}\tag{5.C.3}$$

but $\mathbf{A}(t_r) \equiv \mathbf{A}_0$ is still entirely arbitrary. Thus we would like a theory completely independent of $\mathbf{A}(t_r)$. This is equivalent to the statement above that the Gauge invariant quantities should be independent of \mathbf{f} , as all \mathbf{f} constitutes is a shift in the value of $\mathbf{A}(t_r)$.

We now note that Green's functions $\tilde{G}_{\mathbf{k}}(t, t') \equiv G_{\mathbf{k}+e\mathbf{A}_0}(t, t')$ are unchanged by the Gauge transformation $\mathbf{A}(t) \rightarrow \mathbf{A}(t) + \mathbf{f}$ as the shift $\mathbf{k} \rightarrow \mathbf{k} - e\mathbf{f}$ in the Gauge dependent wave function cancels out the shift $\mathbf{A}_0 \rightarrow \mathbf{A}_0 + \mathbf{f}$. An equivalent finding is that

$$U_{\mathbf{k}+e\mathbf{A}_0}(t, t_r) = T \left(e^{-i \int_{t_r}^t d\tau H_{\mathbf{k}+e\mathbf{A}_0}(\tau)} \right)\tag{5.C.4}$$

but

$$\begin{aligned}H_{\mathbf{k}+e\mathbf{A}_0}(t) &= h_{\mathbf{k}-e\mathbf{A}(t)+e\mathbf{A}_0} \\ &= h_{\mathbf{k}-e\mathbf{A}_{physical}(t)-e\mathbf{A}_0+e\mathbf{A}_0} = h_{\mathbf{k}-e\mathbf{A}_{physical}(t)}\end{aligned}\tag{5.C.5}$$

where $h_{\mathbf{k}}$ is the Dirac Hamiltonian. Therefore $H_{\mathbf{k}+e\mathbf{A}_0}(t)$ is independent of our arbitrary choice of \mathbf{A}_0 , meaning that $U_{\mathbf{k}+e\mathbf{A}_0}(t, t_r)$ and thus $G_{\mathbf{k}+e\mathbf{A}_0}(t, t')$ are gauge invariant as well.

Of course the most natural choice is to set $\mathbf{A}_0 = 0$ so that the (equilibrium) Hamiltonian before the switch on time t_r is simply $h_{\mathbf{k}}$, as one would like it to be. For *this choice* of initial condition the Gauge invariant Greens function and the traditional Greens function are identical.

5.D Linearly Polarized Light

Here we go over the details leading to Eq. (5.3.6) in the main text. Assuming $T_{pump} \ll 2\pi/\omega$,

$$\int_{t'}^t dt'' A_x(t'') = \frac{E_0}{\Omega^2} \left(e^{-t^2/2T_{pump}^2} \sin \Omega t - e^{-t'^2/2T_{pump}^2} \sin \Omega t' \right)$$

and using the identity $e^{ix \sin \Omega t} = \sum_m J_m(x) e^{im\Omega t}$ in the wave functions for the linearly polarized light the photocurrent with $k_y = 0$ reads

$$\begin{aligned} & I(k_x, 0, \omega, t_{\mathcal{O}}) \\ &= \sum_{\alpha} f(\epsilon_{k_x, 0, \alpha}) \left| \sum_m \int_{-\infty}^{\infty} dt_1 J_m(\alpha \mathcal{A}(t_1)) e^{-\frac{(t_1 - t_{\mathcal{O}})^2}{2T_{probe}^2}} e^{-i(\omega - \alpha v_F k_x + \frac{\mu}{\hbar} - m\Omega)t_1} \right|^2 \end{aligned} \quad (5.D.1)$$

In the above, $J_m(\alpha \mathcal{A}(t_1))$ describes a splitting of the eigenstates into sidebands, labeled by m , where the amplitudes of these sidebands depend on time. Meanwhile $s(t_1 - t_{\mathcal{O}}) = e^{-\frac{(t_1 - t_{\mathcal{O}})^2}{2T_{probe}^2}}$ is the profile of the probe pulse and $e^{-i(\omega + \alpha v_F k_x + \frac{\mu}{\hbar} - m\Omega)t_1}$ describes having energies not just at $\pm v_F k_x - \mu$, but also at values $m\hbar\Omega$ above and below these values. The integral above is of course intractable to perform exactly. We can make progress using a series of appropriate approximations. The first is that the probe pulse is much shorter than the pump pulse. Therefore $\mathcal{A}(t)$ changes very slowly over the duration of $e^{-\frac{(t_1 - t_{\mathcal{O}})^2}{2T_{probe}^2}}$. We can therefore simply replace the $J_m(\alpha \mathcal{A}(t_1))$ term with its value at the peak $t_1 = t_{\mathcal{O}}$. However we observe that a better approach is to replace $\mathcal{A}(t) = \frac{eE_0 v_F}{\hbar \Omega^2} e^{-t^2/2T_{pump}^2}$ with a weighted average over the probe pulse. Thus we define

$$A_{eff}(t_{\mathcal{O}}) = \frac{\int dt e^{-\frac{(t - t_{\mathcal{O}})^2}{2T_{probe}^2}} \mathcal{A}(t)}{\int dt e^{-\frac{(t - t_{\mathcal{O}})^2}{2T_{probe}^2}}} \quad (5.D.2)$$

Once we have made this replacement the remaining integral can be done analytically and

gives

$$I(k_x, 0, \omega, t_{\mathcal{O}}) = 2\pi T_{probe}^2 \sum_{\alpha, m, m'} f(\epsilon_{k_x, 0, \alpha}) J_m(\alpha A_{eff}(t_{\mathcal{O}})) J_{m'}(\alpha A_{eff}(t_{\mathcal{O}})) \quad (5.D.3)$$

$$\times \exp\left[-(\omega - \alpha v_F k_x + \frac{\mu}{\hbar} - m\Omega)^2 T_{probe}^2 / 2\right] \exp\left[-(\omega - \alpha v_F k_x + \frac{\mu}{\hbar} - m'\Omega)^2 T_{probe}^2 / 2\right]$$

The width of the peaks described by the Gaussians above are set by the frequency scale $1/T_{probe}$. The two Gaussians describe peaks centred at $\alpha v_F k_x - \frac{\mu}{\hbar} + m\Omega$ and $\alpha v_F k_x - \frac{\mu}{\hbar} + m'\Omega$. Thus the separation between the two peaks is $(m - m')\Omega$. If the decay scale $1/T_{probe}$ is much smaller than the smallest separation Ω , i.e. $1/T_{probe} \ll \Omega$ then the peaks do not overlap at the same frequency and so the major contribution to the double sum comes from the $m' = m$ terms. Working in this approximation gives

$$I(k_x, 0, \omega, t_{\mathcal{O}}) = 2\pi T_{probe}^2 \sum_{\alpha, m} f(\epsilon_{k_x, 0, \alpha}) J_m^2(A_{eff}(t_{\mathcal{O}})) \quad (5.D.4)$$

$$\times \exp\left[-(\omega - \alpha v_F k_x + \frac{\mu}{\hbar} - m\Omega)^2 T_{probe}^2\right]$$

5.E Circularly Polarized Light

We begin with the approximate wave function found in the main text, reproduced here for convenience

$$|\psi_{\Gamma\alpha}(t)\rangle = e^{i\mu(t-t_r)/\hbar} e^{i\Omega t\sigma_z/2} \quad (5.E.1)$$

$$\times e^{-iH_{eff}(t-t_r)/\hbar} e^{-i\Omega t_r\sigma_z/2} |\phi_{\Gamma\alpha}\rangle$$

. We note that in order to find the trace of the Green's function we will require $\langle\phi_{\Gamma,\beta}|\psi_{\Gamma\alpha}(t)\rangle$ (and its complex conjugate). In the distant past the field is turned off and so the Hamiltonian is $h_{\Gamma}(t \rightarrow -\infty) = -\mu\sigma_0$. Thus we are free to choose any "initial" set of states, provided

they are orthonormal. For convenience we choose $\{|\phi_{\Gamma\alpha}\rangle\}$ to be $(1, 0)^T$ and $(0, 1)^T$, which we label $|\phi_\alpha\rangle$ with $\alpha = \pm 1$. From this point forward we will drop the Γ subscript in the interest of brevity. This leads to the following

$$\begin{aligned} \langle \phi_{\Gamma,\beta} | \psi_{\Gamma\alpha}(t) \rangle &= e^{i(\mu+\beta\hbar\Omega/2)t/\hbar} e^{-i(\mu+\alpha\hbar\Omega/2)t_r/\hbar} \\ &\times \langle \phi_\beta | e^{-iH_{eff}(t-t_r)/\hbar} | \phi_\alpha \rangle \end{aligned} \quad (5.E.2)$$

In order to calculate the matrix elements of $e^{-iH_{eff}(t-t_r)/\hbar}$ we write the argument of the exponential as follows

$$\left(-\hbar v_F A_{eff}(t_{\mathcal{O}}) \sigma_y + \frac{\hbar\Omega}{2} \sigma_z \right) = \frac{E_{eff}(t_{\mathcal{O}})}{\hbar} \hat{a} \cdot \vec{\sigma} \quad (5.E.3)$$

where $\hat{a} = \left(-\frac{\hbar v_F A_{eff}(t_{\mathcal{O}})}{E_{eff}(t_{\mathcal{O}})} \hat{y} + \frac{\hbar\Omega}{2 E_{eff}(t_{\mathcal{O}})} \hat{z} \right)$ is a unit vector and we remind the reader that $E_{eff} = \sqrt{(\hbar v_F A_{eff}(t_{\mathcal{O}}))^2 + (\hbar\Omega/2)^2}$. Making use of the identity $e^{-ix\hat{\sigma}} = \cos(x) \sigma_0 - i \sin(x) \hat{a} \cdot \vec{\sigma}$ one can show that

$$\begin{aligned} &\langle \phi_\beta | e^{-iH_{eff}(t-t_r)/\hbar} | \phi_\alpha \rangle \\ &= \sum_{s=\pm 1} e^{i\frac{sE_{eff}(t_{\mathcal{O}})}{\hbar}(t-t_r)} A_{\alpha,\beta}^s \end{aligned} \quad (5.E.4)$$

where $A_{\alpha,\beta}^s = (\delta_{\alpha,\beta} - s\hat{a} \cdot \langle \psi_\beta | \vec{\sigma} | \psi_\alpha \rangle) / 2$ which leads to

$$\begin{aligned} \langle \phi_{\Gamma,\beta} | \psi_{\Gamma\alpha}(t) \rangle &= \\ &\sum_{s=\pm 1} e^{i(\mu+\beta\hbar\Omega/2+sE_{eff}(t_{\mathcal{O}}))t/\hbar} e^{-i(\mu+\alpha\hbar\Omega/2+sE_{eff}(t_{\mathcal{O}}))t_r/\hbar} A_{\alpha,\beta}^s \end{aligned} \quad (5.E.5)$$

Using the above, an equivalent result for $\langle \psi_{\Gamma\alpha}(t') | \phi_{\Gamma\beta} \rangle$, and performing the t_1 and t_2 integrals gives

$$\begin{aligned}
 I(0, 0, \omega, t_{\mathcal{O}}) = & \quad (5.E.6) \\
 & 2\pi T_{probe}^2 \sum_{\alpha\beta, s, s'} f(\epsilon_{\Gamma\alpha}) e^{-i(s-s')E_{eff}(t_{\mathcal{O}})t_r/\hbar} A_{\alpha,\beta}^s (A_{\alpha,\beta}^{s'})^* \\
 \times & \exp \left[-(\omega + \mu/\hbar - \beta\Omega/2 - sE_{eff}(t_{\mathcal{O}})/\hbar)^2 T_{probe}^2/2 \right] \\
 \times & \exp \left[-(\omega - \mu/\hbar - \beta\Omega/2 - s'E_{eff}(t_{\mathcal{O}})/\hbar)^2 T_{probe}^2/2 \right]
 \end{aligned}$$

Recalling that we are working under the assumption $E_{eff}(t_{\mathcal{O}}) = \sqrt{(\hbar v_F A_{eff}(t_{\mathcal{O}}))^2 + (\frac{\hbar\Omega}{2})^2} \geq \hbar\Omega/2 \gg 1/T_{probe}$, the distance separating the peaks in the Gaussians above (which is $2E_{eff}(t_{\mathcal{O}})/\hbar$) is much large than the width of the peaks. We therefore discard terms where $s \neq s'$ which gives us

$$\begin{aligned}
 I(0, 0, \omega, t_{\mathcal{O}}) = & 2\pi T_{probe}^2 \sum_{\alpha\beta, s} f(\epsilon_{\Gamma\alpha}) |A_{\alpha,\beta}^s|^2 \quad (5.E.7) \\
 \times & \exp \left[-(\omega + \mu/\hbar - \beta\Omega/2 - sE_{eff}(t_{\mathcal{O}})/\hbar)^2 T_{probe}^2 \right]
 \end{aligned}$$

We note that the eigenvalues in the distant past are $\epsilon_{\Gamma\alpha} = -\mu$, where are independent of α (as we're at the Dirac point). At this point the only α dependence left in the summand comes from the matrix elements $|A_{\alpha,\beta}^s|^2$. Some algebra shows $\sum_{\alpha} |A_{\alpha,\beta}^s|^2 = \frac{1-s\beta\hat{a}_z}{2}$ leading to our final result

$$\begin{aligned}
 I(0, 0, \omega, t_{\mathcal{O}}) = & 2\pi T_{probe}^2 f(-\mu) \sum_{\beta, s} \left(\frac{1-s\beta\hat{a}_z}{2} \right) \quad (5.E.8) \\
 \times & \exp \left[-(\omega + \mu/\hbar - \beta\Omega/2 - sE_{eff}(t_{\mathcal{O}})/\hbar)^2 T_{probe}^2 \right]
 \end{aligned}$$

References

- ¹Y. H. Wang, H. Steinberg, P. Jarillo-Herrero, and N. Gedik, *Science* **342**, 453–457 (2013).
- ²A. Farrell and T. Pereg-Barnea, *Phys. Rev. Lett.* **115**, 106403 (2015).
- ³A. Farrell and T. Pereg-Barnea, *Phys. Rev. B* **93**, 045121 (2016).
- ⁴B. A. Bernevig, T. L. Hughes, and S.-C. Zhang, *Science* **314**, 1757–1761 (2006).
- ⁵J. E. Moore and L. Balents, *Physical Review B* **75**, 121306 (2007).
- ⁶L. Fu, C. L. Kane, and E. J. Mele, *Physical Review Letters* **98**, 106803 (2007).
- ⁷D. Hsieh, D. Qian, L. Wray, Y. Xia, Y. S. Hor, R. Cava, and M. Z. Hasan, *Nature* **452**, 970–974 (2008).
- ⁸M. König, S. Wiedmann, C. Brüne, A. Roth, H. Buhmann, L. W. Molenkamp, X.-L. Qi, and S.-C. Zhang, *Science* **318**, 766–770 (2007).
- ⁹A. Roth, C. Brüne, H. Buhmann, L. W. Molenkamp, J. Maciejko, X.-L. Qi, and S.-C. Zhang, *Science* **325**, 294–297 (2009).
- ¹⁰J. Li, R.-L. Chu, J. K. Jain, and S.-Q. Shen, *Phys. Rev. Lett.* **102**, 136806 (2009).
- ¹¹J. Borchmann, A. Farrell, and T. Pereg-Barnea, *Phys. Rev. B* **93**, 125133 (2016).
- ¹²N. H. Lindner, G. Refael, and V. Galitski, *Nat Phys* **7**, 490 (2011).
- ¹³Z. Gu, H. A. Fertig, D. P. Arovas, and A. Auerbach, *Phys. Rev. Lett.* **107**, 216601 (2011).
- ¹⁴T. Oka and H. Aoki, *Phys. Rev. B* **79**, 081406 (2009).
- ¹⁵G. Usaj, P. M. Perez-Piskunow, L. E. F. Foa Torres, and C. A. Balseiro, *Phys. Rev. B* **90**, 115423 (2014).
- ¹⁶H. L. Calvo, H. M. Pastawski, S. Roche, and L. E. F. F. Torres, *Applied Physics Letters* **98** (2011).

- ¹⁷L. Foa Torres, P. Perez-Piskunow, C. Balseiro, and G. Usaj, *Unpublished*, arXiv:1409.2482v1 (2014).
- ¹⁸A. Gómez-León and G. Platero, *Phys. Rev. Lett.* **110**, 200403 (2013).
- ¹⁹M. S. Rudner, N. H. Lindner, E. Berg, and M. Levin, *Phys. Rev. X* **3**, 031005 (2013).
- ²⁰T. Kitagawa, E. Berg, M. Rudner, and E. Demler, *Phys. Rev. B* **82**, 235114 (2010).
- ²¹A. Kundu, H. A. Fertig, and B. Seradjeh, *Phys. Rev. Lett.* **113**, 236803 (2014).
- ²²Y. Tenenbaum Katan and D. Podolsky, *Phys. Rev. B* **88**, 224106 (2013).
- ²³L. Jiang, T. Kitagawa, J. Alicea, A. R. Akhmerov, D. Pekker, G. Refael, J. I. Cirac, E. Demler, M. D. Lukin, and P. Zoller, *Phys. Rev. Lett.* **106**, 220402 (2011).
- ²⁴A. Kundu and B. Seradjeh, *Phys. Rev. Lett.* **111**, 136402 (2013).
- ²⁵D. E. Liu, A. Levchenko, and H. U. Baranger, *Phys. Rev. Lett.* **111**, 047002 (2013).
- ²⁶C. We, J. Sun, F. Huang, Y. Li, and W. Liu, *EPL* **104**, 27004 (2013).
- ²⁷P. Wang, Q.-f. Sun, and X. C. Xie, *Phys. Rev. B* **90**, 155407 (2014).
- ²⁸P. Delplace, Á. Gómez-León, and G. Platero, *Phys. Rev. B* **88**, 245422 (2013).
- ²⁹Y. Li, A. Kundu, F. Zhong, and B. Seradjeh, *Phys. Rev. B* **90**, 121401 (2014).
- ³⁰P. Titum, N. H. Lindner, M. C. Rechtsman, and G. Refael, *Phys. Rev. Lett.* **114**, 056801 (2015).
- ³¹K. I. Seetharam, C.-E. Bardyn, N. H. Lindner, M. S. Rudner, and G. Refael, *Unpublished*, arXiv:1502.02664 (2015).
- ³²H. Sambe, *Phys. Rev. A* **7**, 2203–2213 (1973).
- ³³M. C. Rechtsman, J. M. Zeuner, Y. Plotnik, Y. Lumer, D. Podolsky, F. Dreisow, S. Nolte, M. Segev, and A. Szameit, *Nature* **496**, 196–200 (2013).

-
- ³⁴M. Sentef, M. Claassen, A. Kemper, B. Moritz, T. Oka, J. Freericks, and T. Devereaux, *Nature communications* **6** (2015).
- ³⁵L. D'Alessio and M. Rigol, *Phys. Rev. X* **4**, 041048 (2014).
- ³⁶L. D'Alessio and M. Rigol, *Unpublished*, arXiv:1409.6319 (2014).
- ³⁷A. Lazarides, A. Das, and R. Moessner, *Phys. Rev. E* **90**, 012110 (2014).
- ³⁸P. Ponte, A. Chandran, Z. Papić, and D. A. Abanin, *Annals of Physics* **353**, 196–204 (2015).
- ³⁹P. K. Tien and J. P. Gordon, *Phys. Rev.* **129**, 647–651 (1963).
- ⁴⁰J. Freericks, H. Krishnamurthy, and T. Pruschke, *Physical review letters* **102**, 136401 (2009).
- ⁴¹J. Freericks, H. Krishnamurthy, M. Sentef, and T. Devereaux, arXiv preprint arXiv:1403.7585 (2014).

6

Conclusions

6.1 Summary of this Thesis

The main theme of this thesis has been driving and manipulating topological states of matter using externally applied perturbations. In particular, it has explored the use of a Zeeman field for this purpose in a topological superconductor, and the use of time-periodic perturbations for this purpose in topological insulators.

Chapter 2 was interested in interacting, spin-orbit coupled electrons. A renormalization group method approach showed that for a range of parameters in the original model the most dominant pairing channel has either p -wave or f -wave symmetry. Such an interaction will then lead to Cooper pairs with either a p -wave or an f -wave order parameter. This manuscript went on to show that, for an appropriate parameter set, the superconductivity developed in this way should be topological in nature and will therefore support Majorana modes. Thus the main conclusion of this work is that interactions, rather than proximity effect, and an appropriately applied Zeeman field may be used to drive a topological superconducting state.

Chapter 3 explored how a time-periodic, external perturbation may be used to manip-

ulate the transport properties of a 2D topological insulator. This was done by developing an analogue of a photon-assisted tunneling picture, where electrons in the system only access the topologically protected edge states probabilistically. This probabilistic viewpoint thereby reduced the traditional values associated with transport measurement in a topological insulator. Nonetheless, the transport values obtained are still a result of topology and will therefore maintain their robustness property. In this way, this work shows that a time-periodic perturbation may be used to strongly manipulate the topologically protected transport values of a 2D TI.

Chapter 4 continued along the path laid by the manuscript in Chapter 3, with the important distinction that this work started by considering a system that is not topological without the application of a time-periodic field. This work showed that an externally applied, time-periodic field may be used to create topologically protected edge-states with very specific transport properties. Similar to the system in Chapter 3, these specific, topological, transport properties can be manipulated by using the external perturbation. Thus Chapter 4 studies a system where an externally applied perturbation is used to both create a topological state, and to manipulate this topological state after it has been created.

Finally, chapter 5 of this work explored the manipulation of the surface Dirac states in a 3D TI with applied light. This work further supports the theme established in Chapter 3 that these states can be understood in terms of probabilistically occupying side-bands in the periodic system. It showed that different polarizations of light can be used to affect these sidebands in unique ways. Linearly polarized light can create a direct splitting of the Dirac cone into multiple Dirac cones, meanwhile circularly polarized light gaps the Dirac points and creates only two sidebands. The results in Chapter 5 were also discussed in connection with recent experimental progress, where good qualitative agreement is found.

6.2 Future Directions

Before closing this work we will briefly discuss several potential extensions of the work contained herein. We will begin with the work on topological superconductors and finish with potential extensions of the non-equilibrium work on topological insulators.

First, the work in Chapter 2 provided a rigorous analysis of interactions in a 2D spin-orbit coupled electron system. That fact notwithstanding, once the tools of RG analysis were used to establish the symmetry of the superconducting order parameter, a mean-field treatment of the topological invariant (assuming this pairing symmetry) had to be utilized. A useful possible extension would therefore be to incorporate a way to determine the topological class of the system using the more thorough tools of RG analysis.

Second, an interesting possible extension, and unification, of the work in Chapters 3 through 5 would be a calculation of the AC conductivity in a driven topological insulator. The main conclusion of Chapters 3 and 4 was that to recover the traditional transport signatures of a 2D TI, one must employ a sum rule of conductivities at energies separated by the frequency of the driving field. It may be possible to design an AC bias in a way that the AC conductivity somehow achieves, or partially achieves, this goal. This set-up would represent a more concise way of making this measurement. Treating this problem will involve a pump-pulse type methodology and so the formalism of Chapter 5 will be an excellent starting point.

